UNIVERSIDAD AUTÓNOMA DE SAN LUÍS POTOSÍ

Doctorado Institucional en Ingeniería y Ciencia de Materiales

Study on the water retention and carbon sequestration of clay–organic composites in nutrient-poor soils

PARA OBTENER EL GRADO DE

DOCTORA EN INGENIERÍA Y CIENCIA DE MATERIALES

QUE PRESENTA

Cui Zhang

ASESORA

Dra. J. Viridiana García Meza

PATROCINADO POR SECIHTI Beca número 813509

San Luis Potosí, SLP, enero 2026

UNIVERSIDAD AUTÓNOMA DE SAN LUÍS POTOSÍ

Doctorado Institucional en Ingeniería y Ciencia de Materiales

Study on the water retention and carbon sequestration of clay–organic composites in nutrient-poor soils

QUE PARA OBTENER EL GRADO DE

DOCTORA EN INGENIERÍA Y CIENCIA DE MATERIALES

PRESENTA

Cui Zhang

ASESORA

Dra. J. Viridiana García Meza

Sinodales

Dra. Jessica Viridiana García Meza _____

Dr. Alejandro López Valdivieso†

Dr. Edgar D. Páez Pérez _____

Dr. Damiano Sarocchi _____

Dra. Ling Xia _____

Dra. Yanmei Li _____

San Luis Potosí, SLP, enero 2026

Acknowledgement

This work was financially supported by Secretariat of Science, Humanities, Technology and Innovation (SECIHTI) of Mexico, Thanks are given to the Marcos Moshinsky Foundation A.C. for economical support. Cui Zhang thanks to SECIHTI for the scholarship number 813509. The Laboratorio de Geomicrobiología del Instituto de Metalurgia, Universidad Autónoma de San Luis Potosí is gratefully acknowledged.

As I completed my Ph.D. thesis, reflecting on the past four years of my doctoral journey evokes a mix of emotions -joy, challenges, and perseverance. Four years ago, I made the significant decision to resign from a company and embark on a rigorous Ph.D. study at Universidad Autónoma de San Luis Potosí. The successful completion of my Ph.D. would not have been possible without the invaluable support of many individuals, to whom I extend my deepest gratitude.

Foremost, I am profoundly grateful to my advisors, Dra. J. Viridiana García Meza. Dra. Viridiana has always helped me a lot. Academically, she provided constructive feedback and oversaw the initial revisions of my manuscript. In daily life, she has been immensely supportive, doing her utmost to help me adapt to life in Mexico and resolve various difficulties. Upon learning that I was without a scholarship, she generously offered me financial support without hesitation and has always assisted me with the greatest enthusiasm. To help me and my other Chinese classmates settle in, she went above and beyond: she acted as our rental guarantor, invited us to her home for meals, and took us on sightseeing trips around Mexico City. During these outings, she patiently explained the city's history and reminded us of important safety precautions. My gratitude towards my dear supervisor is beyond words.

Dra. Ling Xia has been a guiding light for me. Her guidance throughout my doctoral studies has significantly enhanced my critical thinking and research capabilities. She has kept me on the right path intellectually, making timely adjustments to my research direction. Her dedication, innovative thinking, and passion for research will continue to inspire my future endeavors. I would also like to extend my sincere appreciation to Dr. Ling Xia. Her guidance throughout my doctoral studies has significantly enhanced my critical thinking and research capabilities.

I am deeply grateful to my tutor, Dr. Damiano Sarocchi, Dr. Alejandro López Valdivieso, Dra. Yanmei Li, and Dr. Edgar D. Páez Pérez. Thank them for providing constructive feedback in semester evaluations, which enables me to continuously revise my research. Dr. Damiano is always gentlemanly and amiable; during my semester report, he patiently listened to my presentation in less fluent English and gave me some advice. Dr. Valdivieso is renowned for his outstanding academic abilities and passion for work, which greatly inspires me. Although he has left us, I will always remember him, the knowledgeable, childlike, and fish loving person. Dra. Li also gave me too much encouragement. She warmly invited me and my classmates to visit Guanajuato, making dumplings and cooking big meals for us, allowing us to fully experience the flavor of Chinese New Year in Mexico. I must thank Dr. Edgar D. Páez Pérez for being

willing to join my committee as I approach graduation, for offering valuable insights on my research, and for being willing to witness one of the most important moments of my life together with us. This means a great deal to me.

Furthermore, I need to thank to everyone at the Instituto de Ingeniería y Ciencia de Materiales at Universidad Autónoma de San Luis Potosí, in especial, Dr. Mildred Quintan Ruiz, Eva, Maricela, and Ubaldo. Eva, Maricela, and Ubaldo always patiently answer all the questions I encounter at school, and I really want to give everyone a big hug.

Lastly, I wish to express my heartfelt gratitude to my friends in San Luis Potosí for their unwavering support in both my academic and personal life.

To all who have contributed to my academic and personal growth, I extend my sincerest thanks.

Abstract

Nutrient-poor soils are typically characterized by low nutrient content and poor water retention. Typical examples include saline-alkali soil, phosphogypsum-covered soil, and desert soil. In this study, we employed corresponding strategies for these three soil types: salt-tolerant polymers, natural biocrusts, and clay-based artificial biocrusts. Our aim was to explore feasible approaches for enhancing water retention and carbon sequestration. Simultaneously, we investigated the interactions between inorganic (e.g., clay, phosphogypsum, salinity, pH) and organic (e.g., polymers, microorganisms, soil organic carbon) constituents. By leveraging these interactions, we seek to trigger a synergy that delivers more effective restoration than any single method.

Chapter II: Improving soil water retention is an effective strategy for mitigating soil salinization. Superabsorbent polymers (SAPs), known for their strong water absorption capacity, are widely used as water-retaining agents in agriculture. However, their limited salt tolerance restricts their application in saline-alkali soils. To address this limitation, this study aimed to develop a salt-tolerant superabsorbent polymer (ST-SAP) suitable for use in high-salinity environments. ST-SAP was synthesized using 2-acrylamide-2-methylpropanesulfonic acid (AMPS), acrylic acid (AA), and acrylamide (AM) and was evaluated through swelling and reswelling experiments. The salt-tolerance mechanism of ST-SAP was spectroscopical analyzed using X-ray photoelectron (XPS) and Fourier transform infrared (FT-IR); the analyses were completed by computed tomography (CT). To assess its effectiveness in highly saline soil, ST-SAP was tested in soil samples collected from Lop Nur, Xinjiang, which contained 18.13 wt% total dissolved salts. The synthesized ST-SAP demonstrated outstanding swelling capacity (69.04 g/g) under high-salinity conditions. Notably, its exceptional stability in saline environments was attributed to the complexation reaction between Ca^{2+} and its three hydrophilic functional groups (R-SO_3H, R-COOH, and R-$CONH_2$). Furthermore, the addition of 2 wt% ST-SAP to saline-alkali soil extended the water retention period to 28 days, confirming its effectiveness in improving soil water retention under high-salinity conditions.

Chapter III:

Chapter IV: Artificial biocrusts serve as essential carbon pools in mitigating desertification. However, most research has primarily focused on microbial communities, overlooking the influence of clay minerals on the biocrust carbon pump. This study constructed clay-based artificial biocrusts to examine the role of clay minerals in soil organic carbon (SOC) accumulation. Montmorillonite (MMT) and *Microcoleus vaginatus* were co-inoculated, and key SOC-related parameters were measured, including microbial biomass carbon, SOC content, and chlorophyll a (Chl-*a*). The results showed that by day 84, SOC levels in the MMT-algae groups ($\geqslant$1.4 g dm^{-2}) were more than 3.45 times higher than in the algae-only group, with 1.4 g dm^{-2} identified as the optimal MMT dosage. Additionally, MMT significantly promoted microbial growth and enhanced SOC stability, with microbial proliferation identified

as the primary mechanism driving SOC accumulation. Moreover, MMT favored the proliferation of photosynthetically active microorganisms. These findings suggest that MMT can act as an accelerator of the microbial carbon pump in artificial biocrust development, offering a viable approach and solid theoretical foundation for the rapid restoration of desertified landscapes.

Chapter V: Biocrusts serve as the primary reservoirs of organic carbon in desert environments, with inorganic clays potentially playing a crucial role in this process. However, the specific mechanisms underlying their influence remain largely unexplored. This study investigated the effects of two typical clay minerals, e.g., kaolin (1:1 type) and montmorillonite (2:1 type), on SOC accumulation in artificial biocrusts. After 84 days of cultivation, both kaolin and MMT significantly enhanced SOC levels, increasing them by 5.03-fold and 4.08-fold, respectively, compared to the Algae group (without added clay). Notably, the two clay types exhibited distinct advantages in SOC accumulation. Due to its larger external specific surface area and higher cation exchange capacity, MMT played a greater role in SOC stabilization. In the MMT group, the mineralization quotient (qM), hot-water extractable organic carbon (HWEOC), and molecular structural stability of SOC were 0.3, 0.34, and 1.31 times those of the Algae group, respectively, indicating improved SOC stability. In contrast, kaolin promoted microbial growth and SOC formation more effectively, likely due to its higher dissolved organic carbon (DOC) content. Microbial biomass carbon (MBC), Chl-*a*, photosynthetic performance index (PI_{ABS}), and Shannon diversity index in the kaolin group were 5.67, 2.44, 11.95, and 1.82 times higher than those in the Algae group, respectively. These findings highlight the synergistic role of clay minerals and cyanobacteria in SOC accumulation within artificial biocrust systems, clarify the distinct contributions of kaolin and MMT, and provide new insights for accelerating the rehabilitation of nutrient-poor desert landscapes.

The above results indicate that ST-SAP significantly enhances the water retention capacity of saline–alkali soil. Natural biocrusts and clay-based artificial biocrusts notably promote carbon sequestration in phosphogypsum stockpiles and desert soils, respectively. This study provides effective strategies and theoretical foundations for improving water retention and carbon sequestration in nutrient-poor soils.

Keywords: Nutrient-poor soils; Salt-alkali soils; Salt-tolerant superabsorbent polymer; Phosphogypsum; Biocrusts; Clays; Soil organic carbon; Desert

Resumen

Los suelos pobres en nutrientes se caracterizan típicamente por su bajo contenido de nutrientes y su escasa capacidad de retención de agua. Ejemplos representativos de estos suelos son el suelo salino-alcalino, el suelo cubierto de fosfoyeso y el suelo desértico. En este estudio, empleamos estrategias específicas para estos tres tipos de suelo: polímeros tolerantes a la sal, costras biológicas naturales y costras biológicas artificiales basadas en arcilla. Nuestro objetivo fue explorar métodos viables para

mejorar la retención de agua y el secuestro de carbono. Al mismo tiempo, investigamos las interacciones entre los componentes inorgánicos (p. ej., arcilla, fosfoyeso, salinidad, pH) y los componentes orgánicos (p. ej., polímeros, microorganismos, carbono orgánico del suelo). Al aprovechar estas interacciones, buscamos generar una sinergia que permita una restauración más efectiva que la alcanzada mediante cualquier método individual.

Capítulo II:Mejorar la retención de agua en el suelo es una estrategia efectiva para mitigar la salinización del suelo. Los polímeros superabsorbentes (SAP), conocidos por su fuerte capacidad de absorción de agua, se utilizan ampliamente como agentes retenedores de agua en la agricultura. Sin embargo, su tolerancia limitada a la sal restringe su aplicación en suelos salino-alcalinos. Para abordar esta limitación, este estudio tuvo como objetivo desarrollar un polímero superabsorbente tolerante a la sal (ST-SAP) adecuado para su uso en ambientes de alta salinidad. El ST-SAP se sintetizó utilizando ácido 2-acrilamido-2-metilpropanosulfónico (AMPS), ácido acrílico (AA) y acrilamida (AM), y se evaluó mediante experimentos de hinchamiento y re-hinchamiento. El mecanismo de tolerancia a la sal del ST-SAP se analizó mediante espectroscopía fotoelectrónica de rayos X (XPS), espectroscopía infrarroja por transformada de Fourier (FT-IR) y tomografía computarizada (TC). Para evaluar su eficacia en suelos altamente salinos, se probó el ST-SAP en muestras de suelo recolectadas en Lop Nur, Xinjiang, China, que contenían un 18.13% en peso de sales totales disueltas. El ST-SAP sintetizado demostró una capacidad de hinchamiento sobresaliente (69.04 g/g) en condiciones de alta salinidad. Cabe destacar que su excepcional estabilidad en ambientes salinos se atribuyó a la reacción de complejación entre el Ca^{2+} y sus tres grupos funcionales hidrófilos (R-SO_3H, R-COOH y R-$CONH_2$). Además, la adición de un 2% en peso de ST-SAP al suelo salino-alcalino extendió el período de retención de agua a 28 días, confirmando su eficacia para mejorar la retención de agua del suelo en condiciones de alta salinidad.

Capítulo III: El acumulamiento de fosfoyeso plantea riesgos ecológicos significativos para el medio ambiente circundante. La rehabilitación ecológica in situ impulsada biológicamente representa un enfoque de restauración ecológico. Las costras biológicas juegan un papel irreemplazable en la recuperación ecológica de ambientes degradados, pero reciben menos atención en el contexto del fosfoyeso. Este estudio empleó investigaciones de campo en acumulados o montones de fosfoyeso de diferentes años de almacenamiento con capas de costras biológicas y capas de fosfoyeso. Se observó que después de 12 años, los montones de fosfoyeso se cubrieron completamente con costras biológicas, lo que indica la colonización y estabilización exitosa de costras biológicas en las superficies de fosfoyeso. Para explorar las interacciones entre el fosfoyeso y las costras biológicas, se recolectaron muestras y se sometieron a análisis fisicoquímicos. Los resultados experimentales demostraron que el tamaño de partícula fino (<100 μm), el abundante fósforo disponible y los iones de calcio intercambiables en el fosfoyeso proporcionan condiciones favorables para la formación y desarrollo de costras biológicas. Por el contrario, las interacciones

fosfoyeso-costra biológica mejoran los procesos microbianos del ciclo de nutrientes, particularmente el ciclo del carbono, lo que finalmente conduce a mejoras significativas en las propiedades fisicoquímicas de la superficie del montones de fosfoyeso. Específicamente, el C orgánico del suelo aumentó en un 175.28%, el pH aumentó de 3.4 a 5.6, y el contenido de fluoruro soluble disminuyó al 14.2% de su nivel original.

Capítulo IV: Las costras biológicas artificiales sirven como *pools* de carbono esenciales para mitigar la desertificación. Sin embargo, la mayoría de las investigaciones se han centrado principalmente en las comunidades microbianas, pasando por alto la influencia de los minerales arcillosos en la bomba de carbono de las costras biológicas. Este estudio construyó costras biológicas artificiales basadas en arcilla para examinar el papel de los minerales arcillosos en la acumulación de carbono orgánico del suelo (SOC). Se coinocularon montmorillonita (MMT) *y Microcoleus vaginatus*, y se midieron parámetros clave relacionados con el SOC, incluyendo el carbono microbiano de la biomasa, el contenido de SOC y la clorofila *a* (Chl-*a*). Los resultados mostraron que para el día 84, los niveles de SOC en los grupos MMT-algas (≥1.4 g dm^{-2}) fueron más de 3.45 veces superiores a los del grupo solo con algas, identificándose 1.4 g dm^{-2} como la dosis óptima de MMT. Adicionalmente, la MMT promovió significativamente el crecimiento microbiano y mejoró la estabilidad del SOC, identificándose la proliferación microbiana como el mecanismo principal que impulsa la acumulación de SOC. Además, la MMT favoreció la proliferación de microorganismos fotosintéticamente activos. Estos hallazgos sugieren que la MMT puede actuar como un acelerador de la bomba de carbono microbiana en el desarrollo de costras biológicas artificiales, ofreciendo un enfoque viable y una base teórica sólida para la restauración rápida de paisajes desertificados.

Capítulo V: Las costras biológicas sirven como los reservorios primarios de carbono orgánico en ambientes desérticos, donde las arcillas inorgánicas podrían desempeñar un papel crucial en este proceso. Sin embargo, los mecanismos específicos que subyacen a su influencia permanecen en gran medida inexplorados. Este estudio investigó los efectos de dos minerales arcillosos típicos: caolín (tipo 1:1) y montmorillonita (tipo 2:1), sobre la acumulación de SOC en costras biológicas artificiales. Después de 84 días de cultivo, tanto el caolín como la MMT mejoraron significativamente los niveles de SOC, aumentándolos en 5.03 y 4.08 veces, respectivamente, en comparación con el grupo algas (sin arcilla añadida). Cabe destacar que los dos tipos de arcilla exhibieron ventajas distintas en la acumulación de SOC. Debido a su mayor área superficial externa y mayor capacidad de intercambio catiónico, la MMT jugó un papel más importante en la estabilización del SOC. En el grupo MMT, el cociente de mineralización (qM), el carbono orgánico extraíble con agua caliente (HWEOC) y la estabilidad estructural molecular del SOC fueron 0.3, 0.34 y 1.31 veces los del grupo algas, respectivamente, lo que indica una estabilidad mejorada del SOC. Por el contrario, el caolín promovió el crecimiento microbiano y la formación de SOC de manera más efectiva, probablemente debido a su mayor contenido de carbono orgánico disuelto (DOC). El carbono microbiano de la biomasa (MBC), la Chl-*a*, el

índice de rendimiento fotosintético (PIABS) y el índice de diversidad de Shannon en el grupo de caolín fueron 5.67, 2.44, 11.95 y 1.82 veces mayores que los del grupo Algas, respectivamente. Estos hallazgos resaltan el papel sinérgico de los minerales arcillosos y las cianobacterias en la acumulación de SOC dentro de los sistemas de costras biológicas artificiales, aclaran las contribuciones distintas del caolín y la MMT, y proporcionan nuevas perspectivas para acelerar la rehabilitación de paisajes desérticos pobres en nutrientes.

Los resultados anteriores indican que el ST-SAP mejora significativamente la capacidad de retención de agua del suelo salino-alcalino. Las costras biológicas naturales y las costras biológicas artificiales basadas en arcilla promueven notablemente el secuestro de carbono en los montones de fosfoyeso y en los suelos desérticos, respectivamente. Este estudio proporciona estrategias efectivas y fundamentos teóricos para mejorar la retención de agua y el secuestro de carbono en suelos pobres en nutrientes.

Palabras clave: Suelos pobres en nutrientes; Suelos salino-alcalinos; Polímero superabsorbente tolerante a la sal; Fosfoyeso; Costras biológicas; Arcillas; Carbono orgánico del suelo; Desierto

摘要

贫瘠土壤通常具有养分含量低和保水能力差的特点，其典型代表包括盐碱土、磷石膏覆盖土壤和沙漠土。本研究针对这三种土壤类型，分别采用了相应的修复策略：有机高分子耐盐聚合物、自然生物结皮和粘土基人工生物结皮。我们的目标是探索增强土壤保水能力和促进碳封存的可行途径。同时，我们研究了无机成分（如粘土、磷石膏、盐度、pH 值）与有机成分（如有机高分子聚合物、微生物、土壤有机碳）之间的相互作用。通过利用这些相互作用，我们旨在触发协同效应，实现比任何单一方法更有效的生态修复。

第二章：提高土壤保水能力是缓解土壤盐渍化的有效策略。高吸水性聚合物因其强大的吸水能力而在农业中作为保水剂被广泛使用，但其有限的耐盐性限制了在盐碱土壤中的应用。为解决这一局限，本研究旨在开发一种适用于高盐度环境的耐盐高吸水性聚合物。该 ST-SAP 采用 2-丙烯酰胺-2-甲基丙磺酸（AMPS）、丙烯酸（AA）和丙烯酰胺（AM）合成，并通过溶胀和再溶胀实验进行评估。利用 X 射线光电子能谱、傅里叶变换红外光谱和计算机断层扫描技术分析了 ST-SAP 的耐盐机制。为评估其在高度盐渍化土壤中的有效性，在取自新疆罗布泊（总溶解盐含量为 18.13 wt%）的土壤样品中进行了测试。合成的 ST-SAP 在高盐度条件下表现出卓越的溶胀能力（69.04 g/g）。值得注意的是，其在盐环境中的优异稳定性归因于 Ca^{2+}与其三个亲水官能团（$R-SO_3H$, R-COOH, $R-CONH_2$）之间的

络合反应。此外，向盐碱土中添加 2 wt%的 ST-SAP 可将保水期延长至 28 天，证实了其在改善高盐条件下土壤保水能力方面的有效性。

第三章： 磷石膏的堆存对周围环境构成显著的生态风险。生物驱动的原位生态修复是一种环境友好的恢复方法。生物结皮在退化环境的生态恢复中发挥着不可替代的作用，但在磷石膏环境中的相关研究较少受到关注。本研究对不同堆存年限且已形成生物结皮层磷石膏堆场进行了实地调查。发现经过 12 年后，磷石膏堆场完全被生物结皮覆盖，表明生物结皮在磷石膏表面成功定殖并稳定存在。为探究磷石膏与生物结皮之间的相互作用，分层采集了相关样品并进行理化分析。实验结果表明，磷石膏的细颗粒尺寸（<100 μm）、丰富的有效磷和交换性钙离子为生物结皮的形成与发展提供了有利条件。反过来，磷石膏与生物结皮之间的相互作用增强了微生物养分循环过程，特别是碳循环，最终显著改善了磷石膏堆场表面的理化性质。具体而言，土壤有机碳增加了 175.28%，pH 值从 3.39 升至 5.61，可溶性氟化物含量降至初始水平的 14.20%。

第四章： 人工生物结皮是缓解荒漠化的重要碳库。然而，大多数研究主要聚焦于微生物群落，忽视了粘土矿物对生物结皮"碳泵"的影响。本研究构建了粘土基人工生物结皮，以考察粘土矿物在土壤有机碳积累中的作用。将蒙脱石与具鞘微鞘藻共同接种，并测量了关键的土壤有机碳相关参数，包括微生物生物量碳、土壤有机碳含量和叶绿素 a。结果显示，到第 84 天时，MMT-藻类组别的土壤有机碳水平（≥1.4 g dm^{-2}）是纯藻类组的 3.45 倍以上，且 1.4 g dm^{-2} 被确定为最佳 MMT 添加量。此外，MMT 显著促进了微生物生长并增强了土壤有机碳稳定性，微生物增殖被确定为驱动土壤有机碳积累的主要机制。而且，MMT 有利于光合活性微生物的生长。这些发现表明，MMT 可以在人工生物结皮发育中充当微生物碳泵的"加速器"，为快速恢复荒漠化土壤提供了可行的方法和坚实的理论基础。

第五章： 生物结皮是沙漠环境中有机碳的主要储存库，无机粘土可能在此过程中扮演关键角色。然而，其影响的具体机制在很大程度上仍未得到探索。本研究调查了两种典型粘土矿物——高岭石（1:1 型）和蒙脱石（2:1 型）——对人工生物结皮中土壤有机碳积累的影响。经过 84 天的培养后，与纯藻类组（未添加粘土）相比，高岭石和 MMT 均显著提高了土壤有机碳水平，分别增加了 5.03 倍和 4.08 倍。值得注意的是，两种粘土类型在土壤有机碳积累方面表现出不同的优势。由于其更大的外比表面积和更高的阳离子交换能力，MMT 在土壤有机碳稳定化方面作用更大。在 MMT 组中，土壤有机碳的矿化商、热水可提取有机碳和分子结构稳定性分别是藻类组的 0.3、0.34 和 1.31 倍，表明土壤有机碳稳定性得到改善。相比之下，高岭石更能有效促进微生物生长和土壤有机碳形成，这可能是由于其较高的溶解性有机碳含量。高岭石组的微生物生物量碳、叶绿素 a、光合性能指数和香农多样性指数分别比藻类组高 5.67、2.44、11.95 和 1.82 倍。这些发现强调了粘土矿物和具鞘微鞘藻在人工生物结皮系统土壤有机碳积累中

的协同作用，阐明了高岭石和 MMT 的不同贡献，并为加速贫营养沙漠景观的修复提供了新的见解。

以上结果表明，ST-SAP 显著增强了盐碱土的保水能力；自然生物结皮和粘土基人工生物结皮则分别显著促进了磷石膏堆场和沙漠土壤的碳封存。本研究为改善贫瘠土壤的保水性和碳封存能力提供了有效的策略和理论基础。

关键词： 贫瘠土壤；盐碱土；耐盐高吸水性聚合物；磷石膏；生物结皮；粘土；土壤有机碳；沙漠

Index

Index of Figures

Index of Tables

Chapter I. Introduction

1.1 Justification

1.1.1 Nutrient-poor soils

Nutrient-poor soils often limit plant growth and ecosystem productivity (Orians and Milewski, 2007). The main characteristics of nutrient-poor soils are nutrient deficiency and poor water-holding capacity (Rominger and Meyer, 2019). This study takes salt-alkali soil, phosphogypsum on phosphogypsum stockpiles, and desert soil as examples (Figure 1.1).

About 1.13 billion hectares of land suffered from saline-alkali stress in the world，in which, 60% of the agricultural areas are affected by salinization in Mexico (Zhang et al., 2022). Saline-alkali stress severely reduces food production and results in $27.3 billion in economic losses per year (Ali et al., 2017). More seriously, saline-alkali land is still expanding around the world. Soil salinity primarily arises from the accumulation of various cations, such as sodium (Na^+), potassium (K^+), calcium (Ca^{2+}), magnesium (Mg^{2+}). Among these, Na compounds are generally recognized as the dominant contributors to salinization in most soils (Jat Baloch et al., 2023). The excessive buildup of Na ions severely interferes with the physiological and metabolic functions of plants (Hu and Schmidhalter, 2023). Salt stress is widely acknowledged as one of the major abiotic stresses that hinder plant growth, development, and productivity. High Na levels can trigger the efflux of intracellular K^+ and Ca^{2+}, thereby disturbing ionic balance and nutrient uptake, leading to oxidative damage, stunted growth, and even programmed cell death (Ahanger and Agarwal, 2017). To alleviate this problem, enhancing soil water retention has been recognized as an effective strategy to mitigate soil salinization (Q. Cui et al., 2021). Thus, improving soil water retention of saline-alkali soil is a worldwide challenge.

Phosphogypsum is the primary industrial byproduct of wet-process phosphoric acid production, with approximately 5 tons of phosphogypsum generated per ton of phosphoric acid (Bounaga et al., 2022). Over recent decades, the rapid growth in global population and living standards has significantly increased the demand for food, thereby accelerating the demand for phosphoric acid. Consequently, phosphogypsum production has risen rapidly, with annual outputs estimated at 200–250 million tons (Akfas et al., 2023; Bounaga et al., 2022). However, phosphogypsum has a complex composition, primarily consisting of Ca sulfate dihydrate, along with substantial amounts of incompletely decomposed phosphate rock, sulfates, fluorides, and metals, which make its recycling and treatment challenging (Kijjanapanich et al., 2014; Xiang et al., 2023). Currently, only about 15% of the annually produced phosphogypsum is recycled, while the remaining 85% is either stockpiled or discharged into the ocean. This not only occupies large areas of land but also poses serious ecological threats to soil, surface water, groundwater, and marine ecosystems (Bilal et al., 2023). In situ

ecological restoration driven by biological processes is considered the most economical and environmentally friendly remediation strategy (Bai et al., 2022; Zheng et al., 2022). However, the high gypsum content, high content of soluble fluorides, and strong acidity of phosphogypsum make it difficult for plants to grow (Akfas et al., 2023; Barrow and Hartemink, 2023; Singh et al., 2023).

At present, desertified soils account for more than 21% of the global land area and for more than 20% of the land area in Mexico (Yang et al., 2023; Schaeffer et al., 2025). Desert regions have highly fragile ecosystems due to land desertification and degradation. They suffer from severe biodiversity loss, low vegetation coverage, and a sharp decline in available water resources, which in turn accelerates the expansion of desertified areas (Liu et al., 2023). Soil organic carbon (SOC) is fundamental to sustaining critical biogeochemical processes, making it indispensable for the rehabilitation of desertified ecosystems (Chen et al., 2023; Satdichanh et al., 2023; Wu et al., 2023). The activities of microorganisms -including their growth, metabolism, and decomposition -are key drivers of SOC formation and stabilization (Liang and Balser, 2011; Miltner et al., 2012; H. W. Wu et al., 2024). In recent years, increasing attention has been directed toward the microbial carbon pump (MCP) concept (Feng and Wang, 2023; Jiao et al., 2024; Zhu et al., 2020). This framework suggests that microbial communities transform easily degradable organic compounds into more persistent carbon forms through processes of extracellular modification and intracellular turnover, thereby promoting long-term SOC sequestration (Liang et al., 2017; Zhang et al., 2025b). Within arid and desertified regions, biological soil crusts (biocrusts) serve as integral components of the MCP (Weber et al., 2022; W. Xu et al., 2024). Comprised of diverse microorganisms, extracellular polymeric substances, and mineral particles, biocrusts act as ecosystem engineers that enhance stability and functionality in fragile dryland environments (Cheng et al., 2021; Lan et al., 2014). Hence, biocrusts may help prevent the worsening of desertification.

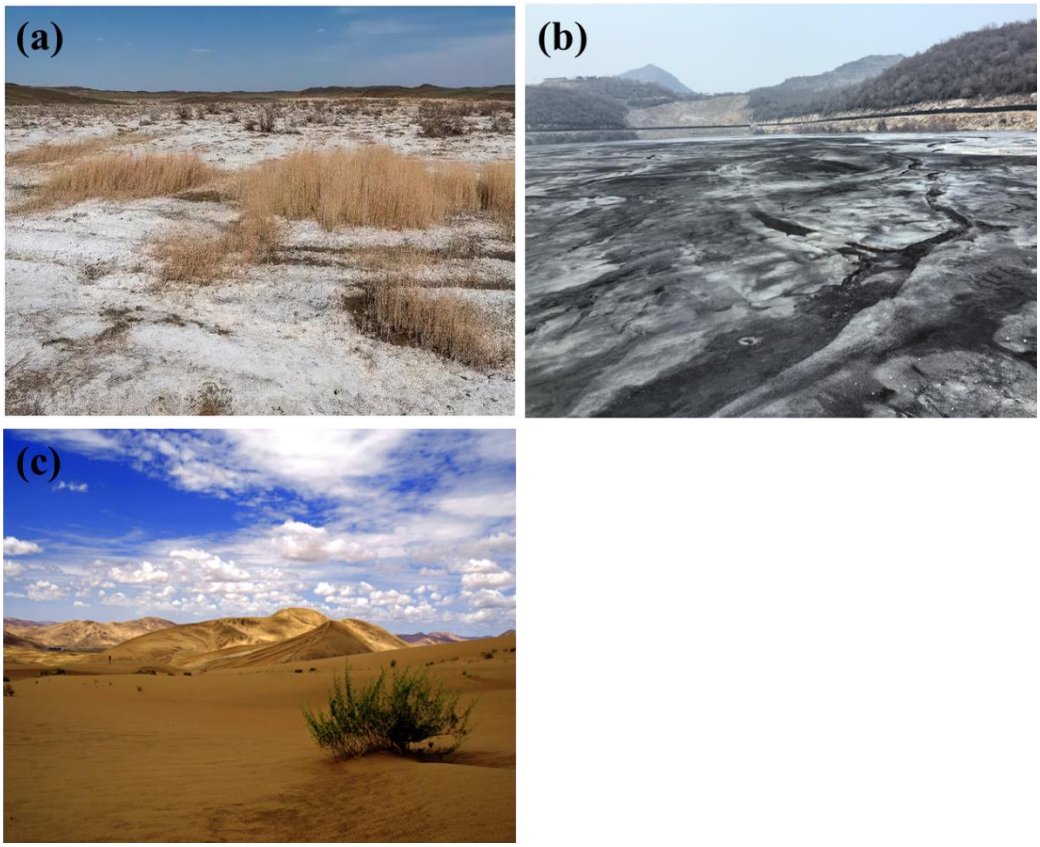

Figure 1.1 (a) Saline-alkali soils. (b) Phosphogypsum stockpiles. (c) Desert

1.1.2 Limitations of existing superabsorbent polymers

Superabsorbent polymers (SAPs) are a kind of polymeric materials distinguished by the presence of strongly hydrophilic functional groups and a cross-linked three-dimensional network (Panic et al., 2010; Zhang and Zhang, 2018). This network architecture endows SAPs with the ability to uptake and retain substantial quantities of aqueous solutions (Figure 1.2). From a structural perspective, hydrogels are hydrophilic polymer networks with a high degree of crosslinking and a water absorption capacity reaching approximately 10 g/g, whereas SAPs can be regarded as lightly cross-linked hydrogels with significantly enhanced water-absorbing performance (Zhang et al., 2021). The water retention behavior of SAPs primarily relies on the hydration of polar functional groups and the osmotic pressure gradient, which together facilitate the diffusion and retention of water molecules within the polymer network (Berradi et al., 2023; C. Zhang et al., 2023).

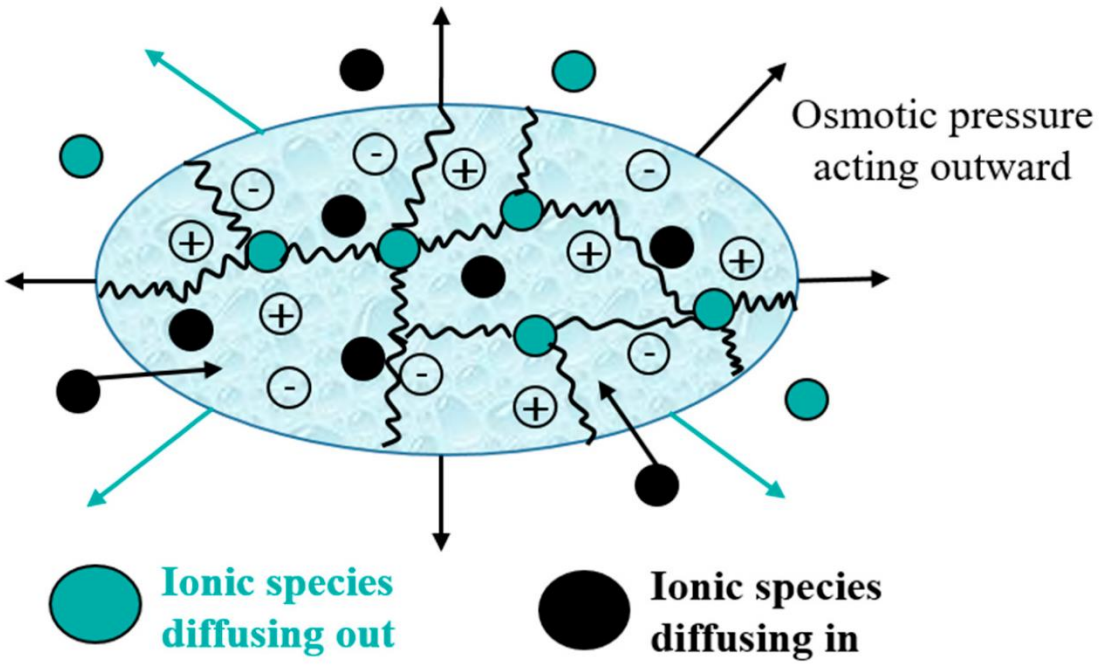

Figure 1.2 The swelling mechanism of the superabsorbent polymers (SAP) (Berradi et al., 2023)

Owing to their exceptional capacity for water uptake, superabsorbent polymers (SAPs) began to replace conventional absorbent materials in disposable hygiene products such as diapers and sanitary pads in the late 1970s. In contrast to traditional absorbents, SAPs possess markedly enhanced abilities for both water absorption and retention, rendering them highly versatile functional materials (Santos et al., 2019). Over the past decades, these polymers have found extensive applications across diverse sectors, including personal hygiene products, agricultural practices, medical and healthcare materials, construction and concrete engineering, as well as industrial wastewater treatment (Li et al., 2016; J. Liu et al., 2020; Rizwan et al., 2022).

However, SAPs have limited effectiveness in saline-alkali soils due to their poor salt tolerance (Ahmed, 2015). To enhance the swelling performance of SAPs in saline conditions, researchers have explored various modifications, including zwitterionic polymers (Zhang et al., 2021), e.g., zwitterionic polymers (Z. M. Wang et al., 2021), inorganic materials (Kabiri and Zohuriaan-Mehr, 2003), and interpenetrating polymer networks (IPNs) (Tally and Atassi, 2015). Despite these efforts, their success remains constrained, primarily because the additives contribute insufficient hydrophilicity rather than increasing the material's crosslinking density (Kabiri et al., 2011, 2010).the swelling capacity of SAP is significantly constrained by the ionic strength of the surrounding solution, particularly in the presence of multivalent cations (Olad et al., 2018; Zhang and Qiao, 2021). However, enhancing the affinity of SAP has been shown to greatly improve its performance, with the diversity of hydrophilic groups also playing a crucial role (Ahmed, 2015; Zhang et al., 2021). Studies have established the hydrophilicity ranking of functional groups as follows: R-SO_3H > R-COOH > R-$CONH_2$ > R-OH (Berthold et al., 1996; Zhang and Qiao, 2021). 2-acrylamide-2-

methylpropanesulfonic acid (AMPS), which contains the highly hydrophilic R-SO_3H group, is widely used as a salt-resistant oil displacement agent in the petroleum industry due to its low cation-binding tendency (Mohamadian et al., 2019; Cai, 2004; Shubnell et al., 1994). Meanwhile, acrylic acid (AA) and acrylamide (AM), which feature R-COOH and R-$CONH_2$ groups, respectively, are commonly utilized in gel-based applications due to their strong hydrophilicity and cost-effectiveness (Ahmed, 2015; Liu et al., 2018). Therefore, a superabsorbent polymer synthesized using AA, AM, and AMPS as monomers may enhance the water absorption performance of the material under high-salinity conditions.

1.1.3 Significance of soil organic carbon in nutrient-poor soils

Soil Organic Carbon (SOC), as a core component of the terrestrial ecosystem carbon cycle, functions in nutrient-poor soils in a role that extends far beyond that of a mere carbon source, serving as a key driver in sustaining ecosystem productivity and nutrient cycling. (Zhang et al., 2025a, 2025b).

Firstly, SOC constitutes a vast, slow-release reservoir of soil nutrients. Essential elements such as N, P and S, which exist within SOC in various organic forms (e.g., humus, microbial biomass carbon, and dissolved organic carbon), can be continuously and steadily supplied to plants as available nutrients through the process of microbially-mediated mineralization (Chalchissa and Kuris, 2024; Chen et al., 2023; Li et al., 2023; Wu et al., 2023). This slow-release pattern not only aligns with the long-term nutritional requirements of plants but also significantly reduces nutrient losses caused by leaching or fixation, thereby establishing a more resilient internal nutrient supply system within impoverished environments.(Witzgall et al., 2021).

Then, SOC profoundly influences nutrient availability and turnover efficiency through the synergy of its physical, chemical, and biological effects (Zhang et al., 2025b). At the physical level, SOC acts as a primary soil cementing agent, promoting the formation of water-stable aggregates (Zhang et al., 2025a). For example, humic substances in organic carbon can bind with soil particles to form stable aggregates, increasing soil resistance to erosion (Gerke, 2018). This directly enhances soil pore structure and water-holding capacity, creating a favorable physical habitat for root extension and microbial activity (Jinger et al., 2025). At the biochemical level, the active SOC pool (such as microbial biomass carbon) serves as the "engine" for soil nutrient transformation (Y. Li et al., 2022). During the decomposition of organic matter, microorganisms secrete organic acids, chelating agents, and specific enzymes (e.g., phosphatases), which effectively activate inherently present, insoluble nutrients like P and K that are fixed by iron-aluminum oxides or embedded within mineral lattices (Jinger et al., 2025). This "*biological activation*" effect is crucial for unlocking the potential fertility in highly weathered nutrient-poor soils (Oechaiyaphum et al., 2020).

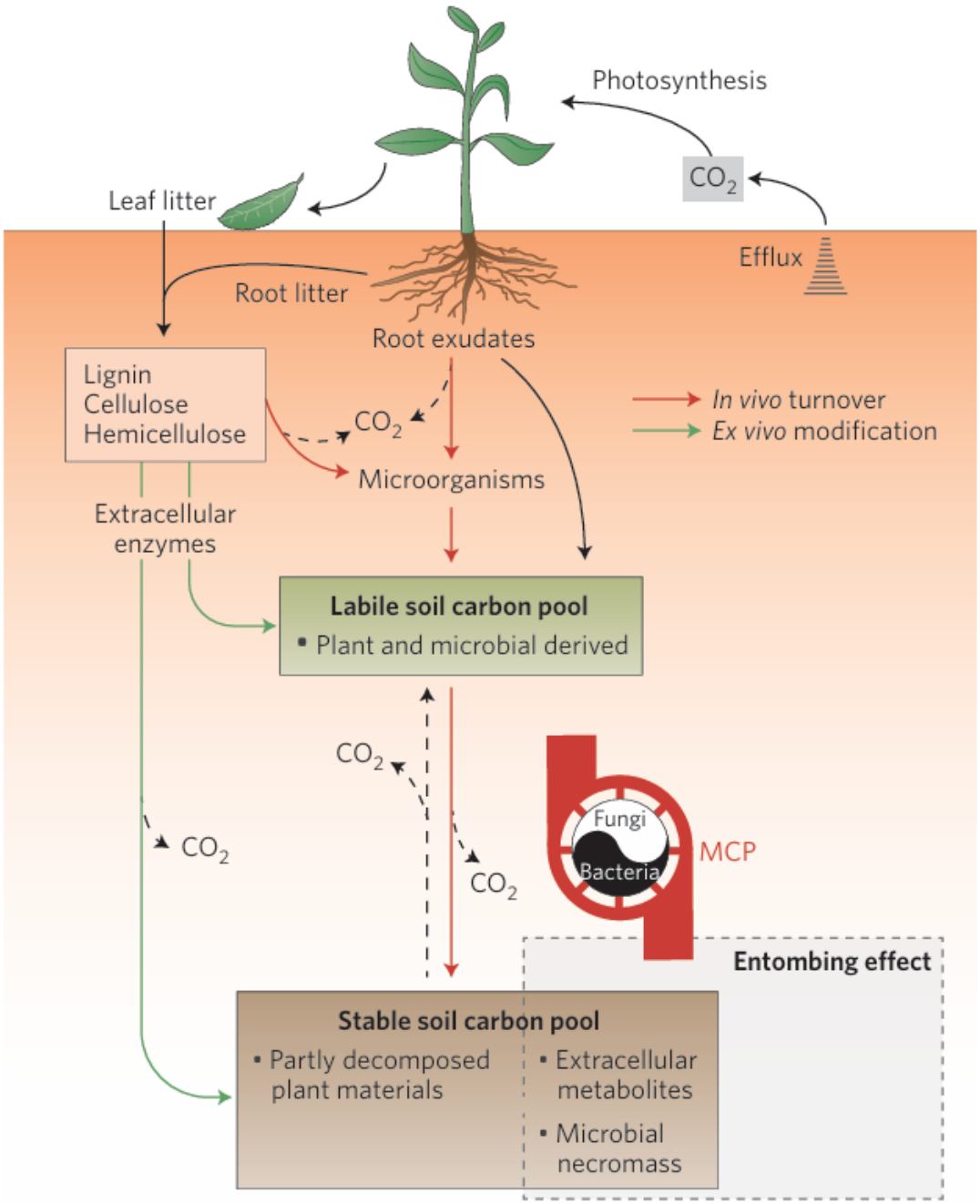

Figure 1.3 Schematic diagram of microbial metabolic processes involved in C cycling in terrestrial ecosystems. MCP: microbial carbon pump (Liang et al., 2017)

In nutrient-poor soils, SOC acts as the central nexus coordinating the synergistic relationship between microbial communities and plant root systems (Fig .1.3) (Huang et al., 2025; Liang et al., 2017). For microorganisms, SOC serves not only as an essential carbon source and energy supply for metabolism and proliferation, but also creates favorable micro-environments by improving soil physical structure, thereby fostering a diverse and metabolically active microbial community (Huang et al., 2025; T. Xue et al., 2024). For plants, the SOC-enhanced soil structure and water retention capacity facilitate extensive root system development, enabling plants under nutrient stress to explore a greater soil volume for nutrient acquisition (Jinger et al., 2025).

In summary, SOC plays a pivotal role in rehabilitating nutrient-poor soils through multiple mechanisms: fertility enhancement, water conservation, soil structure improvement, and the promotion of microbial and plant activities.

1.1.4 Significance of biocrusts in nutrient-poor soils

Biological soil crusts (hereafter referred to as biocrusts) are present in ecosystems worldwide, particularly in environments where limited vascular plant cover allows sunlight to reach the soil surface. They are especially common in water-limited ecosystems (Weber et al., 2022). Biocrusts are complex associations of organic microorganisms and inorganic soil mineral particles (Zhang et al., 2025b).

Biocrusts are composed of a diverse array of photoautotrophic and heterotrophic organisms spanning multiple domains, kingdoms, and phyla. The photoautotrophic components include various lineages such as cyanobacteria, algae, lichens, and bryophytes, but exclude ferns, fern allies, and vascular seed plants. In addition to these cryptogamic photoautotrophs, biocrusts harbor a rich diversity of heterotrophic microorganisms, including fungi, bacteria, and archaea (Büdel et al., 2008). These heterotrophic organisms consume carbon compounds released by photoautotrophs during rainfall events. Biocrusts create a unique habitat that supports a variety of microscopic animals, including protozoa, nematodes, tardigrades, rotifers, and microarthropods. As a result, biocrusts form an entire food web/ecosystem composed of photoautotrophic producers and heterotrophic consumers (Liu et al., 2011; Weber et al., 2022).

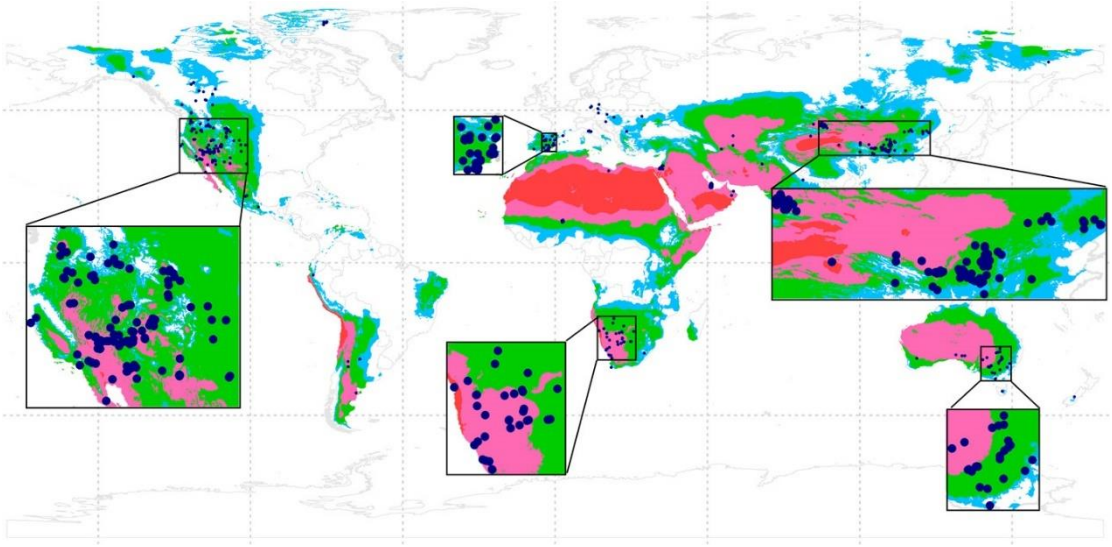

Figure 1.4 The distribution of biocrusts sites in global drylands. Different colors outline four subtypes of drylands (red: hyperarid land; pink: arid land; green: semiarid land; light blue: dry subhumid land). Deep blue points show distributions of biocrust data compiled in the study (Chen et al., 2020)

In nutrient poor arid and semi-arid ecosystems, biocrusts serve as an indispensable layer performing irreplaceable ecological functions (Figure 1.4) (Chen et al., 2020; Román et al., 2020; Rossi et al., 2022). Primarily, cyanobacteria with N_2-fixing

capabilities and other microorganisms within the biocrusts can directly capture atmospheric N_2 and convert it into bioavailable forms (García-Carmona et al., 2020; Román et al., 2020). This process supplies critical external N inputs to the system, effectively alleviating N limitations in the soil. Furthermore, through fungal hyphae and extracellular polymeric substances, the biocrusts bind loose soil particles together, significantly enhancing topsoil stability (Ling et al., 2017). This consolidation provides robust resistance against wind and water erosion while establishing a physical foundation for organic matter accumulation and colonization by organisms from higher trophic levels (Peng et al., 2022; Rossi et al., 2022). Additionally, biocrusts influence surface hydrological processes by modifying water infiltration and evaporation patterns, thereby regulating soil moisture distribution (Guan et al., 2020; S. Li et al., 2021). Simultaneously, these biocrusts function as localized "nutrient islands," concentrating elements such as carbon and N while activating and cycling nutrients through their metabolic activities (Warren, 2014; Zhang et al., 2025b). A study showed that cryptogamic covers, including biocrusts, take up 590 Tg/a of carbon in grasslands and deserts (Maier et al., 2018). In essence, via synergistic mechanisms including N_2 fixation, soil stabilization, hydrological regulation, and nutrient enhancement, biocrusts act as both pioneering colonists and ecosystem stabilizers in oligotrophic environments, representing crucial biological agents for initiating and sustaining the recovery of fragile ecosystems.

1.1.5 Protective effects of clay on SOC and its facilitative role in biocrusts development

Clay minerals, primarily formed through the weathering of aluminosilicates on the surface of the Earth, belong to a class of layered silicates (Zhang et al., 2022). Their layered structures consist of silica tetrahedral sheets and alumina octahedral sheets. These minerals can be classified based on the stacking ratio of these sheets, primarily falling into 1:1-type and 2:1-type clays (Boumaiza et al., 2020).

Kaolin represents a typical 1:1-type clay, characterized by a structural unit layer composed of one silica tetrahedral sheet and one alumina octahedral sheet (Cheng et al., 2024). The layers are tightly bound via hydrogen bonding, resulting in non-expandable interlayer spaces and fixed interlayer domains (Zhang et al., 2022). In contrast, montmorillonite (MMT) is a classic 2:1-type clay. Its structural unit layer consists of an alumina octahedral sheet sandwiched between two silica tetrahedral sheets. A defining feature of MMT is the presence of an expandable interlayer domain between unit layers, accompanied by significant permanent negative charge. This charge originates from isomorphous substitution within the crystal structure (e.g., Al^{3+} replacing Si^{4+}), enabling strong adsorption and retention of cations (e.g., Ca^{2+}, K^{+}, NH_4^{+}) (Tombácz and Szekeres, 2006). These properties endow MMT with a substantial specific surface area and high cation exchange capacity (CEC), making it one of the most physiochemically reactive components in soils (Six et al., 2002). Compared to

MMT, kaolin exhibits lower specific surface area, reduced CEC, and greater chemical stability (Tombácz and Szekeres, 2006).

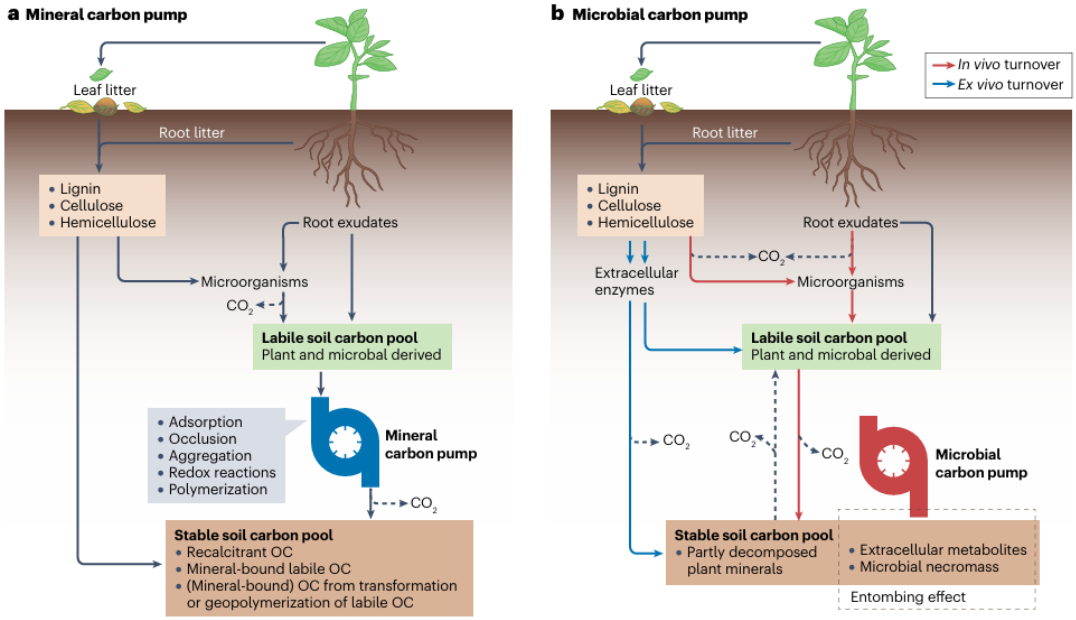

Figure 1.5 The soil mineral (a) and microbial (b) carbon pumps (Xiao et al., 2023)

Clay minerals, particularly 2:1-type MMT, serve as crucial "guardians" for the long-term stabilization of SOC (Figure 1.5) (Montes‐Pulido et al., 2025; Xiao et al., 2023; Xie et al., 2025). (1) Chemical adsorption and complexation: The extensive specific surface area and permanent negative charge of MMT enable it to form stable surface complexes with organic molecules (e.g., via carboxyl or amino functional groups), either directly or through cation bridges (e.g., Ca^{2+}) (Han et al., 2016). This firmly adsorbs organic matter onto its surface, effectively slowing microbial decomposition (Jing et al., 2022; Liu et al., 2023). (2) Intercalation and encapsulation: The expandable interlayer spaces of MMT allow small organic molecules (e.g., amino acids, peptides) to enter, forming organo-mineral complexes. This physical isolation separates organic matter from microorganisms and their secreted enzymes, providing robust physical protection (Wu et al., 2023). Additionally, microaggregates formed by clay minerals in conjunction with iron/aluminum oxides can encapsulate organic matter, creating spatial barriers (Uroz et al., 2015). (3) Formation of physical barriers: After combining with organic matter, clay minerals can coat the surface of organic particles or clog soil pores, thereby impeding the access of microorganisms and enzymes and reducing the rate of SOC mineralization (Liang et al., 2017; Wu et al., 2023). In contrast, kaolin, due to its smaller specific surface area and non-expandable interlayers, is considered to have a weaker capacity for protecting organic carbon compared to MMT (Wattel‐Koekkoek et al., 2003).

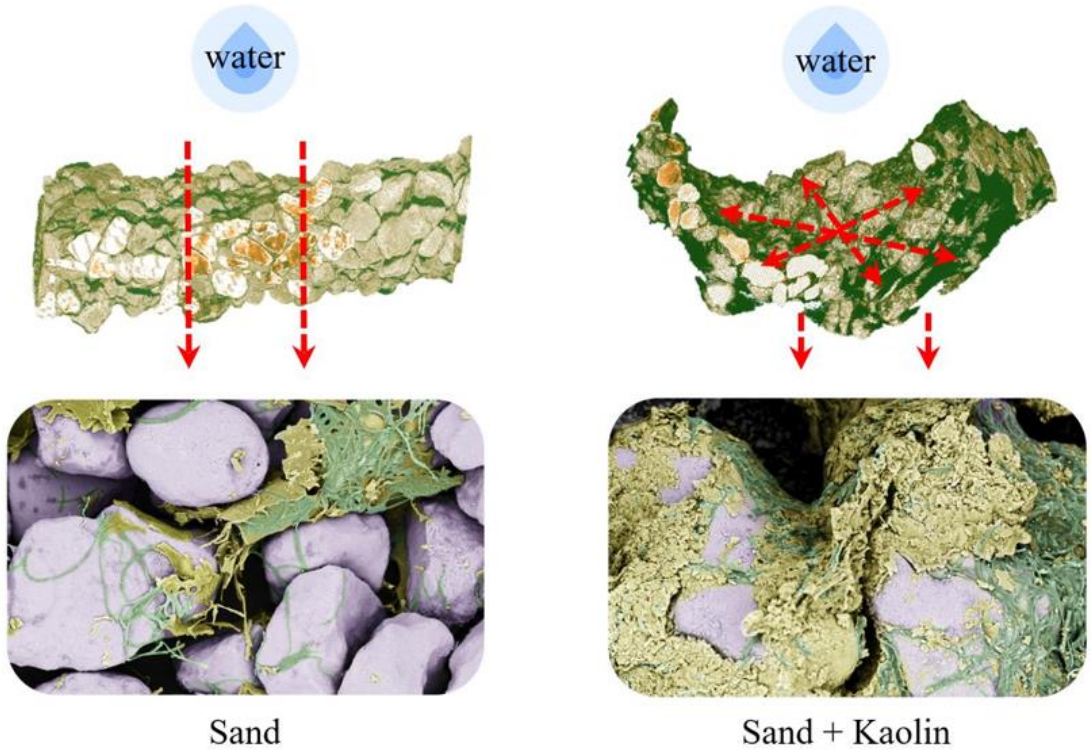

Figure 1.6 Promotion of biocrusts growth by kaolin through enhanced surface soil water retention (Keqiang et al., 2023)

Current research indicates that clay minerals significantly promote the colonization and development of biocrusts (Keqiang et al., 2023; Qian et al., 2024). (1) Fine particle size advantage: Fine-grained particles facilitate microbial colonization and growth, particularly for cyanobacteria (Zhao et al. 2021; Faist et al. 2020). The fine-grained nature of clay undoubtedly accelerates the colonization and growth of biocrusts. (2) Improved surface microhabitat: Clay minerals markedly enhance the water retention capacity of the soil surface. Through capillary action and hygroscopicity, they absorb and retain atmospheric precipitation and condensed water, creating essential moisture conditions for biocrust vitality (Figure 1.6) (Keqiang et al., 2023). Concurrently, their high nutrient adsorption capacity (especially MMT) aids in enriching nutrient elements beneath the crust layer, forming a micro-scale "nutrient reservoir" (Hartmann and Six, 2023; Wu et al., 2023). (3) Promotion of microbial community establishment: The organic matter and nutrients adsorbed on clay particle surfaces provide initial energy and material sources for pioneer N_2-fixing cyanobacteria and other microorganisms. Clay minerals such as MMT can even directly interact with microbial cells, influencing their community structure and metabolic activity, thereby accelerating the formation and succession of biocrusts (Uroz et al., 2015; Wu et al., 2023).

Therefore, clay minerals not only contribute to the protection of SOC but also facilitate the development of biocrusts.

1.2 Rationale and research hypotheses

Nutrient-poor soils—such as saline-alkali soils, phosphogypsum-covered soils, and desert soils—are often regarded as "ecological deserts" or "life-forbidden zones" (Mohanta et al., 2023). Yet, these nutrient-poor soils account for a considerable portion of the global land area and continue to expand (P. Zhang et al., 2022). Low fertility and poor water retention are defining characteristics of such soils (Orians and Milewski, 2007). Therefore, in the ecological restoration of these regions, enhancing water retention and carbon sequestration is key to "breaking the deadlock".

Moreover, against the backdrop of escalating climate change and water resource crises, the potential of vast oligotrophic soils should not be overlooked (F. Yang et al., 2023). From a climate change perspective, the global soil carbon pool is three to four times larger than the atmospheric carbon pool, with desert regions contributing significantly to carbon storage (Lal, 2004; F. Yang et al., 2023). For instance, the carbon sink of the Gurbantunggut Desert of China was 41.69 g C m^{-2} during the period from April to September 2021 (Amar et al., 2023). However, this carbon sink is primarily abiotically driven (F. Yang et al., 2023). When environmental factors shift -such as due to heavy rainfall or warming -large amounts of CO_2 can be released (Ahlström et al., 2015). In contrast, biological carbon sequestration via photosynthesis by biocrusts and vascular plants can lead to more stable carbon fixation (Zhang et al., 2025a). From a water security perspective, improving the water retention capacity of oligotrophic soils is equivalent to creating countless "invisible reservoirs" across vast lands. This effectively reduces surface runoff, replenishes groundwater, alleviates regional drought stress, and provides more reliable water sources for agricultural production and human livelihoods in marginal areas -directly impacting food security and regional stability (Böhm et al., 2021; Patel et al., 2024).

Accordingly, this study addresses the following issues: (I) To tackle the poor water retention of saline-alkali soils, we developed salt-tolerant superabsorbent polymers, offering a potential approach for restoring soils with weak water retention capacities. (II) To address the nutrient poverty and the difficulty of vascular plant survival of phosphogypsum stockpiles, we investigated the interactions between biocrusts and phosphogypsum, aiming to provide an effective method for the eco-friendly treatment of phosphogypsum. (III) To deal with the nutrient deficiency in desert soils, we introduced clay-based artificial biocrusts to promote biological sequestration of soil organic carbon (SOC) in desert environments.

The main innovation of this study lies in integrating the "inorganic-organic" dual perspective to develop a synergistic restoration strategy. By clearing the interactions between inorganic components (e.g., clay, phosphogypsum, salinity, cation exchange capacity, pH) and organic components (e.g., polymeric materials, microorganisms, SOC), we aim to drive a synergistic enhancement effect, achieving superior restoration outcomes compared to single-material or single-method approaches. Furthermore, this study employed high-throughput sequencing (HTS) to characterize the microbial community composition and their environmental functions (C, N, P, and S cycling).

Statistical methods were used to establish correlations between microorganisms and inorganic environmental factors. These systematic investigations into inorganic–organic coordination will provide broader insights for ecological rehabilitation. Based on this, the targeted research hypotheses are as follows:

(1) Since enhancing soil water retention has been widely recognized as an effective strategy to mitigate soil salinization, and that superabsorbent polymers (SAPs) possess strong water absorption and retention capacities, we raised the following scientific question: How can we synthesize a salt-tolerant superabsorbent polymer suitable for saline-alkali soils? Given that sulfonic, carboxyl, amino, and hydroxyl groups exhibit strong hydrophilicity -and that sulfonic groups provide good salt tolerance -we proposed the research hypothesis that: a salt-tolerant superabsorbent polymer applicable to saline–alkali soils could be synthesized using monomers containing sulfonic, carboxyl, amino, and hydroxyl groups.

(2) The large-scale production and difficult disposal of phosphogypsum have already caused serious ecological problems. *In situ* green remediation is undoubtedly the most cost-effective and environmentally friendly disposal approach. Biocrusts possess excellent ecological restoration capabilities. During our field investigation, we observed that a phosphogypsum stockpile had been completely covered by biocrusts. Therefore, we raised the following scientific question: Is there an interaction between phosphogypsum and the biocrusts covering its surface? Accordingly, we proposed the research hypothesis that: the development of biocrusts on the surface of phosphogypsum may serve as an effective approach for its *in situ* remediation.

(3) Soil organic carbon (SOC) is a key factor in the restoration of desert soils, and biocrusts are the primary surface cover in such environments. Clay minerals have been proven to play a significant role not only in protecting SOC but also in promoting the growth of biocrusts. However, the effect of clay on SOC during the construction of artificial biocrusts remains unclear, and few studies have examined how different types of clay influence SOC formation and stabilization. Therefore, we propose the research hypothesis that clay may also promote SOC accumulation during artificial biocrust construction, and that different types of clay have distinct effects on SOC formation and stabilization.

1.3 Objectives

This thesis aims to provide feasible methods and a relevant theoretical basis for the restoration of arid and semi-arid regions, taking saline-alkali land, phosphogypsum stockpiles, and desert areas as examples.

(1) To develop a salt-tolerant superabsorbent polymer (ST-SAP) for improving the water retention capacity of saline alkali land.

(2) To explore the interactions between phosphogypsum and its surface biocrust, to provide a valuable perspective for the disposal of phosphogypsum.

(3) To explore the effects and mechanisms of two types of clays on the formation, stability, and accumulation of SOC, to provide potentially effective strategies for carbon sequestration in nutrient-poor ecosystems such as desert areas.

1.4 References

Ahanger, M.A., Agarwal, R.M., 2017. Salinity stress induced alterations in antioxidant metabolism and nitrogen assimilation in wheat (Triticum aestivum L) as influenced by potassium supplementation. Plant Physiol. Biochem. 115, 449–460. https://doi.org/https://doi.org/10.1016/j.plaphy.2017.04.017

Ahlström, A., Raupach, M.R., Schurgers, G., Smith, B., Arneth, A., Jung, M., Reichstein, M., Canadell, J.G., Friedlingstein, P., Jain, A.K., Kato, E., Poulter, B., Sitch, S., Stocker, B.D., Viovy, N., Wang, Y.P., Wiltshire, A., Zaehle, S., Zeng, N., 2015. The dominant role of semi-arid ecosystems in the trend and variability of the land CO_2 sink. Science. 348, 895-899. https://doi.org/10.1126/science.aaa1668

Ahmed, E.M., 2015. Hydrogel: Preparation, characterization, and applications: A review. J. Adv. Res. 6, 105–121. https://doi.org/https://doi.org/10.1016/j.jare.2013.07.006

Akfas, F., Elghali, A., Aboulaich, A., Munoz, M., Benzaazoua, M., Bodinier, J.-L., 2023. Exploring the potential reuse of phosphogypsum: A waste or a resource? Sci. Total Environ. 908, 168196. https://doi.org/10.1016/j.scitotenv.2023.168196

Ali, S., Rizwan, M., Qayyum, M.F., Ok, Y.S., Ibrahim, M., Riaz, M., Arif, M.S., Hafeez, F., Al-Wabel, M.I., Shahzad, A.N., 2017. Biochar soil amendment on alleviation of drought and salt stress in plants: a critical review. Environ. Sci. Pollut. Res. 24, 12700–12712. https://doi.org/10.1007/s11356-017-8904-x

Amar, G., Mamtimin, A., Wang, YongHui, Wang, Yu, Gao, J., Yang, F., Song, M., Aihaiti, A., Wen, C., Liu, J., 2023. Factors controlling and variations of CO_2 fluxes during the growing season in Gurbantunggut Desert. Ecol. Indic. 154, 110708. https://doi.org/https://doi.org/10.1016/j.ecolind.2023.110708

Bai, D., Yang, X., Lai, J., Wang, Y., Zhang, Y., Luo, X., 2022. In situ restoration of soil ecological function in a coal gangue reclamation area after 10 years of elm/poplar phytoremediation. J. Environ. Manage. 305, 114400. https://doi.org/https://doi.org/10.1016/j.jenvman.2021.114400

Barrow, N.J., Hartemink, A.E., 2023. The effects of pH on nutrient availability depend on both soils and plants. Plant Soil. 487, 21-37. https://doi.org/10.1007/s11104-023-05960-5

Berradi, A., Aziz, F., Achaby, M. El, Ouazzani, N., Mandi, L., 2023. A Comprehensive Review of Polysaccharide-Based Hydrogels as Promising Biomaterials. Polymers (Basel). 15, 2908. https://doi.org/10.3390/polym15132908

Berthold, J., Rinaudo, M., Salmeń, L., 1996. Association of water to polar groups; estimations by an adsorption model for ligno-cellulosic materials. Colloids Surfaces A Physicochem. Eng. Asp. 112, 117–129. https://doi.org/https://doi.org/10.1016/0927-7757(95)03419-6

Bilal, E., Bellefqih, H., Bourgier, V., Mazouz, H., Dumitraş, D.-G., Bard, F., Laborde, M., Caspar, J.P., Guilhot, B., Iatan, L., Bounakhla, M., Iancu, M.A., Marincea, Ş., Essakhraoui, M., Li, B., Diwa, R.R., Ramirez, J.D., Chernysh, Y., Chubur, V.,

Roubík, H., Schmidt, H., Beniazza, R., Cánovas, C.R., Nieto, J.M., Haneklaus, N., 2023. Phosphogypsum circular economy considerations: A critical review from more than 65 storage sites worldwide. J. Clean. Prod. 414, 137561. https://doi.org/10.1016/j.jclepro.2023.137561

Böhm, C., Reyers, M., Knarr, L., Crewell, S., 2021. The Role of Moisture Conveyor Belts for Precipitation in the Atacama Desert. Geophys. Res. Lett. 48, e2021GL094372. https://doi.org/10.1029/2021gl094372

Boumaiza, H., Dutournie, P., Le Meins, J.-M., Limousy, L., Brendle, J., Martin, C., Michau, N., Dzene, L., 2020. Iron-rich clay mineral synthesis using design of experiments approach. Appl. Clay Sci. 199, 105876. https://doi.org/10.1016/j.clay.2020.105876

Bounaga, A., Alsanea, A., Lyamlouli, K., Zhou, C., Zeroual, Y., Boulif, R., Rittmann, B.E., 2022. Microbial transformations by sulfur bacteria can recover value from phosphogypsum: A global problem and a possible solution. Biotechnol. Adv. 57, 107949. https://doi.org/https://doi.org/10.1016/j.biotechadv.2022.107949

Büdel, B., Darienko, T., Deutschewitz, K., Dojani, S., Friedl, T., Mohr, K.I., Salisch, M., Reisser, W., Weber, B., 2008. Southern African biological soil crusts are ubiquitous and highly diverse in drylands, being restricted by rainfall frequency. Microb. Ecol. 57, 229-247. https://doi.org/10.1007/s00248-008-9449-9

Cai, J., 2004. Structural chemistry and properties of metal arenesulfonates. Coord. Chem. Rev. 248, 1061–1083. https://doi.org/10.1016/j.ccr.2004.06.014

Chalchissa, F.B., Kuris, B.K., 2024. Modelling soil organic carbon dynamics under extreme climate and land use and land cover changes in Western Oromia Regional state, Ethiopia. J. Environ. Manage. 350, 119598. https://doi.org/10.1016/j.jenvman.2023.119598

Chen, X.L., Taylor, A.R., Reich, P.B., Hisano, M., Chen, H.Y.H., Chang, S.X., 2023. Tree diversity increases decadal forest soil carbon and nitrogen accrual. Nature 618, 94–101. https://doi.org/10.1038/s41586-023-05941-9

Cheng, C., Gao, M., Zhang, Y.D., Long, M.Z., Wu, Y.J., Li, X.N., 2021. Effects of disturbance to moss biocrusts on soil nutrients, enzyme activities, and microbial communities in degraded karst landscapes in southwest China. Soil Biol. Biochem. 152, 108065. https://doi.org/10.1016/j.soilbio.2020.108065

Cheng, H., Zhou, Y., Xu, P., Zhang, M., Sun, L., 2024. Kaolinite-based form-stable phase change materials for thermal energy storage. J. Energy Storage. 87, 111349. https://doi.org/10.1016/j.est.2024.111349

Cheng, W., Wu, X., Zhang, Y., Wu, D., Meng, L., Chen, Y., Tang, X., 2022. Recent applications of hydrogels in food safety sensing: Role of hydrogels. Trends Food Sci. Technol. https://doi.org/10.1016/j.tifs.2022.10.004

Cui, Q., Xia, J., Yang, H., Liu, J., Shao, P., 2021. Biochar and effective microorganisms promote Sesbania cannabina growth and soil quality in the coastal saline-alkali soil of the Yellow River Delta, China. Sci. Total Environ. 756, 143801. https://doi.org/10.1016/j.scitotenv.2020.143801

Faist, A.M., Antoninka, A.J., Belnap, J., Bowker, M.A., Duniway, M.C., Garcia-Pichel, F., Nelson, C., Reed, S.C., Giraldo-Silva, A., Velasco-Ayuso, S., Barger, N.N., 2020. Inoculation and habitat amelioration efforts in biological soil crust recovery vary by desert and soil texture. Restore. Ecol. 28, S96–S105. https://doi.org/10.1111/rec.13087

Feng, X., Wang, S., 2023. Plant influences on soil microbial carbon pump efficiency. Glob. Chang. Biol. 29, 3854-3856. https://doi.org/10.1111/gcb.16728

García-Carmona, M., Arcenegui, V., García-Orenes, F., Mataix-Solera, J., 2020. The role of mosses in soil stability, fertility and microbiology six years after a post-fire salvage logging management. J. Environ. Manage. 262, 110287. https://doi.org/10.1016/j.jenvman.2020.110287

Gerke, J., 2018. Concepts and Misconceptions of Humic Substances as the Stable Part of Soil Organic Matter: A Review. Agronomy. 8, 76. https://doi.org/10.3390/agronomy8050076

Guan, P., Zhang, X., Cheng, Y., Zheng, H., Liang, W., 2020. Biocrust regulates the effects of water and temperature on soil microbial and nematode communities in a semiarid ecosystem. L. Degrad. Dev. 31, 1335–1343

Han, L., Sun, K., Jin, J., Xing, B., 2016. Some concepts of soil organic carbon characteristics and mineral interaction from a review of literature. Soil Biol. Biochem. 94, 107–121. https://doi.org/10.1016/j.soilbio.2015.11.023

Hartmann, M., Six, J., 2023. Soil structure and microbiome functions in agroecosystems. Nat. Rev. EARTH Environ. 4, 4–18. https://doi.org/10.1038/s43017-022-00366-w

Hu, Y., Schmidhalter, U., 2023. Opportunity and challenges of phenotyping plant salt tolerance. Trends Plant Sci. 28, 552–566.

Huang, Y., Tang, S., Liu, R., Yu, P., Liu, J., Xiao, T., Zhang, Y., Fan, M., Zhang, F., Ni, B., 2025. Soil organic carbon mediates plant immunity-rhizosphere microbiome interactions and controls colonization resistance to microbial inoculants. Cell Host Microbe. https://doi.org/10.1016/j.chom.2025.10.002

Jat Baloch, M.Y., Zhang, W., Sultana, T., Akram, M., Shoumik, B.A. Al, Khan, M.Z., Farooq, M.A., 2023. Utilization of sewage sludge to manage saline–alkali soil and increase crop production: Is it safe or not? Environ. Technol. Innov. 32, 103266. https://doi.org/https://doi.org/10.1016/j.eti.2023.103266

Jiao, N., Luo, T., Chen, Q., Zhao, Z., Xiao, X., Liu, J., Jian, Z., Xie, S., Thomas, H., Herndl, G.J., Benner, R., Gonsior, M., Chen, F., Cai, W.-J., Robinson, C., 2024. The microbial carbon pump and climate change. Nat. Rev. Microbiol. 22, 408-419. https://doi.org/10.1038/s41579-024-01018-0

Jing, F., Sun, Y., Liu, Y., Wan, Z., Chen, J., Tsang, D.C.W., 2022. Interactions between biochar and clay minerals in changing biochar carbon stability. Sci. Total Environ. 809, 151124. https://doi.org/10.1016/j.scitotenv.2021.151124

Jinger, D., Kakade, V.D., Kaushal, R., Bhatnagar, P.R., Ghosh, A., Mahawer, S.K., Dinesh, D., Singh, G., Akula, C., Paramesh, V., Meena, V.S., Roy, T., Islam, S.,

Kumar, D., Uthappa, A.R., Chavan, S.B., Pradhan, A., Kumar, R., Kaledhonkar, M.J., Madhu, M., 2025. Nature-based solutions for enhancing CO_2 sequestration and rehabilitating degraded lands through silvo-aromatic system and soil moisture conservation techniques. J. Environ. Manage. 380, 124904. https://doi.org/https://doi.org/10.1016/j.jenvman.2025.124904

Kabiri, K., Omidian, H., Zohuriaan-Mehr, M.J., Doroudiani, S., 2011. Superabsorbent Hydrogel Composites and Nanocomposites: A Review. Polym. Compos. 32, 277–289. https://doi.org/10.1002/pc.21046

Kabiri, K., Zohuriaan-Mehr, M.J., 2003. Superabsorbent hydrogel composites. Polym. Adv. Technol. 14, 438–444. https://doi.org/10.1002/pat.356

Kabiri, K., Zohuriaan-Mehr, M.J., Mirzadeh, H., Kheirabadi, M., 2010. Solvent-, ion- and pH-specific swelling of poly (2-acrylamido-2-methylpropane sulfonic acid) superabsorbing gels. J. Polym. Res. 17, 203–212. https://doi.org/10.1007/s10965-009-9306-7

Keqiang, Z., Zijia, Z., Cui, Z., Ling, X., Delong, M., Li, W., Shaoxian, S., Sancheze, R.M.T., Farias, M.E., 2023. Rapid artificial biocrust development by cyanobacterial inoculation and clay amendment. L. Degrad. Dev. 34, 3728–3743. https://doi.org/10.1002/ldr.4716

Kijjanapanich, P., Annachhatre, A.P., Lens, P.N.L., 2014. Biological Sulfate Reduction for Treatment of Gypsum Contaminated Soils, Sediments, and Solid Wastes. Crit. Rev. Environ. Sci. Technol. 44, 1037-1070. https://doi.org/10.1080/10643389.2012.743270

Lal, R., 2004. Soil Carbon Sequestration Impacts on Global Climate Change and Food Security. Science. 304, 1623-1627. https://doi.org/10.1126/science.1097396

Lan, S., Zhang, Q., Wu, L., Liu, Y., Zhang, D., Hu, C., 2014. Artificially Accelerating the Reversal of Desertification: Cyanobacterial Inoculation Facilitates the Succession of Vegetation Communities. Environ. Sci. Technol. 48, 307–315. https://doi.org/10.1021/es403785j

Li, S., Yang, S., Wei, X., Jiao, S., Luo, W., Chen, W., Wei, G., 2023. Reduced trace gas oxidizers as a response to organic carbon availability linked to oligotrophs in desert fertile islands. ISME J. 17, 1257–1266. https://doi.org/10.1038/s41396-023-01437-6

Li, X., Li, Q., Xu, X., Su, Y., Yue, Q., Gao, B., 2016. Characterization, swelling and slow-release properties of a new controlled release fertilizer based on wheat straw cellulose hydrogel. J. Taiwan Inst. Chem. Eng. 60, 564–572. https://doi.org/10.1016/j.jtice.2015.10.027

Li, Y., Xie, T., Yang, H., Li, X., 2022. Revegetation enhances soil organic carbon mineralization and its temperature sensitivity in the Tengger Desert, North China. CATENA 218, 106541. https://doi.org/https://doi.org/10.1016/j.catena.2022.106541

Liang, C., Balser, T.C., 2011. Microbial production of recalcitrant organic matter in global soils: implications for productivity and climate policy. Nat. Rev. Microbiol. 9, 75. https://doi.org/10.1038/nrmicro2386-c1

Liang, C., Schimel, J.P., Jastrow, J.D., 2017. The importance of anabolism in microbial control over soil carbon storage. Nat. Microbiol. 2, 1-6. https://doi.org/10.1038/nmicrobiol.2017.105

Ling, T., Tian, C., Ying, L., Wenjie, Z., Jun, R., 2017. Function of Biological and Sand-fixation Polymer Material Based on Attapulgite. J. Desert Res. 37, 276. https://doi.org/10.7522/j.issn.1000-694X.2017.00023

Liu, D., Li, M., Yu, R., Li, H., Shen, Y., Tian, Q., Bu, H., Huang, C., Tan, W., 2023. Interlayer organic matter within hydroxy-interlayered clay minerals enhances soil organic carbon stability under long-term organic fertilization. Appl. Clay Sci. 239, 106963. https://doi.org/10.1016/j.clay.2023.106963

Liu, J., Khayat, K.H., Shi, C., 2020. Effect of superabsorbent polymer characteristics on rheology of ultra-high performance concrete. Cem. Concr. Compos. 112, 103636. https://doi.org/https://doi.org/10.1016/j.cemconcomp.2020.103636

Liu, J., Sun, X., Zuo, Y., Hu, Q., He, X., 2023. Plant species shape the bacterial communities on the phyllosphere in a hyper-arid desert. Microbiol. Res. 269,127314. https://doi.org/10.1016/j.micres.2023.127314

Liu, Y., Li, X., Jia, R., Huang, L., Zhou, Y., Gao, Y., 2011. Effects of biological soil crusts on soil nematode communities following dune stabilization in the Tengger Desert, Northern China. Appl. Soil Ecol. 49, 118-124. https://doi.org/10.1016/j.apsoil.2011.06.007

Liu, P., Dai, J., Liu, J., Zhang, H., Wang, G., Guo, X., Gao, S., 2023. Microplastics exhibit lower carrying effects on the bioaccessibility and cytotoxicity of lead than montmorillonite clay particles. J. Hazard. Mater. 460, 132350. https://doi.org/10.1016/j.jhazmat.2023.132350

Liu, Y., Li, X., Jia, R., Huang, L., Zhou, Y., Gao, Y., 2011. Effects of biological soil crusts on soil nematode communities following dune stabilization in the Tengger Desert, Northern China. Appl. Soil Ecol. 49,118-124. https://doi.org/10.1016/j.apsoil.2011.06.007

Liu, Y., Su, M., Fu, Y., Zhao, P., Xia, M., Zhang, Y., He, B., He, P., 2018. Corrosive environments tolerant, ductile and self-healing hydrogel for highly efficient oil/water separation. Chem. Eng. J. 354, 1185–1196. https://doi.org/10.1016/j.cej.2018.08.071

Maier, S., Tamm, A., Wu, D., Caesar, J., Grube, M., Weber, B., 2018. Photoautotrophic organisms control microbial abundance, diversity, and physiology in different types of biological soil crusts. ISME J. 12, 1032–1046. https://doi.org/10.1038/s41396-018-0062-8

Mandal, S., Chi, H., Moss, R.E., Dhital, P., Babatunde, E.O., Gurav, R., Hwang, S., 2024. Seed gum-based polysaccharides hydrogels for sustainable agriculture: A

review. Int. J. Biol. Macromol. 263, 130339. https://doi.org/10.1016/j.ijbiomac.2024.130339

Miltner, A., Bombach, P., Schmidt-Brücken, B., Kästner, M., 2012. SOM genesis: microbial biomass as a significant source. Biogeochemistry 111, 41–55. https://doi.org/10.1007/s10533-011-9658-z

Mohamadian, N., Ghorbani, H., Wood, D.A., Khoshmardan, M.A., 2019. A hybrid nanocomposite of poly (styrene-methyl methacrylate-acrylic acid)/clay as a novel rheology-improvement additive for drilling fluids. J. Polym. Res. 26, 1–14. https://doi.org/10.1007/s10965-019-1696-6

Mohanta, T.K., Mohanta, Y.K., Kaushik, P., Kumar, J., 2023. Physiology, genomics, and evolutionary aspects of desert plants. J. Adv. Res. 58, 63-78. https://doi.org/10.1016/j.jare.2023.04.019

Montes-Pulido, C.R., Bird, M.I., da Silva Carvalho, L.C., Serrano, J., Quesada, C.A., Feldpausch, T.R., 2025. Climatic and Edaphic Drivers of Soil Organic Carbon and Pyrogenic Carbon Stocks Across Elevation and Disturbance Gradients in Colombian Andean Forests. Glob. Chang. Biol. 31, e70135. https://doi.org/10.1111/gcb.70135

Oechaiyaphum, K., Ullah, H., Shrestha, R.P., Datta, A., 2020. Impact of long-term agricultural management practices on soil organic carbon and soil fertility of paddy fields in Northeastern Thailand. Geoderma Reg. 22, e00307. https://doi.org/10.1016/j.geodrs.2020.e00307

Olad, A., Pourkhiyabi, M., Gharekhani, H., Doustdar, F., 2018. Semi-IPN superabsorbent nanocomposite based on sodium alginate and montmorillonite: Reaction parameters and swelling characteristics. Carbohydr. Polym. 190, 295–306. https://doi.org/10.1016/j.carbpol.2018.02.088

Orians, G.H., Milewski, A. V, 2007. Ecology of Australia: the effects of nutrient-poor soils and intense fires. Biol. Rev. https://doi.org/10.1111/j.1469-185x.2007.00017.x

Panic, V., Adnadjevic, B., Velickovic, S., Jovanovic, J., 2010. The effects of the synthesis parameters on the xerogels structures and on the swelling parameters of the poly(methacrylic acid) hydrogels. Chem. Eng. J. 156, 206–214. https://doi.org/https://doi.org/10.1016/j.cej.2009.10.040

Patel, V.K., Kuttippurath, J., Kashyap, R., 2024. Rise in water vapour driven by moisture transport facilitates water availability for the greening of global deserts. Sci. Total Environ. 946, 174111. https://doi.org/10.1016/j.scitotenv.2024.174111

Peng, J., Wu, X., Ni, S., Wang, J., Song, Y., Cai, C., 2022. Investigating intra-aggregate microstructure characteristics and influencing factors of six soil types along a climatic gradient. Catena 210, 105867. https://doi.org/10.1016/j.catena.2021.105867

Qian, L., Wang, J., Xiao, J., Yang, L., Xia, L., Song, S., Farías, M.E., Wang, Z., Wu, L., 2024. Clay minerals accelerate the formation of indoor biocrusts: Effects and

mechanism. Soil Tillage Res. 244, 106217. https://doi.org/10.1016/j.still.2024.106217

Rizwan, M., Gilani, S.R., Durrani, A.I., Naseem, S., 2022. Kinetic model studies of controlled nutrient release and swelling behavior of combo hydrogel using Acer platanoides cellulose. J. Taiwan Inst. Chem. Eng. 131, 104137. https://doi.org/10.1016/j.jtice.2021.11.004

Qin, C., Wang, H., Zhao, Y., Qi, Y., Wu, N., Zhang, S., Xu, W., 2024. Recent advances of hydrogel in agriculture: Synthesis, mechanism, properties and applications. Eur. Polym. J. 113376. https://doi.org/10.1016/j.eurpolymj.2024.113376

Román, J.R., Chilton, A.M., Cantón, Y., Muñoz-Rojas, M., 2020. Assessing the viability of cyanobacteria pellets for application in arid land restoration. J. Environ. Manage. 270, 110795. https://doi.org/10.1016/j.jenvman.2020.110795

Rominger, K., Meyer, S., 2019. Application of UAV-Based Methodology for Census of an Endangered Plant Species in a Fragile Habitat. Remote Sens. 11, 719. https://doi.org/10.3390/rs11060719

Rossi, F., Mugnai, G., De Philippis, R., 2022. Cyanobacterial biocrust induction: a comprehensive review on a soil rehabilitation-effective biotechnology. Geoderma 415, 115766. https://doi.org/10.1016/j.geoderma.2022.115766

Santos, R.V.A., Costa, G.M.N., Pontes, K. V, 2019. Development of Tailor-Made Superabsorbent Polymers: Review of Key Aspects from Raw Material to Kinetic Model. J. Polym. Environ. 27, 1861–1877. https://doi.org/10.1007/s10924-019-01485-0

Satdichanh, M., Dossa, G.G.O., Yan, K., Tomlinson, K.W., Barton, K.E., Crow, S.E., Winowiecki, L., Vågen, T., Xu, J., Harrison, R.D., 2023. Drivers of soil organic carbon stock during tropical forest succession. J. Ecol. 111, 1722–1734. https://doi.org/10.1111/1365-2745.14141

Ruan, W., Zhang, Z., Cai, M., She, Y., Liu, J., Guo, W., Ma, X., Liao, J., He, X., 2023. Comparative study of the effects of magnesium aluminum silicate and bentonite clay on the properties of magnesium phosphate cement-based grouting material. Constr. Build. Mater. 401, 132852. https://doi.org/10.1016/j.conbuildmat.2023.132852

Schröfl, C., Erk, K.A., Siriwatwechakul, W., Wyrzykowski, M., Snoeck, D., 2021. Recent progress in superabsorbent polymers for concrete. Cem. Concr. Res. 151, 106648. https://doi.org/10.1016/j.cemconres.2021.106648

Shubnell, A.J., Kosnic, E.J., Squattrito, P.J., 1994. Structures of layered metal sulfonate salts: trends in coordination behavior of alkali, alkaline earth and transition metals. Inorganica Chim. Acta 216, 101–112. https://doi.org/10.1016/0020-1693(93)03700-K

Singh, A., Yadav, V.K., Gautam, H., Rathod, L., Chundawat, R.S., Singh, G., Verma, R.K., Sahoo, D.K., Patel, A., 2023. The role of plant growth promoting rhizobacteria in strengthening plant resistance to fluoride toxicity: a review. Front. Microbiol. 14, 1271034. https://doi.org/10.3389/fmicb.2023.1271034

Six, J., Conant, R.T., Paul, E.A., Paustian, K., 2002. Stabilization mechanisms of soil organic matter: implications for C-saturation of soils. Plant Soil 241, 155–176.

Tally, M., Atassi, Y., 2015. Optimized synthesis and swelling properties of a pH-sensitive semi-IPN superabsorbent polymer based on sodium alginate-g-poly (acrylic acid-co-acrylamide) and polyvinylpyrrolidone and obtained via microwave irradiation. J. Polym. Res. 22, 1-13. https://doi.org/10.1007/s10965-015-0822-3

Tombácz, E., Szekeres, M., 2006. Surface charge heterogeneity of kaolinite in aqueous suspension in comparison with montmorillonite. Appl. Clay Sci. 34, 105-124. https://doi.org/10.1016/j.clay.2006.05.009

Uroz, S., Kelly, L.C., Turpault, M.P., Lepleux, C., Frey-Klett, P., 2015. The Mineralosphere Concept: Mineralogical Control of the Distribution and Function of Mineral-associatec Bacterial Communities. TRENDS Microbiol. 23, 751–762. https://doi.org/10.1016/j.tim.2015.10.004

Wang, Z.M., Shi, H.X., Wang, F., Wang, A.R., He, Q., Cuan, S.S., 2021. Synthesis of cassava starch-g-acrylic acid/dimethylaminopropyl methacrylamide: A new hydrogel for brine solution. Carbohydr. Polym. 266, 118109. https://doi.org/10.1016/j.carbpol.2021.118109

Warren, S.D., 2014. Role of biological soil crusts in desert hydrology and geomorphology: implications for military training operations. 22. https://doi.org/10.1130/2014.4122(16)

Wattel-Koekkoek, E.J.W., Buurman, P., Van Der Plicht, J., Wattel, E., Van Breemen, N., 2003. Mean residence time of soil organic matter associated with kaolinite and smectite. Eur. J. Soil Sci. 54, 269–278. https://doi.org/10.1046/j.1365-2389.2003.00512.x

Weber, B., Belnap, J., Budel, B., Antoninka, A.J., Barger, N.N., Chaudhary, V.B., Darrouzet-Nardi, A., Eldridge, D.J., Faist, A.M., Ferrenberg, S., Havrilla, C.A., Huber-Sannwald, E., Issa, O.M., Maestre, F.T., Reed, S.C., Rodriguez-Caballero, E., Tucker, C., Young, K.E., Zhang, Y.M., Zhao, Y.G., Zhou, X.B., Bowker, M.A., 2022. What is a biocrust? A refined, contemporary definition for a broadening research community. Biol. Rev. 97, 1768–1785. https://doi.org/10.1111/brv.12862

Wichterle, O., LÍM, D., 1960. Hydrophilic Gels for Biological Use. Nature. 185, 117-118. https://doi.org/10.1038/185117a0

Witzgall, K., Vidal, A., Schubert, D.I., Höschen, C., Schweizer, S.A., Buegger, F., Pouteau, V., Chenu, C., Mueller, C.W., 2021. Particulate organic matter as a functional soil component for persistent soil organic carbon. Nat. Commun. 12, 4115. https://doi.org/10.1038/s41467-021-24192-8

Wu, H.W., Cui, H.L., Fu, C.X., Li, R., Qi, F.Y., Liu, Z.L., Yang, G., Xiao, K.Q., Qiao, M., 2024. Unveiling the crucial role of soil microorganisms in carbon cycling: A review. Sci. Total Environ. 909, 168627. https://doi.org/10.1016/j.scitotenv.2023.168627

Wu, S., Konhauser, K.O., Chen, B., Huang, L., 2023. “Reactive Mineral Sink” drives soil organic matter dynamics and stabilization. npj Mater. Sustain. 1, 1–12. https://doi.org/10.1038/s44296-023-00003-7

Xiang, J., Qiu, J., Zheng, P., Sun, X., Zhao, Y., Gu, X., 2023. Usage of biowashing to remove impurities and heavy metals in raw phosphogypsum and calcined phosphogypsum for cement paste preparation. Chem. Eng. J. 451, 138594. https://doi.org/https://doi.org/10.1016/j.cej.2022.138594

Xiao, K.Q., Zhao, Y., Liang, C., Zhao, M., Moore, O.W., Otero-Fariña, A., Zhu, Y.G., Johnson, K., Peacock, C.L., 2023. Introducing the soil mineral carbon pump. Nat. Rev. Earth Environ. 4, 135–136. https://doi.org/10.1038/s43017-023-00396-y

Xie, Y., Tang, J., Li, R., Chen, P., 2025. Redistribution of SOC driven by erosion and deposition in cultivated black soils of Northeast China. Catena. 258, 109268. https://doi.org/10.1016/j.catena.2025.109268

Xu, W., Zhao, Yanqiao, Lian, Y., Zhao, Yang, Zhang, Z., 2025. Co-development of biocrust and herbaceous plant communities in sandy areas after cyanobacterial inoculation. Plant Soil. 508, 227-240. https://doi.org/10.1007/s11104-024-06794-5

Xue, T., Zhang, Lixia, Yang, F., Cheng, C., Wang, J., Sang, Q., Yang, S., Zhao, X., Zhang, Liang, 2024. Carbon sink and soil organic carbon sequestration mechanisms in vineyards. J. Clean. Prod. 143217. https://doi.org/10.1016/j.jclepro.2024.143217

Yang, F., Huang, J., Zhou, C., Yang, X., Mamtimin, A., Zheng, X., Huo, W., Ji, F., Han, D., Meng, L., Gao, J., Song, M., Wang, Y., Zhu, C., 2023. Desert Abiotic Carbon Sequestration Weakening by Precipitation. Environ. Sci. Technol. 57, 7174–7184. https://doi.org/10.1021/acs.est.2c09470

Yang, Y., Liang, Z., Zhang, R., Zhou, S., Yang, H., Chen, Y., Zhang, J., Yin, H., Yu, D., 2024. Research Advances in Superabsorbent Polymers. Polymers (Basel). 16, 501. https://doi.org/10.3390/polym16040501

Zhang, C., Chen, X., Zhou, K., Li, J., Meza, J.V.G., Song, S., Montes, M.L., Zamoniddin, N., Xia, L., 2025a. Synergistic effects of clays and cyanobacteria on the accumulation dynamics of soil organic carbon in artificial biocrusts. J. Environ. Manage. 374, 124110. https://doi.org/10.1016/j.jenvman.2025.124110

Zhang, C., Meza, J.V.G., Zhou, K., Liu, J., Song, S., Zhang, M., Meng, D., Chen, J., Xia, L., Hu, X., 2023. Superabsorbent polymer used for saline-alkali soil water retention. J. TAIWAN Inst. Chem. Eng. 145, 104830. https://doi.org/10.1016/j.jtice.2023.104830

Zhang, C., Zhou, K., Wang, Z., Zhou, Z., Meza, J.V.G., Song, S., Kim, H., Montes, M.L., Benzaazoua, M., Xia, L., 2025b. Montmorillonite as an “accelerator” for the microbial carbon pump during artificial biocrust construction. Plant Soil. 1-17. https://doi.org/10.1007/s11104-025-07256-2

Zhang, J.-P., Zhang, F.-S., 2018. Recycling waste polyethylene film for amphoteric superabsorbent resin synthesis. Chem. Eng. J. 331, 169–176. https://doi.org/https://doi.org/10.1016/j.cej.2017.08.058

Zhang, M., Zhang, T., Zhou, L., Lou, W., Zeng, W., Liu, T., Yin, H., Liu, H., Liu, X., Mathivanan, K., 2022. Soil microbial community assembly model in response to heavy metal pollution. Environ. Res. 213, 113576. https://doi.org/10.1016/j.envres.2022.113576

Zhang, P., Bing, X., Jiao, L., Xiao, H., Li, B., Sun, H., 2022. Amelioration effects of coastal saline-alkali soil by ball-milled red phosphorus-loaded biochar. Chem. Eng. J. 431, 133904. https://doi.org/10.1016/j.cej.2021.133904

Zhang, W.X., Wang, P., Liu, S.F., Chen, J., Chen, R., He, X.Y., Ma, G.F., Lei, Z.Q., 2021. Factors affecting the properties of superabsorbent polymer hydrogels and methods to improve their performance: a review. J. Mater. Sci. 56, 16223–16242. https://doi.org/10.1007/s10853-021-06306-1

Zhang, X., Yao, M.-C., Chen, L., Sheng, G.-P., 2022. Lewis Acid-Base Interaction Triggering Electron Delocalization to Enhance the Photodegradation of Extracellular Antibiotic Resistance Genes Adsorbed on Clay Minerals. Environ. Sci. Technol. 56, 17684–17693. https://doi.org/10.1021/acs.est.2c05785

Zhang, Z., Qiao, X., 2021. Influences of cation valence on water absorbency of crosslinked carboxymethyl cellulose. Int. J. Biol. Macromol. 177, 149–156. https://doi.org/10.1016/j.ijbiomac.2021.02.080

Zhao, Y., Xu, W.W., Wang, N., 2021. Effects of covering sand with different soil substrates on the formation and development of artificial biocrusts in a natural desert environment. Soil Tillage Res. 213, 105081. https://doi.org/10.1016/j.still.2021.105081

Zheng, S., Bai, D.-S., Yang, X., Lai, J.-L., Wang, Y.-W., Zhang, Y., Luo, X.-G., 2022. Changes in soil microecology of gangue reclamation areas after 10 years of in situ restoration with herbaceous plants (Artemisia sacrorum and Imperata cylindrica) and trees (Populus spp.). Ecol. Eng. 182, 106719. https://doi.org/10.1016/j.ecoleng.2022.106719

Zhu, X., Jackson, R.D., DeLucia, E.H., Tiedje, J.M., Liang, C., 2020. The soil microbial carbon pump: From conceptual insights to empirical assessments. Glob. Chang. Biol. 26, 6032-6039. https://doi.org/10.1111/gcb.15319

Chapter II. Superabsorbent polymer used for saline-alkali soil water retention

2.1 Introduction

Approximately $1.13x10^{12}$ billion ha of land worldwide are affected by saline-alkali stress (Zhang et al., 2022), severely impacting food production and causing an estimated annual economic loss of $27.3 billion (Ali et al., 2017). Even more concerning, saline-alkali land continues to expand globally, highlighting the urgent need to improve the physicl and chemical properties of such soils (Cui et al., 2021). Previous studies have identified drought and rapid soil water evaporation as primary drivers of soil salinization (Xiong et al., 2022; Zhang et al., 2018). As a result, enhancing soil water retention has been recognized as an effective strategy for mitigating soil salinization (Ali et al., 2017; Zhang et al., 2018). Superabsorbent polymers (SAPs), capable of retaining more than 1,000 times their weight in water (Panic et al., 2010; Zhang and Zhang, 2018), have been widely used in agriculture as water-retaining agents (Li et al., 2016; Rizwan et al., 2022). However, SAPs have limited effectiveness in saline-alkali soils due to their poor salt tolerance (Ahmed, 2015). To enhance the swelling performance of SAPs in saline conditions, researchers have explored various modifications, including zwitterionic polymers (Zhang et al., 2021), e.g., zwitterionic polymers (Wang et al., 2021), inorganic materials (Kabiri and Zohuriaan-Mehr, 2003), and interpenetrating polymer networks (IPNs) (Tally and Atassi, 2015). Despite these efforts, their success remains constrained, primarily because the additives contribute insufficient hydrophilicity rather than increasing the material's crosslinking density (Kabiri et al., 2011). The Flory-Rehner theory (Flory, 1953) provides a quantitative framework for understanding SAP swelling behavior, as described by Yang et al. (2021):

$$Q^{\frac{3}{5}} = \frac{\left(\frac{i}{2V_\mu}/s^{\frac{1}{2}}\right)^2 + \left(\frac{1}{2} - x_1\right)/V_1}{V_E/V_0} \quad \text{(Eq. 1)}$$

where Q: degree of swelling; i/V_μ: charge density of the used material as polymer; S: ionic strength of solution; $(1/2\text{-}x_1)/V_1$: affinity of polymer-solvent; V_E/V_0: density of crosslinking.

Thus, the swelling capacity of SAP is significantly constrained by the ionic strength of the surrounding solution, particularly in the presence of multivalent cations as Equation 1 (Zhang and Qiao, 2021). However, enhancing the affinity of SAP has been shown to greatly improve its performance, with the diversity of hydrophilic groups also playing a crucial role (Zhang et al., 2021). Studies have established the hydrophilicity ranking of functional groups as follows: R-SO_3H > R-COOH > R-$CONH_2$ > R-OH (Berthold et al., 1996; Zhang and Qiao, 2021). 2-acrylamide-2-methylpropanesulfonic acid (AMPS), which contains the highly hydrophilic R-SO_3H group, is widely used as a salt-resistant oil displacement agent in the petroleum industry

due to its low cation-binding tendency (Mohamadian et al., 2019; Cai, 2004; Shubnell et al., 1994). Meanwhile, acrylic acid (AA) and acrylamide (AM), which feature R-COOH and R-$CONH_2$ groups, respectively, are commonly utilized in gel-based applications due to their strong hydrophilicity and cost-effectiveness (Ahmed, 2015; Liu et al., 2018).

Based on these characteristics, AMPS, AA, and AM were selected as monomers for synthesizing salt-tolerant SAP (ST-SAP) for water retention in saline-alkali soils (Mischke et al., 2019). The target soil was sourced from Lop Nur, Xinjiang, China, where saline-alkali stress is particularly severe. Since the molar ratio of hydrophilic monomers plays a decisive role in polymer properties (Wang et al., 2020), their proportions were carefully adjusted to optimize the synergistic effects of the hydrophilic groups.

To evaluate the performance of ST-SAP under high-salinity conditions, swelling behavior was analyzed using swelling kinetics fitting and reswelling experiments. Additionally, the salt-tolerance mechanisms were investigated through computed tomography (CT) and using two spectroscopy technics, the X-ray photoelectron (XPS), and Fourier-transform infrared (FT-IR). Finally, the microscopy using scanning electron (SEM) was employed to assess the water retention capacity of SAP-treated saline-alkali soil.

2.2 Experimental sections

2.2.1 Materials

Saline-alkali soil was provided from Lop Nur, Xinjiang Province, China. Acrylic acid (AA), acrylamide (AM), 2-acrylamido-2-methyl-1-propanesulfonic acid (AMPS)，N,N'-methylenebisacrylamide (MBA), and potassium persulfate (KPS) were purchased from Sinopharm Chemical Reagent Co. LTD, as well as NaOH, HCl, $CaCl_2$, NaCl, KCl, $MgCl_2$ reagent. All reagents were analytical grade and deionized water was processed by a pure water meter (Millipore company, Milli-Q Direct 16, America).

2.2.2 Preparation of ST-SAP

During preparation, the mass of the monomers was kept constant at 25 wt% of the mass of the deionized water and the monomers. First, AA (0.025 mol) and AMPS (0.0075, 0.015, 0.0225, 0.03, and 0.0375 mol, respectively) were dissolved in deionized water and subsequently cooled in ice water (Ahmed, 2015). AM (0.02, 0.04, 0.06, 0.08, and 0.1 mol, respectively), NaOH (adjusted the neutralization degree to 85%), and MBA (n_{MBA}:$n_{AA+AM+AMPS}$ = 0.025%) were added to the solution. Then, the mixture was transferred to a 250 mL three-necked flask equipped with a mechanical stirrer, reflux condenser thermometer, and N_2 for 15 min to remove dissolved oxygen. Subsequently, KPS (n_{KPS}:$n_{AA+AM+AMPS}$ = 0.08%) was added with continuous stirring at 60℃ to generate radicals. After about 10 min, the mixture gradually solidified, and the system was maintained under N_2 atmosphere at 60℃ for 3 h. Finally, the obtained products

were dried by vacuum freeze dryer, ground and sieved to 40-80 mesh (Zhang and Zhang, 2018; Zhang et al., 2006).

2.2.3 Determination of swelling properties

A mixed saline solution was prepared to determine the swelling properties of ST-SAP under high salt condition. The concentrations and pH of the mixed saline solution matched to Table S5.1 (in wt%: 4.13 Na^+ 0.50 K^+, 0.75 Ca^{2+}, and 0.45 Mg^{2+}), at pH 8.5 The weighed reagents (21 g NaCl, 1.92 g KCl, 4.18 g $CaCl_2$, and 3.58 g $MgCl_2$), were dissolved in 200 mL of deionized water to prepare the high-concentration salt solution.

Materials (0.1000 g) were immersed in deionized water and mixed saline solution for 3 h to achieve swelling equilibrium. Then, the swollen ST-SAP was filtered through a 100 meshes nylon net (Zhang and Zhang, 2018). Each experiment was performed in triplicate to calculate the average values. The water absorbing capacity Q_{eq} (g/g) was calculated as the following.

$$Q_{eq}=(M-M_0)/M_0 \quad \text{(Eq. 2)}$$

where M_0 (g) and M (g): weights of the dry and swollen samples, respectively.

To investigate the swelling kinetics of ST-SAP under high salt condition, the product (0.1000±0.0001 g) was immersed in the mixed saline solution at specific time intervals (0, 5, 15, 20, 60, 120, and 180 min). The swelling rate was determined according to Eq. 2.

The swollen ST-SAP (0.1000g) in deionized water and mixed saline solution were placed in an oven at 60 ℃ until dried completely. The polymers were then re-swelling in an equal volume of deionized water and mixed saline solution. The above process was repeated in five cycles to evaluate the reusability.

2.2.4 Determination of water retention properties

The swollen materials (0.1000 g) in mixed saline solution were placed into a 25 ℃ thermostat. Concurrently, an equal amount of mixed saline solution was used as a blank control. The mass loss was measured every 2 h. The water retention capacity of ST-SAP was determined based on the relationship between mass loss and time, which was calculated as follows:

$$W_r(\%) = W_t/W_0\times 100\% \quad \text{(Eq. 3)}$$

where W_0 and W_t are the masses of the completely swollen ST-SAP and the material at a certain time, respectively.

2.2.5 Determination of swelling properties

Two 10-centimeter soil columns without caps were drilled with small holes at the bottom. 1 g ST-SAP (2wt % of saline-alkali soils) (Saha et al., 2020) was well-distributed with saline-alkali soils and the resulting mixture was added to one of the soil columns. The same amount of saline soil was filled into another column as the blank control. The two soil columns were placed into deionized water for several days until constant weight (P. Zhang et al., 2022) . Subsequently, the soil columns were

placed in a thermostat at 25 ℃ and were weighed every two days until the blank control reached a constant weight. The water retention capacity (W_{eq}) of ST-SAP in saline-alkali soil was determined based on the relationship between mass loss and time, which was calculated as follows:

$$W_{ep} = (M_{total} - M_t) / M_1 \times 100\% \quad \text{(Eq. 4)}$$

in which M_{total}: total mass of the swollen ST-SAP/soil (or soil for control), M_t: mass of the swollen ST-SAP-soil (or soil) if t and M_1 is the total mass of water absorbed by ST-SAP-soil (or soil).

2.2.6 Characterization

The concentrations of Na and K were measured spectrometrically using an atomic absorption (Shimadzu Company, AA-6880, Japan) at range 185 to 900 nm; Ca^{2+} and Mg^{2+} concentrations were calculated after EDTA complexometric method.

Fourier Transform Infrared spectroscopy (Thermo Fisher Scientific, Nicolet6700, USA) was used to record the FT-IR spectra of solid and liquid samples in the range of 4000-400 cm^{-1}. The fast scan was performed once per second.

The X-ray photoelectron spectroscopy (XPS) was employed to investigate the structure change after the ST-SAP absorbing Ca^{2+}, with a spectrometer (Thermo Fisher Scientific, ESCALAB Xi+, USA） equipped with a monochromatic Al Ka Xray source.

The morphology of the ST-SAP was characterized by SEM (JSM 7100F, Jeol, Japan). All materials are sprayed with gold before scanning, and the electron microscope acceleration voltage was set at 15kv.

Computed tomography (CT) (Carl Zeiss AG, ZEISS Xradia 620 Versa, Germany) was applied to reconstruct the internal structure of the material, at 1.51 microns voxel resolution.

2.2.7 Statistical analysis

To know the effect of monomers amount on swelling properties, reswelling capacity, and swelling properties in salt solutions of ST-SAP, ANOVA analyses were performed (Esmaeili and Saremnia, 2016; Song et al., 2022). The former was done using SPSS software (V 26)

2.3 Results and discussion

2.3.1 Structure of ST-SAP

In Figure 2.1a, the FT-IR spectra of the ST-SAP displayed a broad stretching vibration band at 3432 cm^{-1} which is attributed to the O-H stretching vibration (Rashidzadeh and Olad, 2014) . This peak is characteristic of -COOH of AA. Furthermore, the spectra also exhibited peaks at 1666 cm^{-1} and 1450 cm^{-1}, which are attributed to the asymmetric and symmetric stretching vibration peaks of COO- of AA, respectively (Wu et al., 2003) . The FT-IR spectra of AM revealed a peak at 1666 cm^{-1}, which corresponds to -C=O. Additionally, the absorption peaks at 3359 cm^{-1} and 3178 cm^{-1} were assigned to -N-H bond stretching vibration (Rashidzadeh and Olad, 2014;

Wu et al., 2003). The characteristic peaks of -SO_3H stretching vibration, belonging to AMPS, were observed at 1243 and 1025 cm^{-1} (Xie et al., 2012; Xiying Jing, Shili Chen, 1992). The presence of all the above peaks in ST-SAP confirms the successful synthesis of poly (AA-co-AM-co-AMPS) ST-SAP.

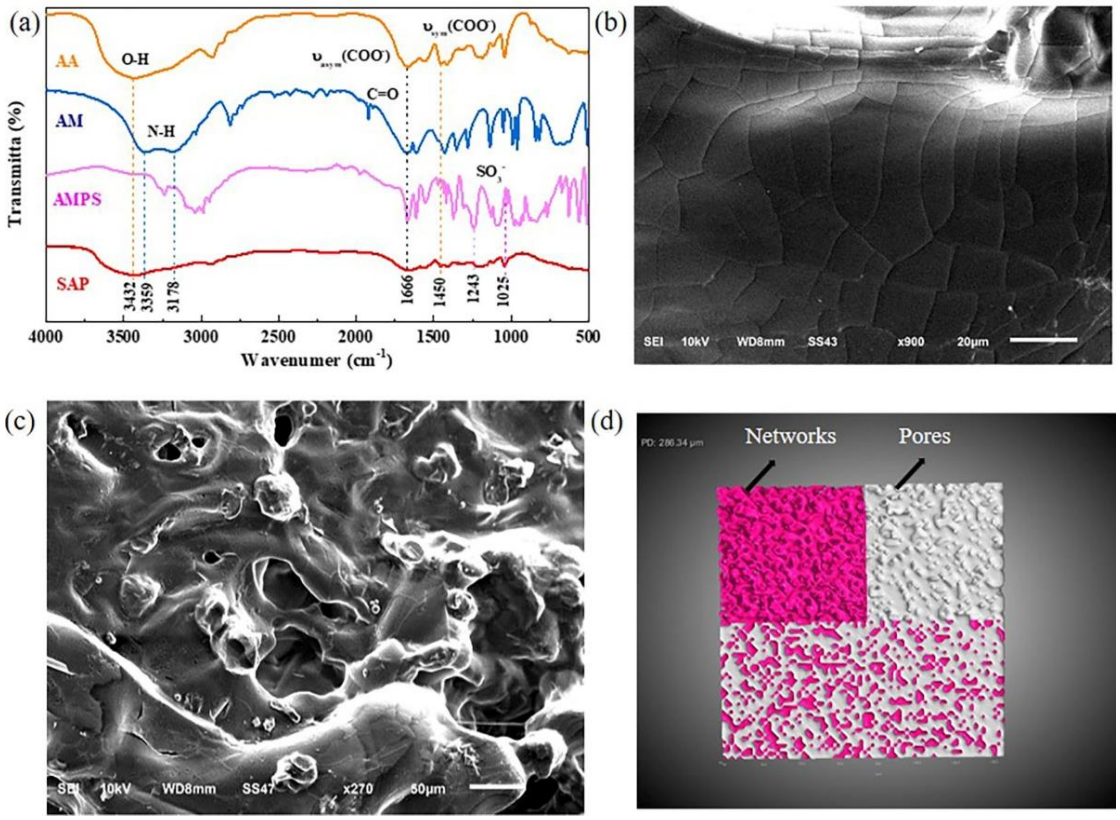

Figure 2.1 (a) spectra after Fourier Transform Infrared analyses of acrylic acid (AA), acrylamide (AM), 2-acrylamide-2-methylpropanesulfonic acid (AMPS), and the synthesizing salt-tolerant superabsorbent polymers (ST-SAP). (b and c) Imagens at scanning electron microscope ST-SAP before and after contacting water, respectively. (d) ST-SAP pore structures (white) inside the swollen networks (pink), showed in 3D

Before being exposed to water, the network structure of ST-SAP was in a contracted state (Xiao et al., 2017; Zohuriaan-Mehr and Kabiri, 2008), characterized by a lack of any discernible pore structure (Figure 2.1b). Upon the addition of water, the network of ST-SAP immediately swelled and acquired a porous morphology (Figure 2.1c). CT is a non-intrusive measurement method without no damage to the object. Utilizing the threshold method of Otsu (Otsu, 1979), reconstructed images of swollen ST-SAP were binarized, which effectively segregated the pores from the bulk ST-SAP (Womack et al., 2022) as is showed in Figure 2.1d. The resulting pore volume ratio was determined to be 67.8%. It should be noted that the pore volume ratio of ST-SAP is not constant; the more water that is absorbed, the more pores there would be in ST-SAP.

2.3.2 Effect of monomers amount on swelling properties

AA content was fixed to simplify the research process (Cheng et al., 2019) (Figure 2.2). The trend of ST-SAP in mixed saline solution closely mirrored that observed in deionized water, which emphasized that increasing polymeric hydrophilicity was an effective way to improve salt tolerance.

When n(AM): n(AA) was 0, surprisingly, the ST-SAP completely dissolved in the solution, which presented the swelling capacities of 0 g/g (Figure 2.2a). It was can be attributed to the strong hydrophilicity of AA and AMPS, which resulted in continuous swelling of the network and accumulation of stresses within the material (Kim and Park, 2004). When the swelling stress reached too high that the material broke up under even tiny external forces. The presence of AM restrained the infinite swelling of the network structure, as the hydrophilicity of the R-$CONH_2$ group in AM is relatively weaker, while the formation of hydrogen bonds increased the degree of cross-linking, ultimately improving the mechanical strength of the material. Additionally, the synergistic interaction of R-$CONH_2$, R-COO^- and R-SO_3H also improved the swelling capacity as well as salt tolerance. However, when n(AM): n(AA) was more than 3.2, the capacity began to decline, as excessive non-ionic groups (R-$CONH_2$) reduced overall hydrophilicity (He et al., 2017).

The swelling capacity of ST-SAP initially increased and then decreased as n(AMPS):n(AA) increased from 0 to 4.0 (Figure 2.2b); while an appropriate increase of AMPS enhanced the swelling capacities, the excessive AMPS resulted in steric hindrance that inhibited the effective formation of hydrophilic substances. When n(AMPS):n(AA) was 1.5, the swelling capacity was again 0. The optimal performance was achieved when the molar ratio of n(AA):n(AM):n(AMPS) was 1:2.4:0.6, as the synergistic effect of the three hydrophilic groups was greatest under the condition (P. Zhang et al., 2022).

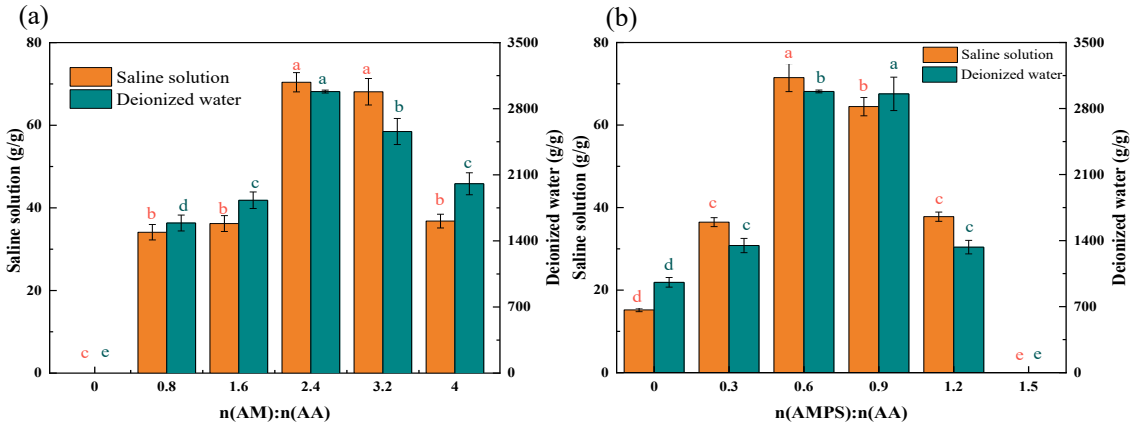

Figure 2.2 Effects of the assayed moles of acrylamide and acrylic (nAm:nAA) (a) and 2-acrylamide-2-methylpropanesulfonic acid and acrylamide (nAMPS:nAA). 0.025 mol AA, 0.015 mol AMPS, AM 0.06 mol. a, b, c: significant differences between treatments ($p < 0.05$)

2.3.3 Swelling properties under high salt condition

2.3.3.1 Swelling kinetics

To investigate the water retention properties of ST-SAP in saline-alkali soil of high salinity, the saline-alkali soil of Lop Nur was selected. The soil samples were composed of 0-30 cm topsoil at different sampling points (Table 3.1).

Table 2.1. The properties of saline-alkali soil from Lop Nur, Xinjiang Province, China.

Properties	Result
CEC	6.452 $cmol^{+}/kg$
Total dissolved salt	18.13%
pH	8.29
Soluble cation contents (Na^+, K^+, Ca^{2+}, Mg^{2+})	4.13 wt% Na^+, 0.50 wt% K^+ 0.75 wt% Ca^{2+}, and 0.45 wt% Mg^{2+}

To investigate the water adsorption efficiency in high saline solution, pseudo-first-order, pseudo-second-order models (Al-Othman et al., 2012; Zhang and Zhang, 2018) were used, which were expressed as follows:

$$Q_t=Q_e\text{-}exp\hat{}(lnQ_e\text{-}k_1t) \quad \text{(Eq. 5)}$$

$$t/Q_t=1/k_2Q_e^2+t/Q_e \quad \text{(Eq. 6)}$$

in which Q_e (g/g) and Q_t (g/g) are defined as the swelling capacity of the materials at equilibrium and time t, respectively. k_1 (min^{-1}), and k_2 (g mol^{-1} min^{-1}) are the rate constant of the pseudo-first-order, and pseudo-second-order model, respectively.

According to Figure 2.3a, the fitting parameters of models are obtained and listed in Table 2.1. The correlation coefficient of the pseudo-first-order model is higher (Simonin, 2016), suggesting a satisfactorily fitting result (Du et al., 2014). In addition, the swelling capacity of ST-SAP was determined to be 69.03 (g/g). Previous studies (refer to Table 2.2) have shown a dearth of research on water-absorbent polymers under high salt concentration, with existing materials generally exhibiting poor salt tolerance. Remarkably, ST-SAP in this study exhibits exceptional swelling performance under high salt conditions.

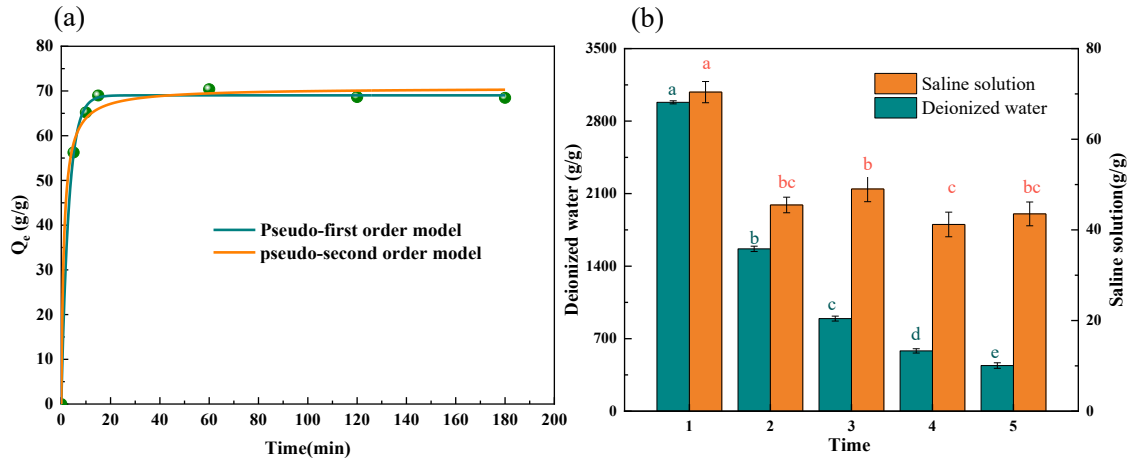

Figure 2.3 (a) Swelling kinetics for water adsorption in mixed saline solution at 25 ℃. (b) The reswelling capacities of the salt-tolerant superabsorbent polymer (ST-SAP) at 25 ℃. Different lowercase letters indicate significant differences between treatments ($p < 0.05$)

Table 2.2. Kinetic parameters for the salt-tolerant superabsorbent polymer (ST-SAP) in mixed saline solution at 25℃

Pseudo-first-order model			Pseudo-second-order model		
Q_e (g/g)	k_1 (min^{-1})	R_1^2	Q_e (g/g)	k_2 (min^{-1})	R_2^2
69.03	0.015	0.999	70.70	0.013	0.994

Table 2.3. Comparison of the swelling capacity of materials

Materials	Swelling capacity (g/g)	Condition	Filtering method	References
Cassava starch-g-AA/DMAPMA hydrogel	20	10 wt% NaCl	100-mesh nylon sieve	Wang et al, 2021
	213.5	rainwater		
FGB	86	Tap-water	-	Liu et al., 2020
	65	0.9 wt% NaCl		
Poly (AA)/attapulgite	20	0.9 wt% $CaCl_2$	100-mesh screen	Li et al., 2005
STSP	145	0.9 wt% NaCl	-	Zhao et al., 2019
ST-SAP	69.026	Mixed saline solution: 10.50 wt% NaCl; 0.96 wt% KCl; 2.09 wt% $CaCl_2$; 1.79 wt% $MgCl_2$	100-mesh nylon sieve	current study

2.3.3.2 Reswelling capacity

The reswelling capacities of ST-SAP during the 1st to 5th cycles were determined (Figure 2.3b). In deionized water, a significant decrease ($P<0.05$) in the swelling capacity of ST-SAP was observed with increasing cycle number, owing to the polymer decomposition to a certain extent (Mohammadbagheri et al., 2021; Zhang and Zhang, 2018). However, in mixed saline solution, no significant difference was noted between the results of the 2nd, 3rd, and 5th cycles ($P>0.05$), nor between the 2nd, 4th, and 5th cycles ($P>0.05$), which indicated the remarkable stability of ST-SAP during the 2nd-5th swelling process. This is because the chemical reaction of ST-SAP with cations in the salt solution increases the degree of cross-linking of the polymer (Kabiri et al., 2011), thus enhancing the structural stability of ST-SAP (Zhang and Qiao, 2021). The phenomenon serves as evidence that ST-SAP can effectively realize multiple reswelling under high salt condition.

2.3.4 Salt-tolerant mechanism under high salt condition

2.3.4.1 Swelling properties under different types and concentrations of salt solutions

The abundant hydrophilic groups formed hydrogen bonds with water to attract a large amount of water (Ahmed, 2015). The ionic groups of ST-SAP generate

intermolecular electrostatic repulsion and the osmotic pressure difference by ionization, which facilitate further swelling of the network structure(Flory, 1953; Zhang et al., 2021). However, the presence of cations greatly reduces the swelling ability of ST-SAP(Olad et al., 2018; Zhang and Qiao, 2021). In the soil sample, Na^+ and Ca^{2+} were the maximum content of monovalent and divalent cations, respectively (in Table 2.1). To investigate the impacts of cations, ST-SAP was added to two salt solutions (NaCl and $CaCl_2$) with varying concentrations. Overall, the swelling capacities decreased significantly with the increase of salt solution concentration (Figure 2.4). This is because the cations complex with hydrophilic groups diminished the polymeric hydrophilicity (Ping et al., 2001; Zhang and Qiao, 2021), screened the electrostatic repulsion of ionic functional groups (Zhang and Zhang, 2018), and reduced the osmotic pressure difference of ST-SAP (Olad et al., 2018).

Interestingly, a non-significant decrease in swelling capacity was observed with increasing concentrations of NaCl solution above 6 wt% and $CaCl_2$ solution above 1.64 wt% ($P>0.05$). A similar phenomenon was reported in other researches (Z. M. Wang et al., 2021), in which absorbed cation complex with the hydrophilic group, enhancing the stability of ST-SAP in high salt solution (Zhang and Qiao, 2021). It was confirmed in the previous content (2.3.2).

In addition, the impact of the Ca solution was more pronounced than that of the Na solution (Figure 2.4). Hence, the Ca solution was chosen for further mechanistic studies.

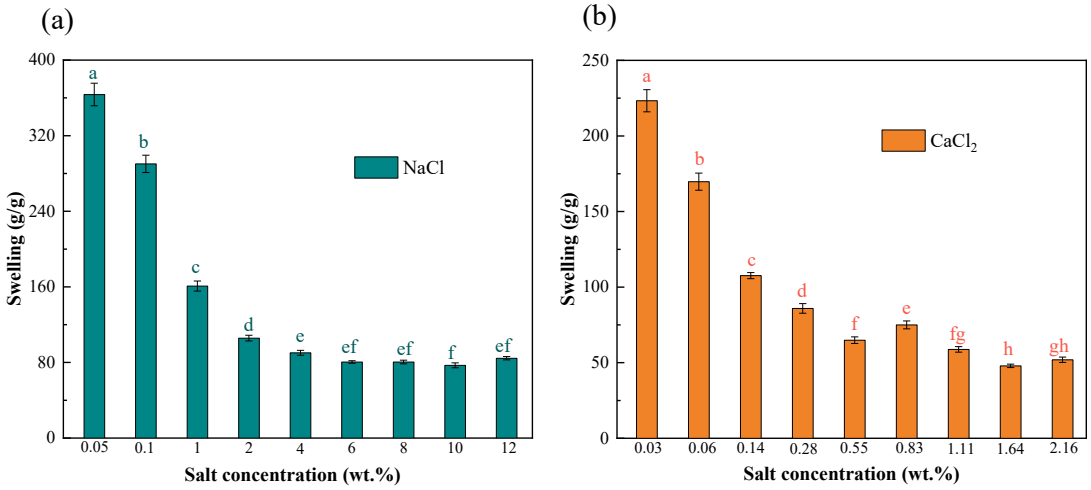

Figure 2.4. Water absorbencies in different salt concentrations and salt solutions. (a) NaCl solution; (b) $CaCl_2$ solution. Different lowercase letters indicate significant differences between treatments ($P < 0.05$)

2.3.4.2 MIP of CT for adsorption of calcium salt in ST-SAP

Due to the significant impact of Ca^{2+} on ST-SAP properties, an adsorption isotherm experiment was performed to examine the adsorption of Ca^{2+} by ST-SAP, which revealed that Ca^{2+} is easily adsorbed onto ST-SAP. Further details are available in the supplementary materials.

To know the Ca^{2+} adsorption by ST-SAP, the ST-SAP (0.1000±0.0001 g) was set at different concentrations of $CaCl_2$ until swelling equilibrium, and results were fitted using the Langmuir and Freundlich models:

Langmuir model:

$$Q_e = k_l Q_m C_e / (1 + k C_e) \quad \text{(Eq. 7)}$$

Freundlich model:

$$Q_e = k_f C_e^{(1/n)} \quad \text{(Eq. 8)}$$

Where C_e (g/L) and Q_e(g/g): equilibrium concentrations of the solution; Q_e (g/g) and Q_m (g/g): balanced and maximum adsorption ratio of ST-SAP, respectively; k_l (L/g): Langmuir constant; k_f (g/g): Freundlich constant, and *1/n*: adsorption intensity index.

The fitting model parameters were listed in Table 3.4. Freundlich fits better to the adsorption process, whose R^2 reached 0.998. Remarkably, 1/n reflects was <0.5, indicating that Ca^{2+} was easily adsorbed in the ST-SAP (Figure 3.5).

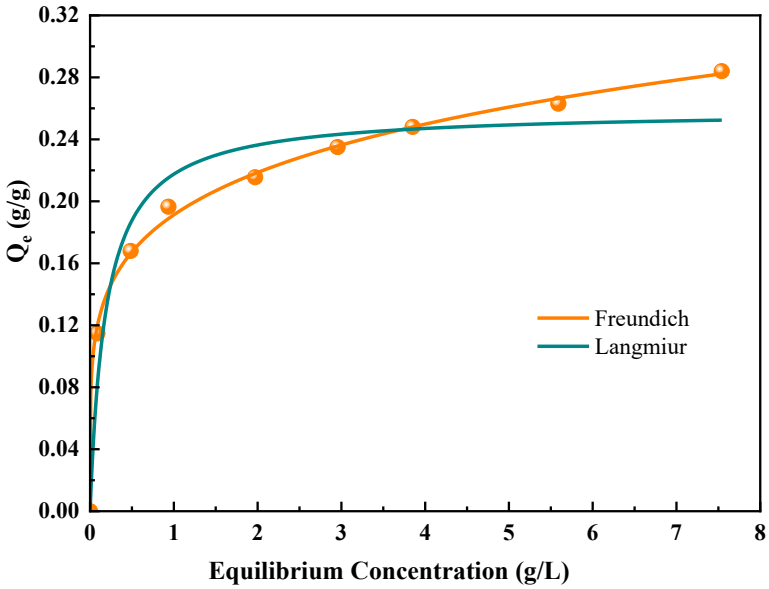

Figure 2.5. Adsorption isotherm for Ca^{2+} absorption

Table 2.4. Adsorption isotherm parameters for the adsorption of Ca^{2+} by the salt-tolerant superabsorbent polymer (ST-SAP)

Langmuir			**Freundlich**		
Q_m (g/g)	k_l (L/g)	R_1^2	1/n	k_f (L/g)	R_2^2
0.259	5.282	0.937	0.193	0.191	0.998

Langmuir			**Freundlich**		
Q_m (g/g)	k_l (L/g)	R_1^2	1/n	k_f (L/g)	R_2^2
0.259	5.282	0.937	0.193	0.191	0.998

The maximum intensity projection (MIP) (Kuhl et al., 2014) utilizes the perspective method to project the pixel with the highest density in the original image

onto a two-dimensional plane, and forms finally a reconstructed image with the maximum density. It is commonly employed in medical diagnostics for assessing physical ailments (Kuhl et al., 2014; L. Zellweger et al., 2022). Herein, MIP of CT was utilized to observe the materials that absorbing deionized water and 2.09 wt% $CaCl_2$ respectively (Figure 2.6). The former (Figs. 2.6a and b) showed a more homogeneous distribution and lower density than the latter (Figs. 2.6c and d). Since the density of Ca^{2+} and Cl^- are significantly different from ST-SAP; Figure 2.6d presents the distributions of Ca^{2+} and Cl^- in ST-SAP. Therefore, in this chapter, the adsorption isotherm results show that Ca is easily adsorbed by ST-SAP, and MIP intuitively presents the distribution of CA in ST-SAP.

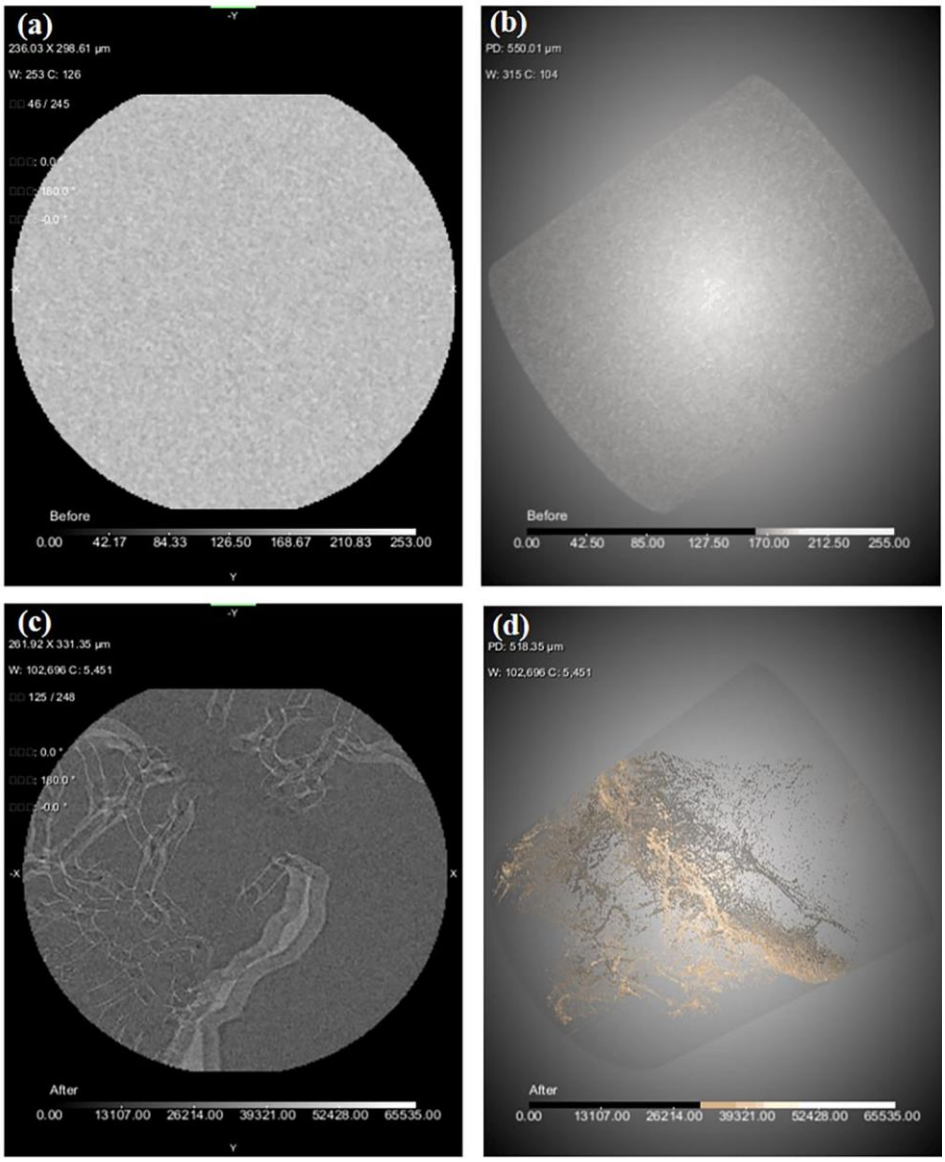

Figure 2.6. 2D images and reconstructed images of the maximum intensity projection of the salt-tolerant superabsorbent polymer after absorbing water (a and b, respectively) and after absorbing soluble $CaCl_2$ (c and d, respectively

2.3.4.3 Spectroscopies of X-ray photoelectron and Fourier transform infrared for complexation mechanism of calcium with ST-SAP

The results of the adsorption isotherm (Figure S5.1, Table S5.2) confirmed that Ca^{2+} was easily adsorbed onto ST-SAP. The adsorption mechanism was further analyzed using X-ray photoelectron and Fourier transform infrared spectroscopies (XPS and FT-IR). The survey spectrum and high-resolution spectra of ST-SAP adsorbing Ca^{2+} (Figure 2.7a) indicates that, after adsorbing, new peaks of Ca appeared in the survey spectra, confirming that Ca^{2+} reacted with ST-SAP. The corresponding change in ion content showed that Ca^{2+} reached 9.92%, while Na decreased from 5.36% to 0.49%. The ion exchange between Ca^{2+} and Na^{+} occurred during the adsorption process due to the stronger affinity of the functional groups of ST-SAP for Ca^{2+} than Na^{+} (Lee et al., 2018).

In Figure 2.7b, the high-resolution C 1s spectra split into four peaks: C-C at 284.8 eV, C=O at 287.99 eV, C-O at 286.3 eV, C-N/C-S at 285.6 eV (Vilani et al., 2007). After absorbing, the binding energy of C=O and C-O increased up to 288.42 eV and 286.56 eV, respectively. Figure 2.7c shows two separate peaks in the O 1s spectra: C-O at 531.42 eV and C=O/S=O at 532.7 eV (Luo et al., 2021). These peaks can be attributed to R-COO-, R-$CONH_2$, and R-SO_3H, respectively, and shifted towards higher binding energy after adsorption. In the S 2p spectra presents two peaks at 167.9 eV and 169.2 eV (Figure 2.7d), corresponding to S $2p_{3/2}$ and S $2p_{1/2}$ respectively, which also shifted towards higher binding energy (Chen et al., 2017). This shift can be attributed to the decreasing oxygen electron cloud density after adsorption (Wu and Li, 2013). Therefore, it can be inferred that R-$CONH_2$, R-SO_3H, R-COO^{-} had complexation reactions with Ca^{2+}.

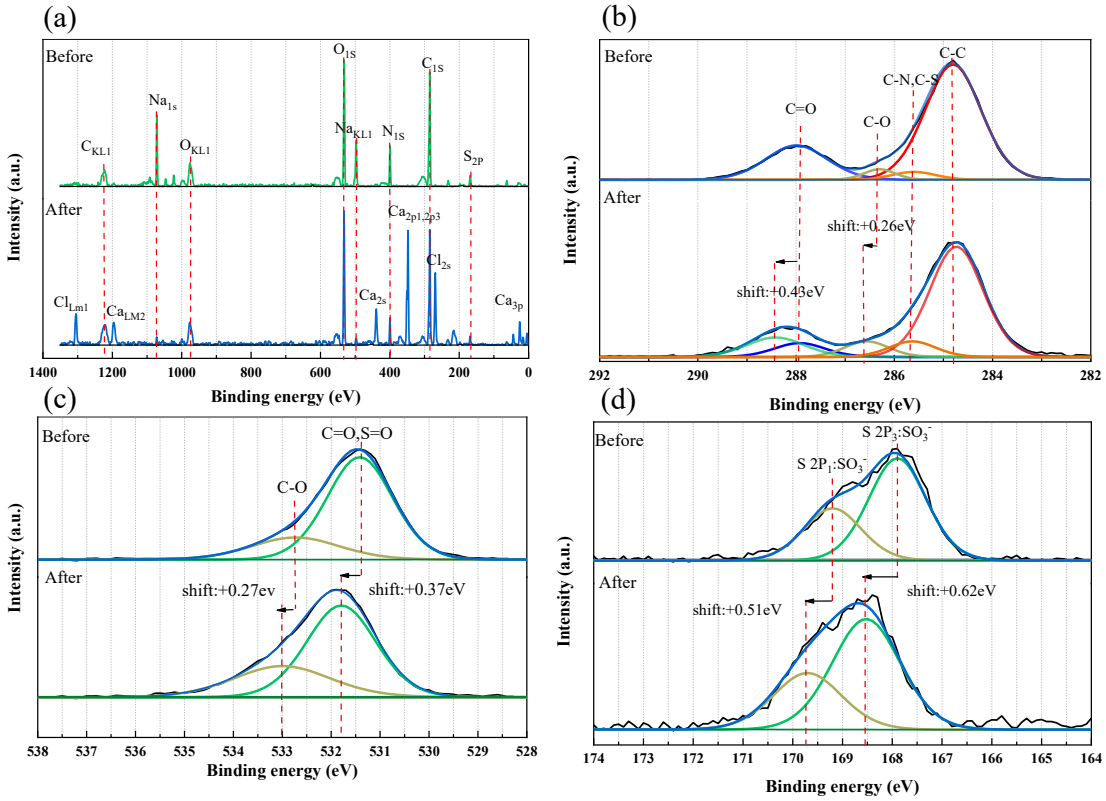

Figure 2.7 X-ray photoelectron spectroscopies of the salt-tolerant superabsorbent polymer (ST-SAP) before and after absorbing Ca^{2+} (a) survey scans spectra; (b, c and d) high-resolution C1s, O 1s, and S 2p spectra, respectively.

According to Pluharova et al. (2014), Ca was coordinated and collinear with an O atom in the amide (Figure 2.8a). Sulfonic acid (-SO_3H) group has a poor binding ability to metallic cations, only one O atom combined with Ca two sulfonates, $-S(=O)_2-O^-$ (Figure 2.8b) (Bagaria et al., 2013Shubnell et al., 1994).

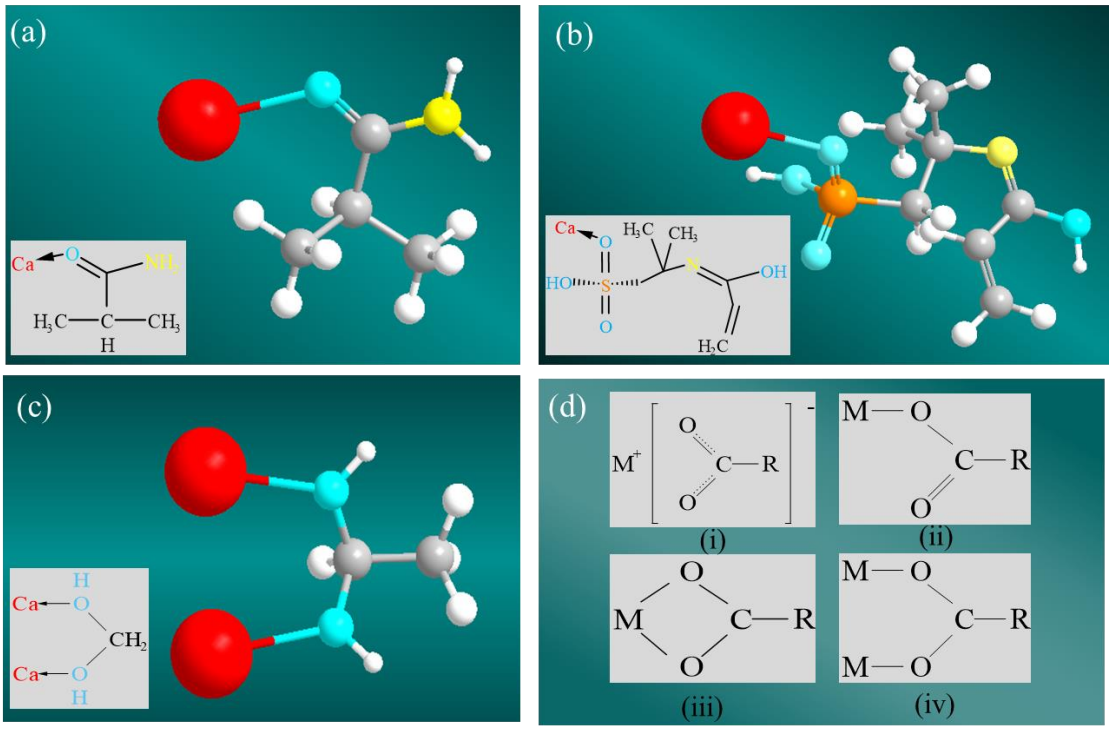

Figure 2.8. (a to c) Schematic diagrams of the coordination binding of Ca^{2+} to three functional groups: amide group, sulfonic acid group, and carboxylate group, respectively. (d) Four types of metal-carboxylate complexes form: (i) an ionic or uncoordinated form, (ii) unidentate coordination, (iii) bidentate chelating coordination, and (iv) bidentate bridging coordination

The formation of metal-carboxylate complexes can be classified into four types according to Mehrotra and Bohra (1983) and Barajas et al. (2022): (i) an ionic or uncoordinated form, (ii) unidentate coordination, (iii) bidentate chelating coordination, and (iv) bidentate bridging coordination (Figure 2.8d).

The coordination mode is determined by steric hindrance (Plank and Sachsenhauser, 2009). Qian et al. (2017) theorized that $CaCl_2$/PAA formed a tetradentate complex when the coordination interaction between Ca^{2+} and R-COO^- was saturated. Zhang and Qiao (2021) proposed that the coordination of R-COO^- and Ca^{2+} was bidentate chelating. In order to elucidate the interaction mechanism between Ca^{2+} and R-COO^- in the network structure of ST-SAP, the material adsorbing Ca^{2+} was characterized by Fourier-transform infrared (Gliemann, 1978).

In the region of 1350-1750 cm^{-1} at the FT-IR spectrum, the difference between $\nu_{asym}(COO^{-})$ and $\nu_{sym}(COO^{-})$ bands are used to determine the type of metal-carboxylate coordination (Filipiuk et al., 2005; Palacios et al., 2004; Papageorgiou et al., 2010). The different coordination modes correspond to different frequencies, which are sensitive to the structure of the carboxylate group and metallic properties. Therefore, metal-carboxylate coordination type can be determined by the difference (i.e., $\Delta\nu$ CO_{asym}-CO_{sym}), as Nakamoto (Gliemann, 1978).

For the bidentate chelating coordination:

$$\Delta\nu(COO^{-})_{complex} \ll \Delta\nu(COO^{-})_{Na} \quad \text{(Eq. 9)}$$

For the bidentate bridging coordination:

$$\Delta\nu(COO^{-})_{complex} \leqslant \Delta\nu(COO^{-})_{Na} \quad \text{(Eq. 10)}$$

For monodentate geometry of the carboxylate group:

$$\Delta\nu(COO^{-})_{complex} \gg \Delta\nu(COO^{-})_{Na} \quad \text{(Eq. 11)}$$

The previous study (Zhang and Qiao, 2021) cleared that the R-COOH has been coordinated with the Na^{+} during the polymerization process. Therefore, $\Delta\nu(COO^{-})_{Na}$ corresponded the difference between $\nu_{asym}(COO^{-})$ and $\nu_{sym}(COO^{-})$ bands (Figure 2.9).

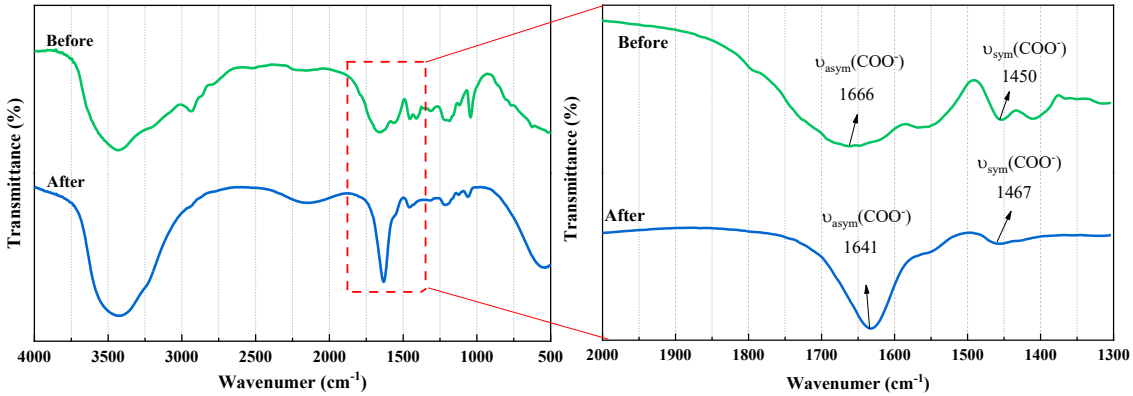

Figure 2.9. The Fourier transform infrared spectra of ST-SAP before and after absorbing Ca^{2+}. The partial enlargement of the 2000-1300 cm^{-1} spectrum

Table 2.5. Fourier Transform Infrared absorption peaks of $\nu_{asym}(COO^{-})$, $\nu_{sym}(COO^{-})$ and the differences

Parameters	$\nu_{asym}(COO^{-})$	$\nu_{sym}(COO^{-})$	$\Delta\nu(COO^{-})$
Na^{+}	1670	1450	220
Ca^{2+}	1641	1467	174

According to the Figure 2.9 and Table 2.3, the value for $\Delta\nu(COO\text{-})_{Ca}$ was less than or equal to $\Delta\nu(COO\text{-})_{Na}$, which is consistent with the finding of Sergios K (Papageorgiou et al., 2010). Based on Equation 9, the Ca-carboxylate coordination type

of ST-SAP is bidentate bridging form (Figure 2.8c). The above results demonstrate that all three hydrophilic monomers (R-COO^-, R-$CONH_2$, R-SO_3H) complex with Ca^{2+}, which contribute to the excellent stability of ST-SAP during the reswelling process and in different concentrations of salt solutions (as described in chapters 5.3.3.2 and 5.3.4.1).

2.3.5 Water retention properties under high salt condition

2.3.5.1 Slow-release water property after adsorbing mixed saline solution

The foregoing study indicated that ST-SAP exhibit favorable swelling properties under high salt condition, which was a prerequisite for excellent slow-release properties. To further evaluate the slow-release performance, the release time of ST-SAP absorbing mixed saline solution was measured. The result showed that ST-SAP prolonged the water retention time of mixed saline solution by 20 h (Figure 2.10a). Water presented three states in ST-SAP: free water, freezable bound water, and non-freezable. While free water was lost at first by evaporation, freezable bound and non-freezable water directly or indirectly forming hydrogen bonds with hydrophilic groups in ST-SAP structures, making their release more difficult than that of free water. Freezable bound and non-freezable water are important factors contributing to water retention properties. An excellent slow-release water properties of ST-SAP under high salt conditions was obtained (Figure 2.10a).

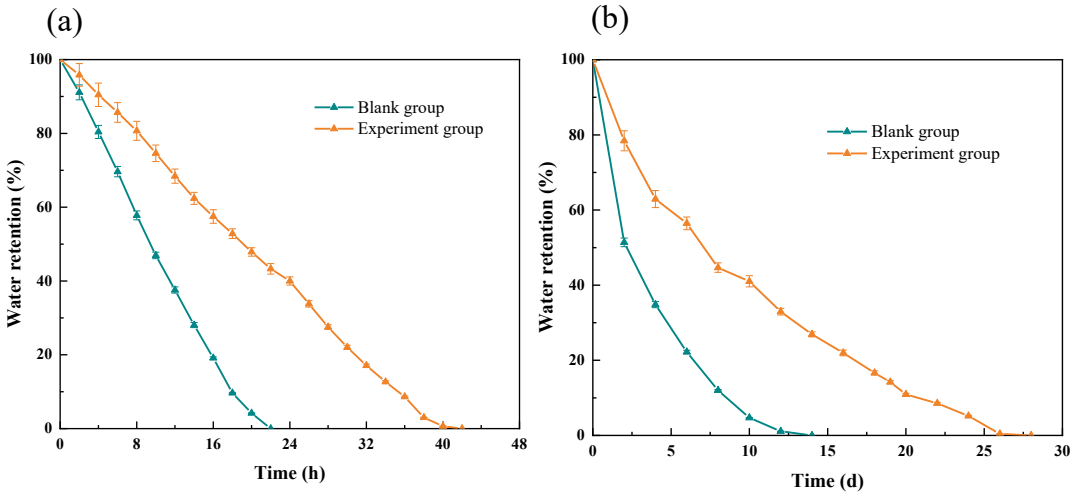

Figure 2.10. (a) Water retention time after adsorbing mixed saline solution. (b) Water retention properties applying to high salinity soil

2.3.5.2 Water retention properties applying in saline-alkali soil of high salinity

ST-SAP was added to Lop Nur saline-alkali soil, and the water retention time was evaluated. Compared with the blank control, the soil moisture retention time was prolonged to 28 days after adding ST-SAP (Figure 2.11b). This can be attributed to the favorable slow-release water characteristic of ST-SAP, as discussed in section 3.5.1. In contrast to previous studies, the moisture retention time of carboxylated nanocellulose superabsorbent polymer prepared by Ruth (Barajas et al., 2022), was 25-33 days for

soils with lower salinity (14 mg/Kg Na^{+}, 156 mg/Kg K^{+}, 521 mg/Kg Ca^{2+}, and 139 mg/Kg Mg^{2+}). FGB (C. Liu et al., 2020) kept 11.5 days at 50 ℃. With 4 wt% CHCAUR (Narayanan et al., 2018), soil kept moisture for 17 days at 35 ℃. NaHMC-g-P (AA-co-AMPS)/laterite ST-SAP (Cheng et al., 2019) kept for 100-120 h at room temperature. Therefore, ST-SAP is highly effective in improving moisture retention of saline soil.

The morphologies of the two soil groups were observed (Figure 2.11) after the soil samples reaching a constant weight. The soil with ST-SAP was encased in the polymer, which may further reduce soil moisture evaporation (Figure 2.11d).

In addition, ST-SAP facilitates the formation of large soil aggregates, resulting in a change in the original dense structure of soil (Figure 2.11c). The loose and porous soil structure facilitated the transport of water, nutrients, air, and dissolved organic carbon (Kraychenko et al., 2019). It indicates that the application of ST-SAP in saline-alkali land not only inhibited the evaporation of water but also improved the soil quality.

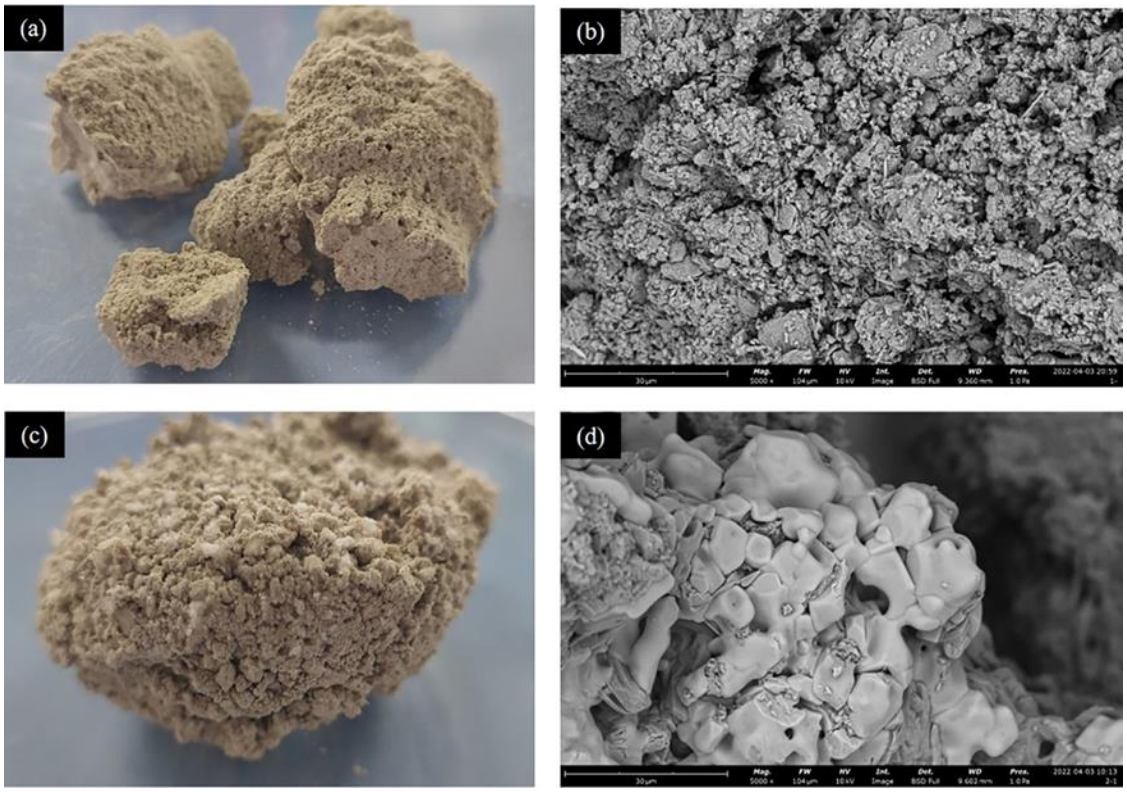

Figure 2.10. Soil photographs after complete water evaporation. (a-b) Soil without ST-SAP ((a) photo taken with a camera;(b) SEM image). (c-d) Soil with 2%(wt) ST-SAP ((a and c) photos taken with a camera; (b and d) SEM images). ST-SAP: the salt-tolerant superabsorbent polymer (ST-SAP); SEM: Scanning electron microscope

2.4 Conclusions

This research, in essence, comes to the following conclusions.

(1) With the three strong hydrophilic groups (R-SO_3H, R-COOH, R-$CONH_2$), ST-SAP has excellent swelling ability, which reaches up to 69.04 g/g under high salt condition.

(2) ST-SAP can effectively realize multiple reswelling under high salt condition.

(3) The complexation reaction between Ca^{2+} and three hydrophilic groups of ST-SAP contributes to its remarkable stability under high salt condition.

(4) With 2 wt% ST-SAP, the moisture of saline-alkali soil could be prolonged to 28 days.

These findings highlight the strong potential of ST-SAP for practical applications in saline-alkali land management and agricultural water conservation.

The main content in this chapter was published:

- ✓ **Zhang C**, García-Meza JV, Zhou KQ, et al. Superabsorbent polymer used for saline-alkali soil water retention[J]. Journal of the Taiwan Institute of Chemical Engineers, 2023, 145: 104830. (JCR Q1; IF=6.3). (**JCR Q1; IF 6.3**)

2.5 References

Ahmed, E.M., 2015. Hydrogel: Preparation, characterization, and applications: A review. J. Adv. Res. 6, 105–121. https://doi.org/https://doi.org/10.1016/j.jare.2013.07.006

Al-Othman, Z.A., Ali, R., Naushad, M., 2012. Hexavalent chromium removal from aqueous medium by activated carbon prepared from peanut shell: Adsorption kinetics, equilibrium and thermodynamic studies. Chem. Eng. J. 184, 238–247. https://doi.org/10.1016/j.cej.2012.01.048

Ali, S., Rizwan, M., Qayyum, M.F., Ok, Y.S., Ibrahim, M., Riaz, M., Arif, M.S., Hafeez, F., Al-Wabel, M.I., Shahzad, A.N., 2017. Biochar soil amendment on alleviation of drought and salt stress in plants: a critical review. Environ. Sci. Pollut. Res. 24, 12700–12712. https://doi.org/10.1007/s11356-017-8904-x

Bagaria, H.G., Xue, Z., Neilson, B.M., Worthen, A.J., Yoon, K.Y., Nayak, S., Cheng, V., Lee, J.H., Bielawski, C.W., Johnston, K.P., 2013. Iron Oxide Nanoparticles Grafted with Sulfonated Copolymers are Stable in Concentrated Brine at Elevated Temperatures and Weakly Adsorb on Silica. ACS Appl. Mater. Interfaces 5, 3329–3339. https://doi.org/10.1021/am4003974

Barajas, R.M., Wong, V., Little, K., Patti, A.F., Garnier, G., 2022. Carboxylated nanocellulose superabsorbent: Biodegradation and soil water retention properties. J. Appl. Polym. Sci. 139. https://doi.org/10.1002/app.51495

Berthold, J., Rinaudo, M., Salmeń, L., 1996. Association of water to polar groups; estimations by an adsorption model for ligno-cellulosic materials. Colloids Surfaces A Physicochem. Eng. Asp. 112, 117–129. https://doi.org/https://doi.org/10.1016/0927-7757(95)03419-6

Cai, J., 2004. Structural chemistry and properties of metal arenesulfonates. Coord. Chem. Rev. 248, 1061–1083. https://doi.org/10.1016/j.ccr.2004.06.014

Chen, K., He, J., Li, Y., Cai, X., Zhang, K., Liu, T., Hu, Y., Lin, D., Kong, L., Liu, J., 2017. Removal of cadmium and lead ions from water by sulfonated magnetic nanoparticle adsorbents. J. Colloid Interface Sci. 494, 307–316. https://doi.org/https://doi.org/10.1016/j.jcis.2017.01.082

Cheng, S., Liu, X., Zhen, J., Lei, Z., 2019. Preparation of superabsorbent resin with fast water absorption rate based on hydroxymethyl cellulose sodium and its application. Carbohydr. Polym. 225, 115214. https://doi.org/10.1016/j.carbpol.2019.115214

Cui, Q., Xia, J., Yang, H., Liu, J., Shao, P., 2021. Biochar and effective microorganisms promote Sesbania cannabina growth and soil quality in the coastal saline-alkali soil of the Yellow River Delta, China. Sci. Total Environ. 756, 143801. https://doi.org/10.1016/j.scitotenv.2020.143801

Du, Q.J., Sun, J.K., Li, Y.H., Yang, X.X., Wang, X.H., Wang, Z.H., Xia, L.H., 2014. Highly enhanced adsorption of congo red onto graphene oxide/chitosan fibers by wet-chemical etching off silica nanoparticles. Chem. Eng. J. 245, 99–106. https://doi.org/10.1016/j.cej.2014.02.006

Esmaeili, A., Saremnia, B., 2016. Synthesis and characterization of NaA zeolite nanoparticles from Hordeum vulgare L. husk for the separation of total petroleum hydrocarbon by an adsorption process. J. Taiwan Inst. Chem. Eng. 61, 276–286. https://doi.org/10.1016/j.jtice.2015.12.031

Filipiuk, D., Fuks, L., Majdan, M., 2005. Transition metal complexes with uronic acids. J. Mol. Struct. 744, 705–709.

Flory, P.J., 1953. Principles of polymer chemistry. Cornell university press.

Gliemann, G., 1978. K. Nakamoto: Infrared and Raman Spectra of Inorganic and Coordination Compounds. John Wiley and Sons, New York, Chichester, Brisbane, Toronto 1978. 3. Aufl., XV, 448 Seiten mit 109 Abbildungen und 95 Tabellen. Preis: $31, 15.

He, G., Ke, W., Chen, X., Kong, Y., Zheng, H., Yin, Y., Cai, W., 2017. Preparation and properties of quaternary ammonium chitosan-g-poly(acrylic acid-co-acrylamide) superabsorbent hydrogels. React. Funct. Polym. 111, 14–21. https://doi.org/https://doi.org/10.1016/j.reactfunctpolym.2016.12.001

He, Q., Ren, Jia, Ren, Junkai, Pang, K., Ma, Z., Zhu, X., Song, R., 2017. Polymethylene-b-poly (acrylic acid) diblock copolymers: Aggregation and crystallization in the presence of CaCl2. Eur. Polym. J. 95, 174–185. https://doi.org/10.1016/j.eurpolymj.2017.08.003

Kabiri, K., Omidian, H., Zohuriaan-Mehr, M.J., Doroudiani, S., 2011. Superabsorbent Hydrogel Composites and Nanocomposites: A Review. Polym. Compos. 32, 277–289. https://doi.org/10.1002/pc.21046

Kabiri, K., Zohuriaan-Mehr, M.J., 2003. Superabsorbent hydrogel composites. Polym. Adv. Technol. 14, 438–444. https://doi.org/10.1002/pat.356

Kabiri, K., Zohuriaan-Mehr, M.J., Mirzadeh, H., Kheirabadi, M., 2010. Solvent-, ion- and pH-specific swelling of poly(2-acrylamido-2-methylpropane sulfonic acid) superabsorbing gels. J. Polym. Res. 17, 203–212. https://doi.org/10.1007/s10965-009-9306-7

Kim, D., Park, K., 2004. Swelling and mechanical properties of superporous hydrogels of poly (acrylamide-co-acrylic acid)/polyethylenimine interpenetrating polymer networks. Polymer (Guildf). 45, 189–196. https://doi.org/10.1016/j.polymer.2003.10.047

Kraychenko, A.N., Guber, A.K., Razavi, B.S., Koestel, J., Quigley, M.Y., Robertson, G.P., Kuzyakov, Y., 2019. Microbial spatial footprint as a driver of soil carbon stabilization. Nat. Commun. 10. https://doi.org/10.1038/s41467-019-11057-4

Kuhl, C.K., Schrading, S., Strobel, K., Schild, H.H., Hilgers, R.-D., Bieling, H.B., 2014. Abbreviated Breast Magnetic Resonance Imaging (MRI): First Postcontrast Subtracted Images and Maximum-Intensity Projection—A Novel Approach to Breast Cancer Screening With MRI. J. Clin. Oncol. 32, 2304–2310. https://doi.org/10.1200/JCO.2013.52.5386

Lee, H.X.D., Wong, H.S., Buenfeld, N.R., 2018. Effect of alkalinity and calcium concentration of pore solution on the swelling and ionic exchange of

superabsorbent polymers in cement paste. Cem. Concr. Compos. 88, 150–164. https://doi.org/10.1016/j.cemconcomp.2018.02.005

Li, A., Zhang, J., Wang, A., 2007. Utilization of starch and clay for the preparation of superabsorbent composite. Bioresour. Technol. 98, 327–332. https://doi.org/10.1016/j.biortech.2005.12.026

Li, X., Li, Q., Xu, X., Su, Y., Yue, Q., Gao, B., 2016. Characterization, swelling and slow-release properties of a new controlled release fertilizer based on wheat straw cellulose hydrogel. J. Taiwan Inst. Chem. Eng. 60, 564–572.

Liu, C., Lei, F., Li, P., Jiang, J., Wang, K., 2020. Borax crosslinked fenugreek galactomannan hydrogel as potential water-retaining agent in agriculture. Carbohydr. Polym. 236. https://doi.org/10.1016/j.carbpol.2020.116100

Liu, Y., Su, M., Fu, Y., Zhao, P., Xia, M., Zhang, Y., He, B., He, P., 2018. Corrosive environments tolerant, ductile and self-healing hydrogel for highly efficient oil/water separation. Chem. Eng. J. 354, 1185–1196. https://doi.org/10.1016/j.cej.2018.08.071

Luo, Q., Huang, X., Luo, Y., Yuan, H., Ren, T., Li, X., Xu, D., Guo, X., Wu, Y., 2021. Fluorescent chitosan-based hydrogel incorporating titanate and cellulose nanofibers modified with carbon dots for adsorption and detection of Cr(VI). Chem. Eng. J. 407, 127050. https://doi.org/https://doi.org/10.1016/j.cej.2020.127050

Mehrotra, R.C., Bohra, R., 1983. Metal carboxylates. Academic Press.

Mischke, S., Zhang, C.J., Liu, C.L., Zhang, J.F., Jiao, P.C., Plessen, B., 2019. The Holocene salinity history of Lake Lop Nur (Tarim Basin, NW China) inferred from ostracods, foraminifera, ooids and stable isotope data. Glob. Planet. Change 175, 1–12. https://doi.org/10.1016/j.gloplacha.2019.01.017

Mohamadian, N., Ghorbani, H., Wood, D.A., Khoshmardan, M.A., 2019. A hybrid nanocomposite of poly (styrene-methyl methacrylate-acrylic acid)/clay as a novel rheology-improvement additive for drilling fluids. J. Polym. Res. 26, 1–14.

Mohammadbagheri, Z., Rahmati, A., Hoshyarmanesh, P., 2021. Synthesis of a novel superabsorbent with slow-release urea fertilizer using modified cellulose as a grafting agent and flexible copolymer. Int. J. Biol. Macromol. 182, 1893–1905. https://doi.org/https://doi.org/10.1016/j.ijbiomac.2021.05.191

Narayanan, A., Kartik, R., Sangeetha, E., Dhamodharan, R., 2018. Super water absorbing polymeric gel from chitosan, citric acid and urea: Synthesis and mechanism of water absorption. Carbohydr. Polym. 191, 152–160. https://doi.org/https://doi.org/10.1016/j.carbpol.2018.03.028

Olad, A., Pourkhiyabi, M., Gharekhani, H., Doustdar, F., 2018. Semi-IPN superabsorbent nanocomposite based on sodium alginate and montmorillonite: Reaction parameters and swelling characteristics. Carbohydr. Polym. 190, 295–306. https://doi.org/10.1016/j.carbpol.2018.02.088

Otsu, N., 1979. A threshold selection method from gray-level histograms. IEEE Trans. Syst. Man. Cybern. 9, 62–66.

Palacios, E.G., Juarez-Lopez, G., Monhemius, A.J., 2004. Infrared spectroscopy of metal carboxylates - II. Analysis of Fe(III), Ni and Zn carboxylate solutions. HYDROMETALLURGY 72, 139–148. https://doi.org/10.1016/S0304-386X(03)00137-3

Panic, V., Adnadjevic, B., Velickovic, S., Jovanovic, J., 2010. The effects of the synthesis parameters on the xerogels structures and on the swelling parameters of the poly(methacrylic acid) hydrogels. Chem. Eng. J. 156, 206–214. https://doi.org/https://doi.org/10.1016/j.cej.2009.10.040

Papageorgiou, S.K., Kouvelos, E.P., Favvas, E.P., Sapalidis, A.A., Romanos, G.E., Katsaros, F.K., 2010. Metal-carboxylate interactions in metal-alginate complexes studied with FTIR spectroscopy. Carbohydr. Res. 345, 469–473. https://doi.org/10.1016/j.carres.2009.12.010

Ping, Z.H., Nguyen, Q.T., Chen, S.M., Zhou, J.Q., Ding, Y.D., 2001. States of water in different hydrophilic polymers Ð DSC and FTIR studies 42.

Plank, J., Sachsenhauser, B., 2009. Experimental determination of the effective anionic charge density of polycarboxylate superplasticizers in cement pore solution. Cem. Concr. Res. 39, 1–5. https://doi.org/10.1016/j.cemconres.2008.09.001

Pluharova, E., Baer, M.D., Mundy, C.J., Schmidt, B., Jungwirth, P., 2014. Aqueous Cation-Amide Binding: Free Energies and IR Spectral Signatures by Ab Initio Molecular Dynamics. J. Phys. Chem. Lett. 5, 2235–2240. https://doi.org/10.1021/jz500976m

Rashidzadeh, A., Olad, A., 2014. Slow-released NPK fertilizer encapsulated by NaAlg-g-poly(AA-co-AAm)/MMT superabsorbent nanocomposite. Carbohydr. Polym. 114, 269–278. https://doi.org/10.1016/j.carbpol.2014.08.010

Rizwan, M., Gilani, S.R., Durrani, A.I., Naseem, S., 2022. Kinetic model studies of controlled nutrient release and swelling behavior of combo hydrogel using Acer platanoides cellulose. J. Taiwan Inst. Chem. Eng. 131, 104137.

Saha, A., Sekharan, S., Manna, U., 2020. Superabsorbent hydrogel (SAH) as a soil amendment for drought management: A review. SOIL TILLAGE Res. 204. https://doi.org/10.1016/j.still.2020.104736

Schreiner, S., Dawant, B.M., Paschal, C.B., Galloway, R.L., 1996. The importance of ray pathlengths when measuring objects in maximum intensity projection images. IEEE Trans. Med. Imaging 15, 560–567. https://doi.org/10.1109/42.511759

Shubnell, A.J., Kosnic, E.J., Squattrito, P.J., 1994. Structures of layered metal sulfonate salts: trends in coordination behavior of alkali, alkaline earth and transition metals. Inorganica Chim. Acta 216, 101–112.

Simonin, J.-P., 2016. On the comparison of pseudo-first order and pseudo-second order rate laws in the modeling of adsorption kinetics. Chem. Eng. J. 300, 254–263. https://doi.org/https://doi.org/10.1016/j.cej.2016.04.079

Song, L., Qian, J., Zhang, F., Kong, X., Li, H., Luan, S., Zhang, Q., Kang, Z., Han, Z., Zhang, Z., 2022. An ecological remediation model combining optimal substrate amelioration and native hyperaccumulator colonization in non-ferrous metal

tailings pond. J. Environ. Manage. 322. https://doi.org/10.1016/j.jenvman.2022.116141

Tally, M., Atassi, Y., 2015. Optimized synthesis and swelling properties of a pH-sensitive semi-IPN superabsorbent polymer based on sodium alginate-g-poly(acrylic acid-co-acrylamide) and polyvinylpyrrolidone and obtained via microwave irradiation. J. Polym. Res. 22. https://doi.org/10.1007/s10965-015-0822-3

Vilani, C., Weibel, D.E., Zamora, R.R.M., Habert, A.C., Achete, C.A., 2007. Study of the influence of the acrylic acid plasma parameters on silicon and polyurethane substrates using XPS and AFM. Appl. Surf. Sci. 254, 131–134. https://doi.org/https://doi.org/10.1016/j.apsusc.2007.07.060

Wang, P.-H., Lin, C.-H., Wen, T.-C., 2020. Tough and antifouling polyampholyte hydrogels via photopolymerization of equivalent ionic monomers with poly(ethylene glycol) diacrylate. J. TAIWAN Inst. Chem. Eng. 113, 101–106. https://doi.org/10.1016/j.jtice.2020.08.027

Wang, Z.M., Shi, H.X., Wang, F., Wang, A.R., He, Q., Cuan, S.S., 2021. Synthesis of cassava starch-g-acrylic acid/dimethylaminopropyl methacrylamide: A new hydrogel for brine solution. Carbohydr. Polym. 266. https://doi.org/10.1016/j.carbpol.2021.118109

Wei, L.M., Zhu, Y.Q., Deng, J.S., Li, Y.H., Li, M.H., Lu, H.T., Zhao, Y.W., 2021. Visualization of Thrombus Enhancement on Thin-Slab Maximum Intensity Projection of CT Angiography: An Imaging Sign for Predicting Stroke Source and Thrombus Compositions. Radiology 298, 374–381. https://doi.org/10.1148/radiol.2020201548

Womack, N.C., Piccoli, I., Camarotto, C., Squartini, A., Guerrini, G., Gross, S., Maggini, M., Cabrera, M.L., Morari, F., 2022. Hydrogel application for improving soil pore network in agroecosystems. Preliminary results on three different soils. CATENA 208, 105759. https://doi.org/https://doi.org/10.1016/j.catena.2021.105759

Wu, J.H., Wei, Y.L., Lin, H.M., Lin, S.B., 2003. Study on starch-graft-acrylamide/mineral powder superabsorbent composite. Polymer (Guildf). 44, 6513–6520. https://doi.org/10.1016/S0032-3861(03)00728-6

Wu, N., Li, Z., 2013. Synthesis and characterization of poly(HEA/MALA) hydrogel and its application in removal of heavy metal ions from water. Chem. Eng. J. 215–216, 894–902. https://doi.org/https://doi.org/10.1016/j.cej.2012.11.084

Xiao, X., Yu, L., Xie, F., Bao, X., Liu, H., Ji, Z., Chen, L., 2017. One-step method to prepare starch-based superabsorbent polymer for slow release of fertilizer. Chem. Eng. J. 309, 607–616. https://doi.org/10.1016/j.cej.2016.10.101

Xie, L., Liu, M., Ni, B., Wang, Y., 2012. Utilization of Wheat Straw for the Preparation of Coated Controlled-Release Fertilizer with the Function of Water Retention. J. Agric. Food Chem. 60, 6921–6928. https://doi.org/10.1021/jf3001235

Xiong, H., Peng, H., Kong, Y., Wang, N., Yang, F., 2022. Soil & Tillage Research High salt tolerance hydrogel prepared of hydroxyethyl starch and its ability to increase soil water holding capacity and decrease water evaporation 222. https://doi.org/10.1016/j.still.2022.105427

Xiying Jing, Shili Chen, S.M., 1992. A Practical Guide to Infrared Spectroscopy. Tianjin Science and Technology, Tianjin.

Yang, M.M., Wu, J.H., Graham, G.M., Lin, J.M., Huang, M.L., 2021. Hotspots, Frontiers, and Emerging Trends of Superabsorbent Polymer Research: A Comprehensive Review. Front. Chem. 9. https://doi.org/10.3389/fchem.2021.688127

Zellweger, C., Berger, N., Wieler, J., Cioni, D., Neri, E., Boss, A., Frauenfelder, T., Marcon, M., 2022. Breast Computed Tomography: Diagnostic Performance of the Maximum Intensity Projection Reformations as a Stand-Alone Method for the Detection and Characterization of Breast Findings. Invest. Radiol. 57, 205–211. https://doi.org/10.1097/RLI.0000000000000829

Zhang, J.-P., Zhang, F.-S., 2018. Recycling waste polyethylene film for amphoteric superabsorbent resin synthesis. Chem. Eng. J. 331, 169–176. https://doi.org/https://doi.org/10.1016/j.cej.2017.08.058

Zhang, J., Li, A., Wang, A., 2006. Study on superabsorbent composite. VI. Preparation, characterization and swelling behaviors of starch phosphate-graft-acrylamide/attapulgite superabsorbent composite. Carbohydr. Polym. 65, 150–158. https://doi.org/10.1016/j.carbpol.2005.12.035

Zhang, M., Dong, B., Qiao, Y., Yang, H., Wang, Y., Liu, M., 2018. Effects of sub-soil plastic film mulch on soil water and salt content and water utilization by winter wheat under different soil salinities. F. Crop. Res. 225, 130–140. https://doi.org/10.1016/j.fcr.2018.06.010

Zhang, P., Bing, X., Jiao, L., Xiao, H., Li, B., Sun, H., 2022. Amelioration effects of coastal saline-alkali soil by ball-milled red phosphorus-loaded biochar. Chem. Eng. J. 431, 133904. https://doi.org/10.1016/j.cej.2021.133904

Zhang, W.X., Wang, P., Liu, S.F., Chen, J., Chen, R., He, X.Y., Ma, G.F., Lei, Z.Q., 2021. Factors affecting the properties of superabsorbent polymer hydrogels and methods to improve their performance: a review. J. Mater. Sci. 56, 16223–16242. https://doi.org/10.1007/s10853-021-06306-1

Zhang, Z., Qiao, X., 2021. Influences of cation valence on water absorbency of crosslinked carboxymethyl cellulose. Int. J. Biol. Macromol. 177, 149–156. https://doi.org/10.1016/j.ijbiomac.2021.02.080

Zhao, C., Zhang, M., Liu, Z., Guo, Y., Zhang, Q., 2019. Salt-Tolerant Superabsorbent Polymer with High Capacity of Water-Nutrient Retention Derived from Sulfamic Acid-Modified Starch. ACS OMEGA 4, 5923–5930. https://doi.org/10.1021/acsomega.9b00486

Zohuriaan-Mehr, M.J., Kabiri, K., 2008. Superabsorbent polymer materials: A review. Iran. Polym. J. 17, 451–477

Chapter III. Occurrence of biocrusts and their positive effects on microbial nutrient cycling on phosphogypsum

3.1 Introduction

Chapter IV. Montmorillonite as an “accelerator” for the microbial carbon pump during artificial biocrust construction

4.1 Introduction

The desertification of land has been intensified in the las year, resulting in 21% of the global land desertified (F. Yang et al., 2023). Because the organic carbon of solil (SOC) has a vital role in strengthening soil structure and maintaining key biogeochemical functions, its input is essential to restore desertified lands (Chen et al., 2023). This goal could be achieved using microorganism (Liang and Balser, 2011; H. W. Wu et al., 2024). In recent years, the microbial carbon pump (MCP) theory has gained increasing attention (Feng and Wang, 2023; Jiao et al., 2024). According to this theory, microbes convert labile organic matter into stable organic carbon through ex vivo modification and in vivo turnover, underscoring their crucial role in SOC sequestration (Liang et al., 2017). In desertified regions, biological soil crusts (biocrusts) function as essential components of the MCP (Weber et al., 2022; W. Xu et al., 2024). Composed of microorganisms, microbial secretions, and inorganic soil particles, biocrusts act as ecosystem engineers in these fragile environments (Cheng et al., 2021; Lan et al., 2014). However, the natural formation and development of biocrusts is a slow process (X. B. Zhou et al., 2020). Compared to natural biocrusts, artificial biocrusts significantly reduce the time required for formation, making them an area of growing research interest (Xie et al., 2024). The development of artificial biocrusts involves culturing cyanobacteria, lichens, or mosses from natural biocrusts under controlled conditions to increase biomass, followed by their inoculation onto arid or semi-arid lands. Current research has primarily focused on the biological aspects, including large-scale microalgae cultivation, improving the environmental adaptability of inoculated algae, and assessing their effectiveness in soil rehabilitation (Giraldo-Silva et al. 2019; Wang et al. 2020; Zhao et al. 2023). However, limited studies have explored strategies for accelerating biocrust development and enhancing SOC accumulation by modifying the abiotic components of the system.

Inorganic minerals, particularly the clay minerals, Fe (II)-Al (III)-oxides, and Fe (II)-Al (III)-hydroxides, play a critical role in SOC accumulation dynamics (Chen et al., 2022; Kleber et al., 2021). In the recent study, Wu et al. (2023) introduced the "active mineral pool" model, which outlines the influence of minerals on soil organic matter through biological, chemical, and physical processes. However, in hybrid systems such as biocrusts—where microorganisms interact with inorganic minerals—the role of inorganic components has often been overlooked (Weber et al. 2022). Clay minerals, as a major constituent of fine soil and sediment particles (Kleber et al., 2021), are particularly important in biocrust formation, as fine-grained particles facilitate their development (Zhao et al., 2021b). Studies have demonstrated that clay minerals effectively promote biocrust growth (Zhou et al. 2023). Therefore, this study

aims to further investigate the role of clay minerals in SOC accumulation within artificial biocrusts.

Montmorillonite is a representative clay mineral, known for its dual role in SOC dynamics—protecting SOC (Arthur et al., 2023) and influencing microbial community evolution (Jiang et al., 2022). *Microcoleus vaginatus*, a stress-resistant cyanobacteria, is widely used as an inoculum for artificial biocrust formation (J. Wang et al., 2020). Based on this, montmorillonite was co-inoculated with *M. vaginatus* in this study to construct artificial biocrusts under laboratory conditions. To assess the influence of montmorillonite on SOC accumulation within the artificial biocrust system, key parameters were measured, including SOC content, microbial biomass carbon, SOC stability, and SOC mineralization. Additionally, high-throughput sequencing of the 16S rDNA gene and internal transcribed spacer (ITS) region was performed to analyze changes in microbial community structure and function. This study aimed to elucidate the role and mechanisms of clay minerals, particularly montmorillonite, in the biocrust carbon pump and to explore effective strategies for restoring desertified lands.

4.2 Materials and methods

4.2.1 Montmorillonite and algal solution preparation

A of high purity montmorillonite, $Na_{0.3}Al_2[(Si, Al)_4O_{10}](OH)_2 \cdot 2H_2O$ (Chifeng Ningcheng Bentonite Co., China), and pretreated by ion exchange to obtain Na-based montmorillonite. Specifically, the montmorillonite was mixed with ultrapure water at a solid-to-liquid mass ratio of 1:20 and stirred for 3 h at 1000 rpm min^{-1}, followed by centrifugation to remove impurities. The purified montmorillonite was then subjected to ion exchange by immersing it in 1 M NaCl to solid-to-liquid mass ratio of 1:20 and stirring at 90 °C for 3 h with water bath heating, followed by centrifugation at 1000 rpm min^{-1} for 5 min. The resulting Na-based montmorillonite (hereafter referred to as montmorillonite) was characterized by XRD analysis (Figure S4.1), and its structure was identified as $Na_{0.3}Al_2[(Si, Al)_4O_{10}] (OH)_2 \cdot 2H_2O$ (JCPDS no:43-0688). The physical and chemical properties of the montmorillonite are presented in Table S4.1.

Microcoleus vaginatus (PCC 9802) was isolated from natural biocrusts in the Qubqi Desert as described by Xie et al. (2007). The stock culture was grown within BG-11 medium in a light incubator at 25 ± 2°C with a radiation of 40 μ E m^{-2} s^{-1} and a light-dark ratio of 14:10 (L. Wu et al., 2022). The bulk algal biomass was disrupted by a liquidizer (BG-JS2, Midea, China), and the suspension was diluted with sterile water to obtain a homogeneous solution with a chlorophyll a (Chl-*a*) concentration of 7.3 μg mL^{-1}.

4.2.2 Experimental design

Montmorillonite and *M. vaginatus* were inoculated into cylindrical culture dishes with a radius of 150 mm and a height of 15 mm. 200 g of sandy soil was dispersed

evenly on the bottom of the dishes. The sandy soil was sourced from the Kubuqi Desert: certain physical and chemical characteristics of the sample are detailed in Table S4.1. The experimental groups were divided into six categories. Four experimental microcosms were mixed with 30 mL microalgal solution (with a 7.3 μg mL^{-1} concentration of Chl-*a*) and montmorillonite at 0, 0.7, 1.2, 1.4, and 2.1 g dm^{-2}, referred to hereinafter as 0-M, 0.7-M, 1.4-M, and 2.1-M, respectively. Additionally, two control check (CK) groups were established: CK-M and CK-Soil, where CK-M had no microalgal solution but 2.1 g dm^{-2} of montmorillonite, while the CK-Soil group was bare sand. Six replicates were prepared of each microcosm. After inoculation, each dish received 10 ml of BG-11 nutrient solution and was cultured for 84 days without the addition of further nutrient. Ultrapure water was added during the cultivation process to maintain 60% of the water holding capacity, and samples were collected periodically (days 0, 7, 14, 28, 42, 56, 84).

4.2.3 Physical and chemical analyses

The pH was determined at a soil: water ratio of 1:5 (w/v) employing the S20 SevenEasy pH meter (Mettler Toledo, OH, USA) (Rakhsh et al., 2020). The cation exchange capacity (CEC) of the samples was measured using the hexamine cobalt trichloride solution extraction method (Ciesielski et al., 1997). The crystal structure of the treated montmorillonite was characterized via an X-ray diffractometer (XRD) (Empyrean, Netherlands). The particle size of montmorillonite and sandy soil were characterized by a laser particle size analyzer (Malvern, Mastersizer 2000, UK). The microstructures of the biocrusts were visualized by scanning electron microscope (Phenom 6.0, Thermo Fisher Scientific, US).

SOC content was determined using the dichromate oxidation method (Walkly, 1934; Z. Xue et al., 2024), while total I (TP) and available I (AP) were quantified using the alkali fusion-Mo-Sb anti-spectrophotometric method, and the $NaHCaO_3$ solution-Mo-Sb anti-spectrophotometric method, respectively (Tan et al., 2023). Available N (AN) was measured using the alkali dissolution diffusion method (Wang et al. 2024). Total C (TC) and total N (TN) were analyzed using an elemental analyzer (Isoprime Ltd, Germany).

4.2.4 Physiological measurements

Chlorophyll a (Chl-*a*) was determined using the ethanol extraction method (Mugnai et al., 2018; Zhao et al., 2021a) based on Eq. (1). Microbial biomass carbon was extracted using the chloroform-fumigation-extraction method with an experimental conversion factor (E) of 0.45 for calculating microbial biomass carbon (Vance et al., 1987).

$$\textit{Chlorophyll a}\ \text{concentration}\ (\mu g\ cm^{-2}) = \frac{11.9035 \times A665 \times V}{S} \quad \text{(Eq. 1)}$$

where V (mL) and S (cm^2) represent the volume of ethanol and the sampling area, respectively.

4.2.5 Determination of SOC mineralization and stability

Biological stability, chemical stability, and molecular structure stability are commonly used as indicators for evaluating SOC stability (Hou et al., 2019; Plante et al., 2011). Biological stability is assessed by the mineralization of SOC (Kallenbach et al., 2016). As described by Francaviglia (Francaviglia et al., 2017), a 25-day cultivation period was carried out for the six experimental microcosms in sealed light-shielded containers. Subsequently, several indicators related to SOC mineralization were computed, including basal respiration (C_{bas}), cumulative respiration (C_{cum}), metabolic quotient (q_{CO2}), and mineralization quotient (q_M). The biological stability ($S_{biological}$) of the six experimental microcosms was determined as:

$$S_{biological} = 1 - q_M \quad \text{(Eq. 2)}$$

chemical stability ($S_{chemical}$) was assessed using the water bath method (Hou et al., 2019). SOC content in the soil samples before and after treatment at 70 °C was measured. The chemical organic carbon index of the system was calculated as the ratio between SOC before and after (SOC_{before} and (SOC_{after}, respectively) assays, as:

$$S_{chemical} = SOC_{after}/SOC_{before} \quad \text{(Eq. 3)}$$

The molecular structure stability ($S_{molecular}$) was characterized using solid-state ^{13}C NMR technology. Following established methods (Prietzel et al., 2018), Gaussian fitting was applied to the C NEXAFS spectra obtained for the different carbon peaks: namely, carboxyl C, aryl C, oxygen-alkyl C, and alkyl C, denoted by peak areas P_1, P_2, P_3 and P_4, respectively. The comprehensive molecular structure stability index was determined by the ratio of aryl C, alkyl C, and oxygen-alkyl C, as shown in Eq. (4). The proportion of carboxyl C ($P_{carboxyl}$) was used to reflect the ability of clay minerals to bind SOC (Curti et al., 2021; Gu et al., 1994), which was calculated by:

$$S_{molecular} = (P_2+P_4)/P_3 \quad \text{(Eq. 4)}$$

$$P_{carboxyl} = p_1/(p_1+p_2+p_3+p_4) \quad \text{(Eq. 5)}$$

4.2.6 High-throughput sequencing and analysis

DNA was extracted using the MagaBio DNA Soil Kit (Bioer Technology, CHN). The concentration and purity of DNA were measured using NanoDrop One (Thermo Fisher Scientific, USA). Polymerase chain reaction (PCR) amplification targeted the 16S rDNA V3V4-1 bacterial region and the ITS2 fungal region, using forward and reverse primers 338F (5′-ACTCCTACGGGAGGCAGCAG-3′) and 806R (5′-GGACTACHVGGGTWTCTAAT-3′) for bacteria, as well as ITS3-F (5′-GCATCGATGAAGAACGCAGC-3′) and ITS4-R (5′-TCCTCCGCTTATTGATATGC-3′) for fungi. Databases were established following the standard procedure of the NEBNext UltraII DNA Library Prep Kit for Illumina (New England Biolabs, USA). The amplified sequences were sequenced using PE250 on the Illumina Nova 6000 platform. The processed sequence data were clustered into operational taxonomic units (OTUs) at a 97% sequence similarity threshold (Lu et al., 2024; Wang et al., 2023). The OTUs for bacteria and fungi were aligned with the Silva

database and Unite database, respectively, to generate species information tables. Alpha diversity analysis was conducted based on the abundance table of OTUs.

4.2.7 Statistical analyses

The data were tested for significance using a one-way analysis of variance (ANOVA) (Duncan's multiple ranges; $p < 0.05$) using SPSS 20.0 (IBM, USA). Additionally, the correlation relationships between SOC and various indicators were examed using Pearson correlation and the Mantel test.

4.3 Results

4.3.1 The growth of microorganisms

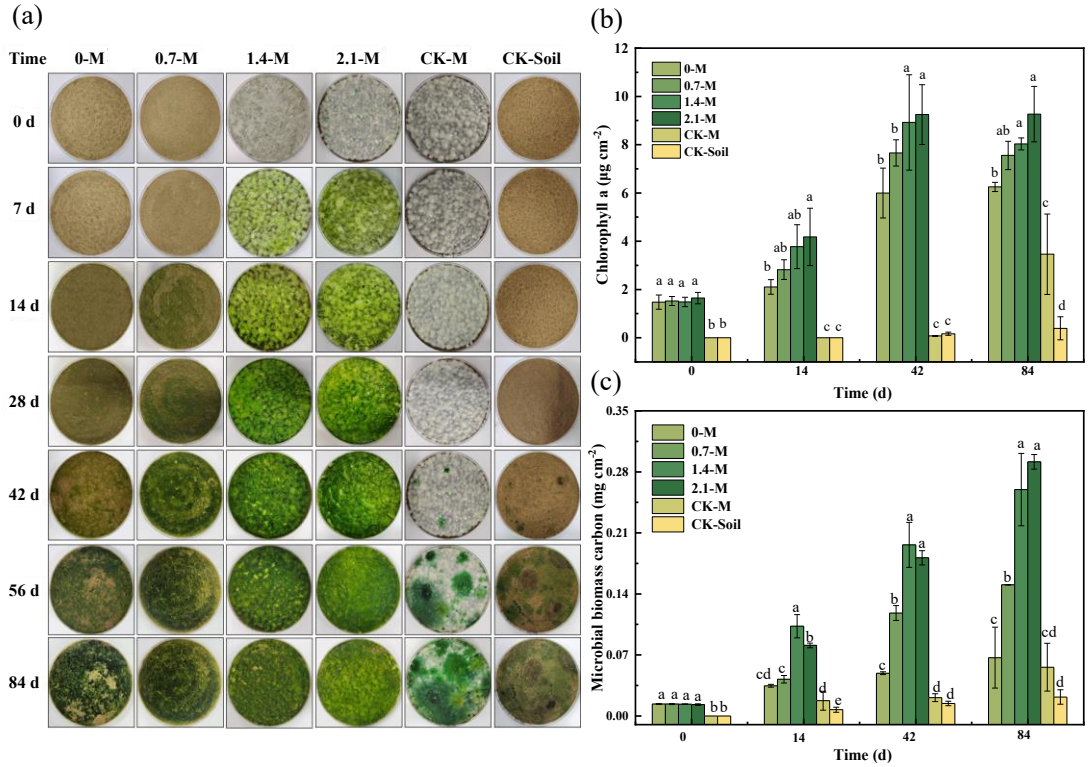

Figure 4.1 Changes in the six microcosms over time (a). Changes in Chl-*a* (b) and microbial biomass carbon (c) over time. Different letters assigned to values denote statistically significant differences ($p < 0.05$). Error bars denote standard deviations. Chl-*a*: chlorophyll *a*; d: day

Figure 4.1a illustrates the temporal evolution of the six microcosms. In particular, the 1.4-M and 2.1-M microcosms exhibited deepening of the green color by the 7th day, followed by a continuous intensification of coloration. By day 42, microbial communities became visible in the CK-M and CK-Soil microcosms due to the airborne spread of microorganisms. Chl-*a* serves as a robust indicator for assessing photosynthetic microorganisms (Lan et al., 2011). As shown in Figure 4.1b, montmorillonite, particularly at an area mass density exceeding 1.4 g dm^{-2}, significantly stimulated the proliferation of photosynthetic microorganisms ($p < 0.05$). Furthermore,

microbial biomass carbon is commonly employed as a proxy for microbial biomass (Finstad et al., 2023; Ning et al., 2021). The notable increase in microbial biomass carbon suggested that montmorillonite (≥ 1.4 g dm^{-2}) significantly accelerated microbial growth ($p < 0.05$) (Figure 3.1c).

4.3.2 The stability of SOC

Table 4.1 Indicators of SOC mineralization in each experimental microcosm

Parameter	0-M	0.7-M	1.4-M	2.1-M	CK-M	CK-Soil
C_{bas} (mg C_{CO2}·cm^{-2} soil·d^{-1})	0.047± 0.006a	0.050± 0.030a	0.35± 0.001a	0.040± 0.004a	0.044± 0.007a	0.045± 0.010a
C_{cum} (mg C_{CO2}·cm^{-2} soil)	0.269± 0.040a	0.239± 0.019b	0.271± 0.048b	0.300± 0.017b	0.1546± 0.032c	0.269± 0.041c
q_{CO2} (mg C_{CO2}·cm^{-2}·h^{-1} C_{mic}^{-1})	0.010± 0.007a	0.002± 0.000c	0.001± 0.000c	0.001± 0.000c	0.0023± 0.0029b c	0.006± 0.002b
q_M (%)	31.447± 3.684a	14.274± 2.163bc	10.930± 0.890cd	9.476± 1.695d	13.04± 2.7abc	16.143± 3.923b

Note: C_{bas}: basal respiration, C_{cum}: cumulative respiration, q_{CO2}: metabolic quotient, q_M: mineralization quotient, CK: control check

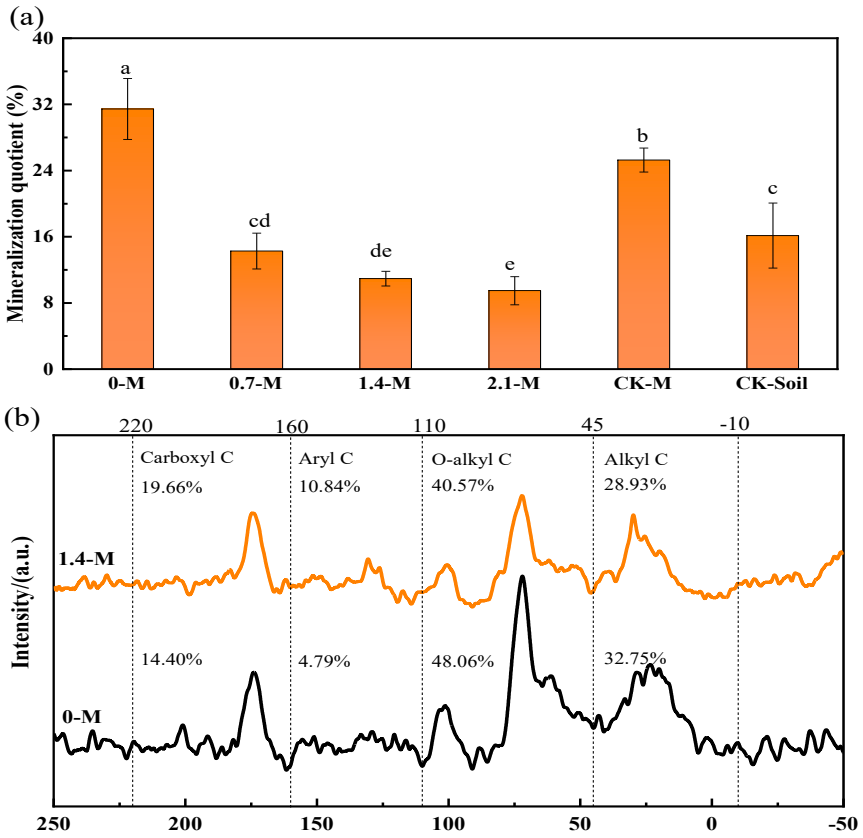

Figure 4.2. qM (a) and C NEXAFS spectrum (b) on day 84. Different letters assigned to values denote statistically significant differences ($p < 0.05$). Error bars denote standard deviations. qM:

Mineralization quotient. The chemical shift regions 10-45, 45-110, 110-160, and 160-220 ppm represent alkyl C, O-alkyl C, aryl C, and carboxyl C, respectively

Table 4.2 Stability of soil organic carbon (SOC) in two experimental microcosms, 0-M and 1.4M

Type	0-M	1.4-M
Biological stability（%）	68.55	90.52
Chemical stability（%）	78.68	92.67
Molecular structural stability（%）	78.11	98.05

As the main path of SOC consumption (Breidenbach et al., 2022; Fu et al., 2022), SOC mineralization was also measured. Co-inoculation of montmorillonite and microalgae, particularly in the 1.4-M and 2.1-M microcosms, significantly reduced C_{bas}, C_{cum}, q_{CO2}, and q_M within the biocrust system ($p < 0.05$) (Figure 4.2a, Table 4.1). The value of q_M serves as a direct indicator of SOC mineralization (Francaviglia et al., 2017). Figure 4.2a shows a noticeable trend in which decreased mineralization of SOC correlates with increased addition of montmorillonite.

Table 4.2 illustrates that the biological, chemical, and molecular structure stabilities of the 1.4-M microcosm exceed those with inoculated algae. Furthermore, the higher the content of carboxyl C, the stronger the binding ability of SOC with minerals (Curti et al., 2021; Gu et al., 1994). Figure 4.2b shows that the 1.4-M microcosm has a higher carboxyl carbon content. Recalcitrant carbon (aryl C) also exhibited a higher content in 1.4-M (Figure 4.2b) due to the specific adsorption of aryl C on clay (Rakhsh et al., 2020). The results indicate that the addition of montmorillonite ($\geqslant$ 1.4 g dm^{-2}) significantly enhanced the stability of SOC.

4.3.3 SOC accumulation

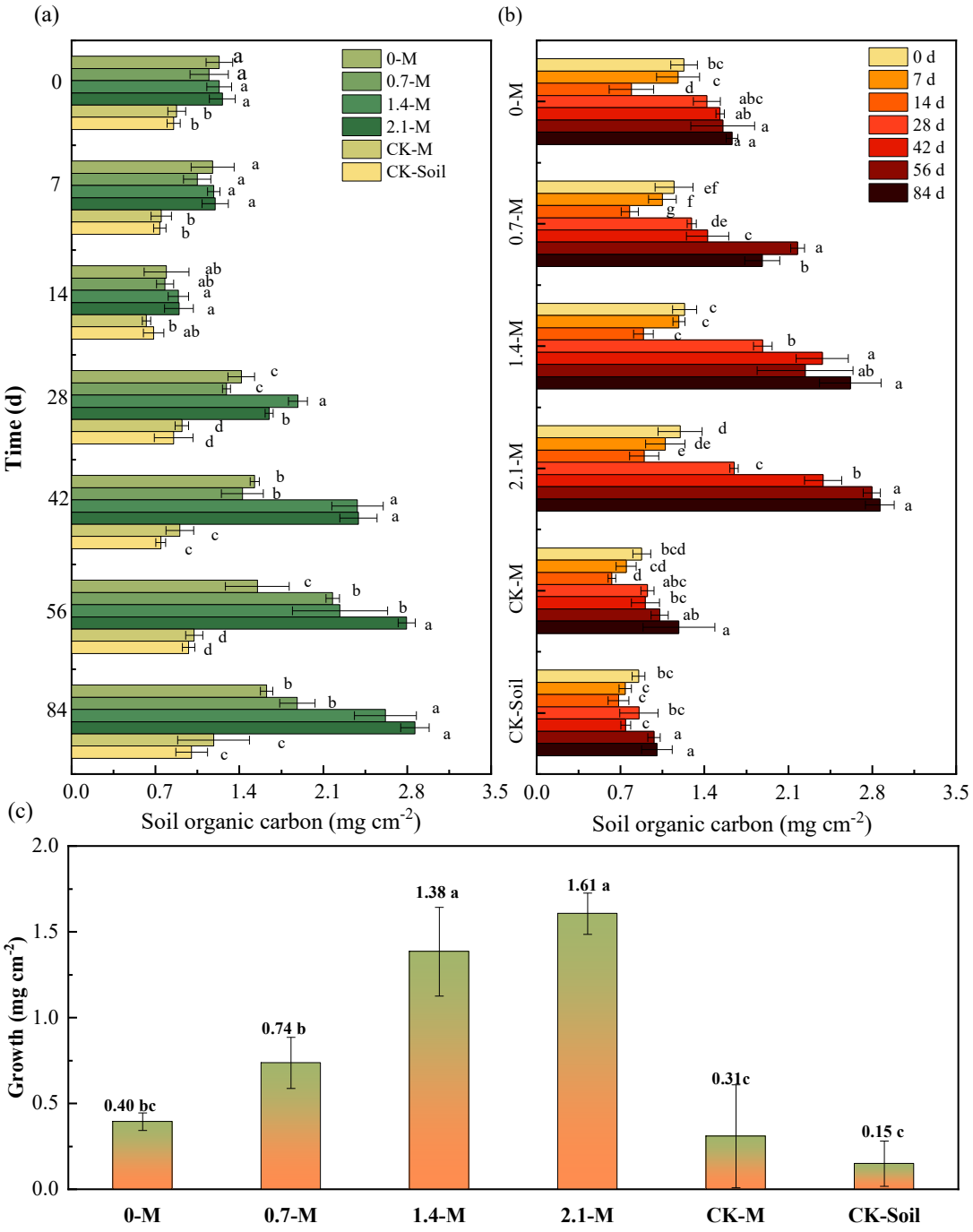

Figure 4.3 Changes in SOC content over time. (a) Significance analysis between six experimental microcosms at different time points; (b) Significance analysis of each microcosm at each time point; (c) The increase in SOC relative to original SOC at day 84. Different letters assigned to values denote statistically significant differences ($p < 0.05$). Error bars denote standard deviations. SOC: soil organic carbon, CK: control check

During the 84-day culture period, the SOC dynamics of the six experimental microcosms exhibited an unconventional trend of initial decline followed by a subsequent increase (Figs. 4.3a and 4.3b). During the initial 0-14 days, the rate of nutrient consumption outweighed early SOC formation. Subsequently, from days 14 to

84, a pronounced increase of SOC occurred, with the 1.4-M and 2.1-M microcosms exhibiting maximum SOC content. The SOC content reached a stabilized phase during days 56-84 (Figure 4.3b). Additionally, it should be noted that the SOC content in the CK-M microcosm was markedly lower than that in the 0-M microcosm, indicating the irreplaceable role of microorganisms in the carbon pump as Chao proposed (Liang et al., 2017). On day 84, SOC content in the 1.4-M and 2.1-M microcosms exceeded that of the 0-M by 3.5-4.0 times (Figure 4.3c), demonstrating the accelerating effect of montmorillonite on the accumulation of SOC in artificial biocrusts. Furthermore, there was no significant difference in SOC accumulation and growth between the 1.4-M and 2.1-M microcosms, indicating that 1.4 g dm^{-2} is the optimal dosage for the addition of montmorillonite.

4.3.4 Microbial structure succession

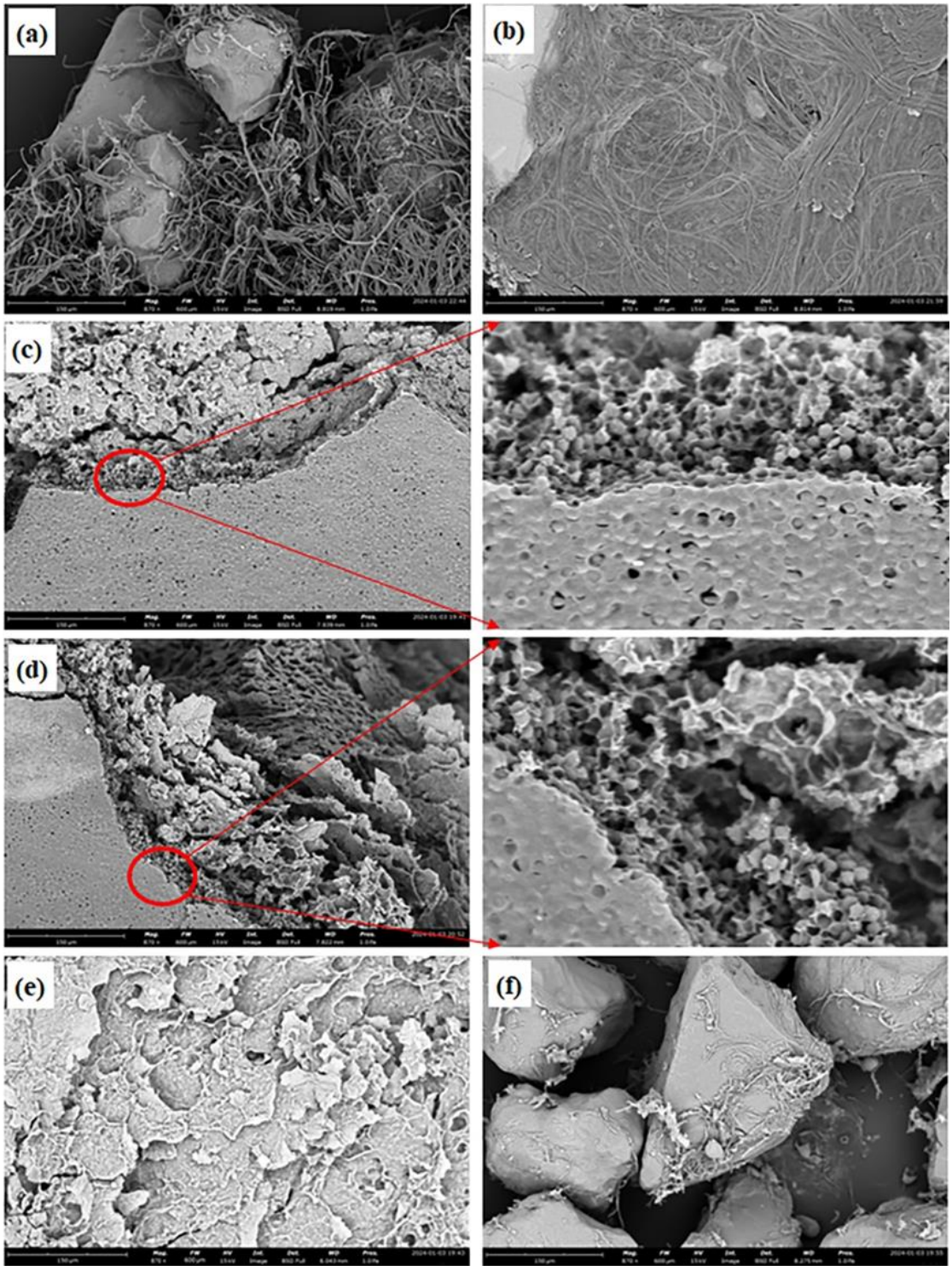

Figure 4.4 Scanning electron microscope (SEM) pictures of experimental microcosms 0-M (a), 0.7-M (b), 1.4-M (c), 2.1-M (d), CK-M (e), CK-Soil (f). CK: control

If the montmorillonite added exceeded 1.4 g dm^{-2}, the filamentous microorganisms decreased significantly and were replaced by spherical microorganisms (Figure 4.4). Interestingly, the microcosms with montmorillonite ($\geqslant$1.4 g dm^{-2}) exhibited the house-

of-cards structure (P. Li et al., 2022), with abundant microorganisms inhabiting it (Figure 4.4c and Figure 4.4d).

Table 4.3 Alpha diversity indices of bacteria in experimental microcosms.

Microcosm	Observed features	Shannon	Simpson	ACE	chao1	cover
0-M	817.33± 114.61ab	3.12± 0.26ab	0.68± 0.05a	822.61± 115.66ab	818.94± 115.18ab	1.00± 1.20×10^{-5}abc
0.7-M	560.67± 126.34b	2.27± 0.21b	0.52± 0.02	565.39± 129.20b	562.51 ±128.24b	1.00± 5.72×10^{-5}ab
1.4-M	952.67± 195.31a	4.00± 1.01a	0.70± 0.16a	959.36± 197.30a	954.52 ±196.10a	1.00± 5.87×10^{-5}c
2.1-M	1027.00± 108.40a	4.12± 0.85a	0.71± 0.14a	1032.11± 108.56a	1028.36 ±108.60a	1.00± 7.00×10^{-6}bc
CK-M	569.67± 59.37b	2.10± 0.08b	0.59± 0.04a	571.52± 59.58b	569.91 ±59.37b	1.00± 3.50×10^{-6}a
CK-Soil	586.67± 214.17b	2.60± 0.18b	0.59± 0.03a	591.10± 217.34b	587.83 ±215.33b	1.00± 4.81×10^{-5}ab

Note: Different letters assigned to values denote statistically significant differences ($p < 0.05$). CK: control check

Table 4.4 Alpha diversity indices of fungi.

Microcosm	Observed features	Shannon	Simpson	ACE	chao1	cover
0-M	72.00± 20.66b	0.87± 0.34bc	0.23± 0.11bc	72.00± 20.66b	72.00± 20.66b	1.00±0.00
0.7-M	67.00± 9.00b	1.19± 0.16b	0.36± 0.06b	67.33± 9.45b	67.33± 9.45b	1.00±0.00
1.4-M	53.67± 9.71b	0.46± 0.22c	0.12± 0.07cd	53.67± 9.71b	53.67± 9.71b	1.00±0.00
2.1-M	43.00± 13.08b	0.30± 0.02c	0.06± 0.01c	43.00± 13.08b	43.00± 13.08b	1.00±0.00
CK-M	132.67± 28.01ab	0.80± 0.11bc	0.19± 0.04cd	132.67± 28.01ab	132.67± 28.01ab	1.00±0.00
CK-Soil	217.00±106.23a	2.93±0.64a	0.72±0.08a	217.00±106.23a	217.00±106.23a	1.00±0.00

Note：Different letters assigned to values denote statistically significant differences ($p < 0.05$). CK：control check

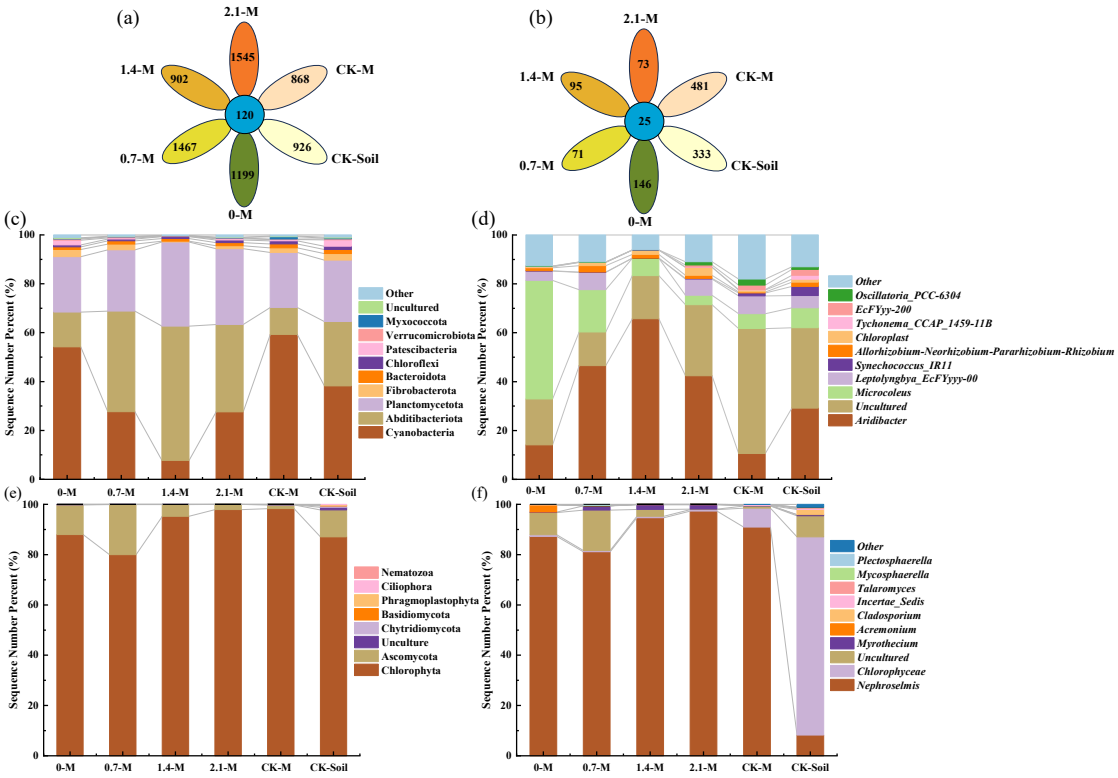

Figure 4.5 Common and unique OTUs of bacteria (a) and fungi (b) at the genus level. The composition of the main bacterial communities at the phylum (c) and genus (d) levels. The composition of the main fungal communities at the phylum (e) and genus (f) levels. CK: control check

We also investigated the microbial community structure of the six microcosms. A total of 24,526 sequences from 18 samples were acquired by 16S rDNA technology. The high coverage (>99%) indicated that the sequencing depth was sufficient to describe the bacterial community of each sample (Table 4.3) (Wang et al., 2023). The Venn diagram illustrated that the OTUs shared among the six microcosms constitute only 7.77-12.93% (Figure 4.5a), suggesting the profound impacts of algae and montmorillonite on soil bacterial community structure (Jia et al., 2021). The alpha diversity metrics Shannon, Simpson, ACE, and Chao1 indices indicated increased bacterial community diversity and richness in systems supplemented with 1.4 g dm^{-2} and 2.1 g dm^{-2} montmorillonite (Table 4.3).

Additionally, ITS2 technology was used to generate a total of 2268 sequences from 18 samples, achieving high coverage (>99%) and adequate sequencing depth to characterize the fungal community within each sample. Analysis of Venn diagrams (Figure 4.5b) and alpha diversity revealed an apparent inhibition of fungal abundance and diversity after algae inoculation and montmorillonite addition (Table 4.4). The bacteria and fungi within the six microcosms appeared to demonstrate a phenomenon of mutual growth and decline.

A total of 29 bacterial phyla and 652 bacterial genera were identified across all samples. Cyanobacteria, Abditibacteriota, and Planctomycetota emerged as dominant

bacterial taxa (Figure 4.5c). In particular, the addition of montmorillonite resulted in a reduction in the dominant proportion of Cyanobacteria while increasing the abundance of Abditibacteriota. Abditibacteriota is recognized for its prevalence in extreme terrestrial environments and has remarkable adaptability to low-nutrient conditions (Tahon et al., 2018). At the genus level, the addition of montmorillonite significantly decreased the dominant proportion of *Microcoleus*, a genus of filamentous algae that includes the original inoculated algae (Figure 4.5d). According to previous studies (Mugnai et al., 2024b; Zhao et al., 2024), the microbial community structure of biocrusts changes during succession, with the dominance of Cyanobacteria being replaced, indicating that the biocrust system has undergone succession. In the group with montmorillonite, the decrease in the abundance of *Microcoleus vaginatus* or its homologous algae suggests that the addition of montmorillonite may have further promoted succession in the biocrust. Montmorillonite also promoted the proportion of *Aridibacter* (Figure 3.5d), commonly found in alkaline clay environments (Huber et al., 2014). These results reflect the regulating action of montmorillonite on the structure of biological communities.

A total of eight fungal phyla and 42 fungal genera were identified across all samples. At the phylum level, Chlorophyta and Ascomycota exhibited absolute dominance as the primary fungal taxa (Figure 4.5e). At the genus level, *Nephroselmis* emerged as the predominant genus in all experimental microcosms except for the CK-Soil (Figure 4.5f). In particular, the genus is characterized by large pyrenoids and thylakoid-pyrenoid complexes within bacterial cells, indicative of exceptionally high CO_2 enrichment and adaptive photosynthetic structures (Cheng et al., 2018). *Nephroselmis* exhibited the highest abundance percentage in the 1.4-M and 2.1-M microcosms, with an average abundance ratio of 94.67-97.33%.

Table S2 shows that 1.4-M and 2.1-M exhibited notable advantages of the ability of photoautotrophy-Cyanobacteria, phototrophy, photosynthesis, and photosynthesis-antenna proteins. It was mutually confirmed by the promoting effect of montmorillonite on photosynthetic microorganisms.

Overall, montmorillonite significantly regulated the microbial community structure, leading to a notable growth of photosynthetic microorganisms and oligotrophic-adapted microbes. Furthermore, the 1.4-M and 2.1-M microcosms exhibited higher photosynthetic capabilities.

4.4 Discussion

4.4.1 The accelerating effect of montmorillonite on microbial growth

The results show the accelerating effect of montmorillonite on microbial growth, primarily attributable to the following factors (Figure 4.1). Firstly, fine-grained particles facilitate the colonization and growth of microorganisms, particularly Cyanobacteria (Zhao et al. 2021; Faist et al. 2020). The fine particle advantage of

montmorillonite (Table S4.1) undoubtedly contributes to accelerating the growth of microbial communities within artificial biocrusts.

Secondly, prior studies (Hartmann and Six, 2023; Wu et al., 2023) have highlighted that spatial heterogeneity enhances microbial abundance and diversity. The unique house-of-cards structure (Benna et al., 1999) of montmorillonite creates pore spaces that not only absorb essential water, oxygen, and nutrients for microbes to grow but also establish diverse microenvironments, promoting both microbial abundance and diversity. As a typical clay, montmorillonite contains numerous trace elements (such as Na, Mg, Mn, and Fe), which are essential as electron donors, terminal electron acceptors (Kleber et al., 2021; X. Yang et al., 2021), cofactors, or vital nutrients for bacterial physiology (Uroz et al. 2015; Yang et al. 2023; Tan et al. 2023).

Furthermore, the availability of soil surface water is crucial for algal crust growth (Zhou et al. 2023; Xu et al. 2023): the strong hydration effect of montmorillonite can extend the duration of soil surface water availability (Chen et al., 2024), ensuring sustained water availability for biocrusts inhabiting shallow soil layers.

Indoor experiments have shown that montmorillonite is a highly promising additive for the development of biocrusts. However, for complex real-world desertified land, much more work is needed in the future.

In real-world desertified land, rainfall is typically irregular, and soils in desertified regions are predominantly sandy, characterized by high permeability and poor water retention (Fattahi et al., 2020). Montmorillonite, known for its strong hydration capacity, is often incorporated into superabsorbent hydrogels and could potentially reduce permeability and improve water retention in desertified soils (Etemadi Baloch et al., 2021). Current views on the impact of biocrusts on runoff are inconsistent, with pore clogging and water repellency identified as two major factors influencing runoff generation (Kidron et al., 2022). Could the hydrophilicity and water absorption capacity of montmorillonite make the impact on runoff more significant? Under natural conditions with irregular rainfall, the influence of montmorillonite on microbial development within biocrust systems, as well as its effects on soil permeability and runoff in desertified soils, undoubtedly warrants further investigation.

Extreme precipitation events are becoming increasingly frequent in desertified areas (Zhang et al., 2024), and intense rainfall causes severe disturbances to the surface, significantly hindering the sustained development of biocrusts. Given its strong hydration capacity, ion exchange properties (Song et al., 2019), and colloidal characteristics, montmorillonite can enhance the adhesion performance of certain binders (Sun et al., 2021). Could montmorillonite aid biocrusts resisting the impact of extreme rainfall? Furthermore, could xanthan gum, Na, alginate, or similar compounds be incorporated into montmorillonite to produce polymer-based sand stabilizers (Khaleghi and Heidarvand, 2023), further improving resistance to disturbances from more complex environmental factors?

4.4.2 The optimization effect of montmorillonite on the microbial community

The addition of montmorillonite was shown to induce significant changes in the microbial community structure.

At the bacterial phylum level, the proportion of Cyanobacteria in the montmorillonite -microalgae co-inoculation microcosm decreased. However, the results of the functional annotation revealed that the addition of montmorillonite (≥ 1.4 g dm^{-2}) increased photosynthesis-Cyanobacteria ability. This indicates that montmorillonite only preferred Cyanobacteria with photosynthesis ability, consistent with the research result of Tan et al. (2022). Furthermore, the proportion of Abditibacteriota increased. This could be attributed to the stronger stability (Figure 4.2) and the difficulty in decomposing SOC in montmorillonite-based biocrusts, making the oligotrophic adaptive microorganisms in the microbial community more adaptable (Tahon et al., 2018).

Regarding fungi, the addition of montmorillonite amplified the abundance of *Chlorophyta*, characterized by chloroplasts akin to those of higher plants and with robust photosynthetic capabilities (Murik et al., 2024). At the genus level, montmorillonite (≥ 1.4 g dm^{-2}) augmented the abundance of *Nephroselmis* to more than 94.67%, exhibitings efficient CO_2 absorption and photosynthesis ability (Cheng et al., 2018). Both indicate the selectivity of montmorillonite-based biocrusts towards microorganisms with strong photosynthesis activity. This was also confirmed in the function of microbial communities (Table S4.2).

These observations underscore that montmorillonite (≥ 1.4 g dm^{-2}) effectively modulates the microbial community, especially favoring the proliferation of phototrophic microorganisms with strong photosynthetic capabilities. Moreover, the current study has only studied the effects of montmorillonite on microbial community structure during the period of SOC accumulation stability. Future research should expand the time scale and spatial range to study the long-term dynamics of microbial communities in montmorillonite-based artificial biocrusts and their impact on the restoration of higher plants.

4.4.3 Montmorillonite as an accelerator for the microbial carbon pump

Microbial growth served as the primary driving force behind SOC formation (Liang et al., 2017). The addition of montmorillonite (≥ 1.4 g dm^{-2}) notably accelerated the development of biocrust (Section 3.4.1) and regulated the mass propagation of photosynthetic microorganisms (Section 3.4.2). Stability is an important condition for SOC accumulation (Baumann et al., 2021). The strong and selective adsorption capacity of SOC by montmorillonite significantly enhanced its stability. By accelerating microbial growth, regulating microbial communities, and improving SOC stability, montmorillonite (≥ 1.4 g dm^{-2}) markedly promoted the accumulation of SOC (Figure 4.3). To study the most influential factor accelerating SOC accumulation by montmorillonite, Pearson correlation analysis assessed relevant indicators within experimental microcosms co-inoculated with montmorillonite-microalgae. As shown

in Figure 4.6, the Pearson coefficient between microbial biomass carbon and SOC accumulation attains its highest value of 0.92 ($p < 0.001$). This indicates that microbial mass is the predominant factor for SOC accumulation. Liang et al. (2017) proposed a microbial carbon pump emphasizing the driving role of microorganisms in the improvement of SOC. In the montmorillonite-based artificial biocrust system, montmorillonite promoted microbial growth, serving as an accelerator for microbial growth and SOC accumulation. Consequently, we explicitly propose the concept that montmorillonite can function as an "accelerator" for the biocrust carbon pump (Figure 4.7).

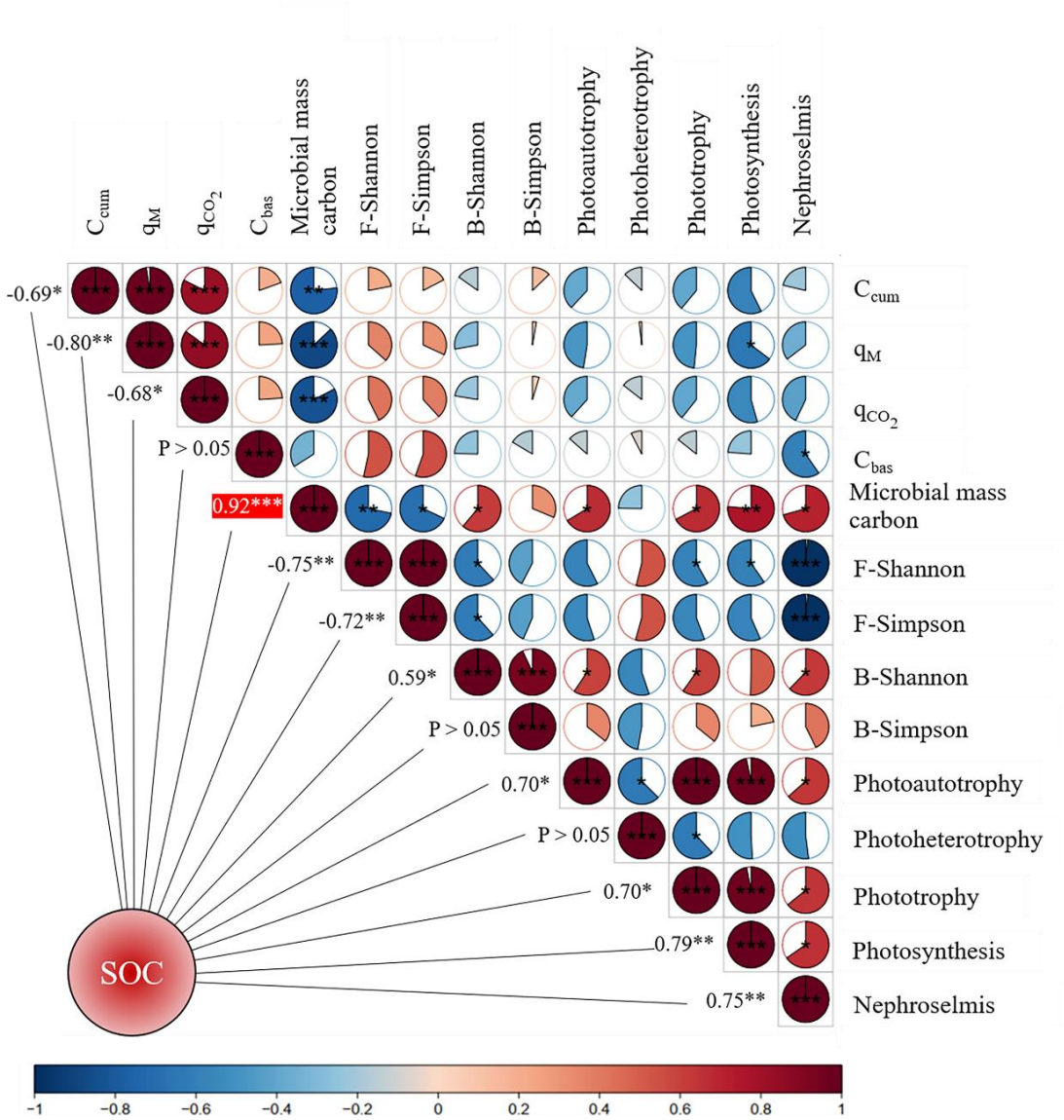

Figure 4.6 Correlation analysis between SOC and related indicators, as well as between these indicators. The numbers in the figure represent the Pearson correlation coefficients between SOC and related indicators. The color and area filled in the circle represent the Pearson coefficients between these indicators. F-Shannon, F-Simpson, B-Shannon, and B-Simpson represent the Shannon index of fungi, the Simpson index of fungi, the Shannon index of bacteria, and the Simpson index of bacteria, respectively. The symbols *, **, and *** represent statistically significant levels at $p < 0.05$, $p < 0.01$, and $p < 0.001$, respectively. C_{cum}: cumulative respiration, q_M: mineralization quotient, q_{CO2}: metabolic quotient, C_{bas}: basal respiration, CK: control check

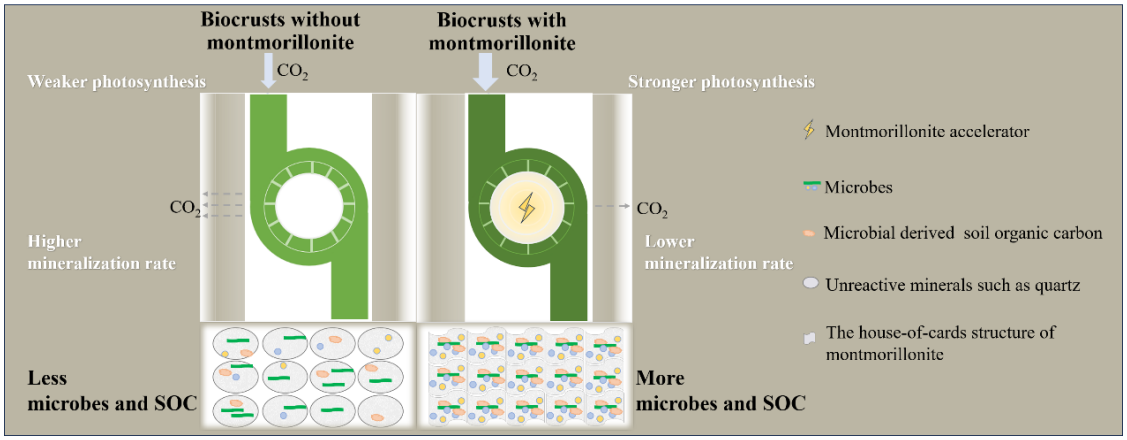

Figure 4.7 Schematic diagram of montmorillonite as an "accelerator" in the biocrust carbon pump. After montmorillonite was added, more microbial growth and SOC accumulation were observed in the biocrust, as montmorillonite drove stronger photosynthesis and resulted in lower SOC mineralization

4.5 Conclusions

This study aimed to investigate the impact of clay minerals on the dynamics of SOC accumulation in artificial biocrust systems. We determined that the optimal addition of montmorillonite was 1.4 g dm^{-2}, leading to a 3.45-fold increase in SOC content after 84 days of cultivation. Three key findings emerged from the montmorillonite-based artificial biocrust system. First, montmorillonite significantly accelerated microbial growth; second, it specifically regulated microbial communities, promoting the proliferation of photosynthetically active microorganisms; third, the growth of microbial biomass driven by montmorillonite was the primary factor driving SOC accumulation. Based on these results, we propose that montmorillonite acts as an accelerator for the biocrust carbon pump during the formation of artificial biocrusts. While this study provides valuable insights, it is limited to laboratory conditions. Future research in natural settings is needed to examine the effects of montmorillonite-based artificial biocrusts on processes such as water infiltration, surface runoff, evaporation, and soil erosion in desertified areas, thereby enhancing our understanding of ecosystem functions and biodiversity under desert environmental conditions.

The main content in this chapter was published:

- ✓ **Zhang C**, Zhou KQ, Wang Z, et al. Montmorillonite as an "accelerator" for the microbial carbon pump during artificial biocrust construction[J]. Plant and Soil, 2025 1-17. (JCR Q1; IF 4.1)

4.6 References

Arthur E, Tuller M, Norgaard T, et al, 2023. Contribution of organic carbon to the total specific surface area of soils with varying clay mineralogy. Geoderma. 430, 116314. https://doi.org/10.1016/j.geoderma.2022.116314

Baumann K, Eckhardt KU, Acksel A, et al, 2021. Contribution of biological soil crusts to soil organic matter composition and stability in temperate forests. Soil Biol Biochem. 160, 108315. https://doi.org/10.1016/j.soilbio.2021.108315

Benna M, Kbir-Ariguib N, Magnin A, Bergaya F, 1999. Effect of pH on rheological properties of purified sodium bentonite suspensions. J Colloid Interface Sci. 218, 442-455. https://doi.org/10.1006/jcis.1999.6420

Breidenbach A, Schleuss PM, Liu SB, et al, 2022. Microbial functional changes mark irreversible course of Tibetan grassland degradation. Nat Commun. 13, 2681. https://doi.org/10.1038/s41467-022-30047-7

Chen M, Zhang S, Liu L, et al, 2022. Organic fertilization increased soil organic carbon stability and sequestration by improving aggregate stability and iron oxide transformation in saline-alkaline soil. Plant Soil. 474, 233-249. https://doi.org/10.1007/s11104-022-05326-3

Chen WQ, Sedighi M, Curvalle F, Jivkov AP, 2024. Elevated temperature effects (T >100 °C) on the interfacial water and microstructure swelling of Na-montmorillonite. Chem Eng. 481, 148647. https://doi.org/10.1016/j.cej.2024.148647

Chen XL, Taylor AR, Reich PB, et al, 2023. Tree diversity increases decadal forest soil carbon and nitrogen accrual. Nature. 618, 94-101. https://doi.org/10.1038/s41586-023-05941-9

Cheng C, Gao M, Zhang YD, et al, 2021. Effects of disturbance to moss biocrusts on soil nutrients, enzyme activities, and microbial communities in degraded karst landscapes in southwest China. Soil Biol Biochem. 152, 108065. https://doi.org/10.1016/j.soilbio.2020.108065

Cheng QL, Xu LG, Cheng FM, et al, 2018. Bicarbonate-rich wastewater as a carbon fertilizer for culture of *Dictyosphaerium* sp. of a giant pyrenoid. J Clean Prod. 202, 439-443. https://doi.org/10.1016/j.jclepro.2018.08.066

Ciesielski H, Sterckeman T, Santerne M, Willery JP, 1997. A comparison between three methods for the determination of cation exchange capacity and exchangeable cations in soils. Agronomie. 17, 9–16.

Curti L, Moore OW, Babakhani P, et al, 2021. Carboxyl-richness controls organic carbon preservation during coprecipitation with iron (oxyhydr)oxides in the natural environment. Commun Earth Environ. 2, 229. https://doi.org/10.1038/s43247-021-00301-9

Etemadi Baloch F, Afzali D, Fathirad F, 2021. Design of acrylic acid/nanoclay grafted polysaccharide hydrogels as superabsorbent for controlled release of chlorpyrifos. Appl Clay Sci. 211, 106194. https://doi.org/https://doi.org/10.1016/j.clay.2021.106194

Faist AM, Antoninka AJ, Belnap J, et al, 2020. Inoculation and habitat amelioration efforts in biological soil crust recovery vary by desert and soil texture. Restor Ecol. 28, S96-S105. https://doi.org/10.1111/rec.13087

Finstad KM, Nuccio EE, Grant KE, et al, 2023. Radiocarbon analysis of soil microbial biomass via direct chloroform extraction. Radiocarbon. 66, 854-862. https://doi.org/10.1017/RDC.2023.80

Feng X, Wang S, 2023. Plant influences on soil microbial carbon pump efficiency. Glob Chang Biol. 29, 3854-3856. https://doi.org/10.1111/gcb.16728

Finstad KM, Nuccio EE, Grant KE, et al, 2023. Radiocarbon analysis of soil microbial biomass via direct chloroform extraction. Radiocarbon. 66, 854-862. https://doi.org/10.1017/RDC.2023.80

Francaviglia R, Renzi G, Ledda L, Benedetti A, 2017. Organic carbon pools and soil biological fertility are affected by land use intensity in Mediterranean ecosystems of Sardinia, Italy. Sci Total Environ. 599, 789-796. https://doi.org/10.1016/j.scitotenv.2017.05.021

Fu XH, Song QL, Li SQ, et al, 2022. Dynamic changes in bacterial community structure are associated with distinct priming effect patterns. Soil Biol Biochem. 169,108671. https://doi.org/10.1016/j.soilbio.2022.108671

Giraldo-Silva A, Nelson C, Barger NN, Garcia-Pichel F, 2019. Nursing biocrusts: isolation, cultivation, and fitness test of indigenous cyanobacteria. Restor Ecol. 27, 793-803. https://doi.org/10.1111/rec.12920

Gu B, Schmitt J, Chen Z, et al, 1994. Adsorption and desorption of natural organic matter on iron oxide: mechanisms and models. Environ Sci Technol. 28, 38-46. https://doi.org/10.1021/es00050a007

Hartmann M, Six J, 2023. Soil structure and microbiome functions in agroecosystems. Nat Rev Earth Environ. 4, 4-18. https://doi.org/10.1038/s43017-022-00366-w

Hou YH, Chen Y, Chen X, et al, 2019. Changes in soil organic matter stability with depth in two alpine ecosystems on the Tibetan Plateau. Geoderma. 351, 153-162. https://doi.org/10.1016/j.geoderma.2019.05.034

Huber KJ, Wüst PK, Rohde M, et al, 2014. *Aridibacter famidurans* gen. nov., sp. nov. and *Aridibacter kavangonensis* sp. nov., two novel members of subdivision 4 of the Acidobacteria isolated from semiarid savannah soil. Int J Syst Evol Microbiol. 64, 1866-1875. https://doi.org/10.1099/ijs.0.060236-0

Jia AQ, Xu L, Wang Y, 2021. Venn diagrams in bioinformatics. Brief Bioinform. 22, bbab108. https://doi.org/10.1093/bib/bbab108

Jiang Z, An N, Chu YX, et al, 2022. Growth, biofilm formation and atrazine degrading gene (trzN) expression of *Arthrobacter* sp. DNS10 cultured with montmorillonite, kaolinite and goethite. Chemosphere. 307, 135904. https://doi.org/10.1016/j.chemosphere.2022.135904

Jiao N, Herndl GJ, Hansell DA, et al, 2010. Microbial production of recalcitrant dissolved organic matter: long-term carbon storage in the global ocean. Nat Rev Microbiol. 8, 593-599. https://doi.org/10.1038/nrmicro2386

Kallenbach CM, Frey SD, Grandy AS, 2016. Direct evidence for microbial-derived soil organic matter formation and its ecophysiological controls. Nat Commun. 7, 13630. https://doi.org/10.1038/ncomms13630

Zhou KQ, Zhang ZJ, Zhang C, et al, 2023. Rapid artificial biocrust development by cyanobacterial inoculation and clay amendment. L Degrad Dev. 34, 3728-3743. https://doi.org/10.1002/ldr.4716

Khaleghi M, Heidarvand M, 2023. A novel study on hydro-mechanical characteristics of biopolymer-stabilized dune sand. J Clean Prod. 398, 136518. https://doi.org/https://doi.org/10.1016/j.jclepro.2023.136518

Kidron GJ, Lichner L, Fischer T, et al, 2022. Mechanisms for biocrust-modulated runoff generation – A review. Earth-Science Rev. 231, 104100. https://doi.org/10.1016/j.earscirev.2022.104100

Kleber M, Bourg IC, Coward EK, et al, 2021. Dynamic interactions at the mineral-organic matter interface. Nat Rev Earth Environ. 2, 402-421. https://doi.org/10.1038/s43017-021-00162-y

Lan S, Zhang Q, Wu L, et al, 2014. Artificially accelerating the reversal of desertification: Cyanobacterial inoculation facilitates the succession of vegetation communities. Environ Sci Technol. 48, 307-315. https://doi.org/10.1021/es403785j

Lan SB, Wu L, Zhang DL, et al, 2011. Ethanol outperforms multiple solvents in the extraction of chlorophyll-a from biological soil crusts. Soil Biol Biochem. 43, 857-861. https://doi.org/10.1016/j.soilbio.2010.12.007

Li P, Hu M, Liu M, et al, 2022. Thixotropic and hydration effects of Mg/Al-layered double hydroxide and sodium montmorillonite composite dispersion on oil well cement paste. Cem Concr Compos. 134, 104785. https://doi.org/https://doi.org/10.1016/j.cemconcomp.2022.104785

Liang C, Balser TC, 2011. Microbial production of recalcitrant organic matter in global soils: implications for productivity and climate policy. Nat Rev Microbiol. 9, 75-75. https://doi.org/10.1038/nrmicro2386-c1

Liang C, Schimel JP, Jastrow JD, 2017. The importance of anabolism in microbial control over soil carbon storage. Nat Microbiol. 2, 1-6. https://doi.org/10.1038/nmicrobiol.2017.105

Lu Z, Wang H, Wang Z, et al, 2024. Critical steps in the restoration of coal mine soils: Microbial-accelerated soil reconstruction. J Environ Manage. 368, 122200. https://doi.org/https://doi.org/10.1016/j.jenvman.2024.122200

Miltner A, Bombach P, Schmidt-Brücken B, Kästner M, 2012. SOM genesis: Microbial biomass as a significant source. Biogeochemistry. 111, 41-55. https://doi.org/10.1007/s10533-011-9658-z

Mugnai G, Pinchuk I, Borruso L, et al, 2024. The hidden network of biocrust successional stages in the High Arctic: Revealing abiotic and biotic factors shaping microbial and metazoan communities. Sci Total Environ. 926, 171786. https://doi.org/https://doi.org/10.1016/j.scitotenv.2024.171786

Mugnai G, Rossi F, Felde V, et al, 2018. The potential of the cyanobacterium *Leptolyngbya ohadii* as inoculum for stabilizing bare sandy substrates. Soil Biol Biochem. 127, 318-328. https://doi.org/10.1016/j.soilbio.2018.08.007

Murik O, Geffen O, Shotland Y, et al, 2024. Genomic imprints of unparalleled growth. New Phytol. 241, 1144-1160. https://doi.org/10.1111/nph.19444

Ning QS, Hättenschwiler S, Lü XT, et al, 2021. Carbon limitation overrides acidification in mediating soil microbial activity to nitrogen enrichment in a temperate grassland. Glob Chang Biol. 27, 5976-5988. https://doi.org/10.1111/gcb.15819

Plante AF, Fernández JM, Haddix ML, et al, 2011. Biological, chemical and thermal indices of soil organic matter stability in four grassland soils. Soil Biol Biochem. 43, 1051-1058. https://doi.org/10.1016/j.soilbio.2011.01.024

Prietzel J, Müller S, Kogel-Knabner I, et al, 2018. Comparison of soil organic carbon speciation using C NEXAFS and CPMAS ^{13}C NMR spectroscopy. Sci Total Environ. 628, 906-918. https://doi.org/10.1016/j.scitotenv.2018.02.121

Rakhsh F, Golchin A, Al Agha AB, Nelson PN, 2020. Mineralization of organic carbon and formation of microbial biomass in soil: Effects of clay content and composition and the mechanisms involved. Soil Biol Biochem. 151, 108036. https://doi.org/10.1016/j.soilbio.2020.108036

Satdichanh M, Dossa GGO, Yan K, et al, 2023. Drivers of soil organic carbon stock during tropical forest succession. J Ecol. 111, 1722-1734. https://doi.org/10.1111/1365-2745.14141

Song J, Zhang S, Li G, et al, 2019. Preparation of montmorillonite modified biochar with various temperatures and their mechanism for Zn ion removal. J Hazard Mater. 391, 121692. https://doi.org/10.1016/j.jhazmat.2019.121692

Sun Z, Sun B, Bai Y, Gao Z, 2021. Economical improvement on the performances of a soybean flour-based adhesive for wood composites via montmorillonite hybridization. Compos Part B Eng. 217, 108920. https://doi.org/https://doi.org/10.1016/j.compositesb.2021.108920

Tahon G, Tytgat B, Lebbe L, et al, 2018. *Abditibacterium utsteinense* sp. nov. the first cultivated member of candidate phylum FBP, isolated from ice-free Antarctic soil samples. Syst Appl Microbiol. 41, 279-290. https://doi.org/10.1016/j.syapm.2018.01.009

Tan J, Wang X, Zhang M, et al, 2023. *Chlorella sorokiniana* FK-montmorillonite interaction enhanced remediation of heavy metals in tailings. Sci Total Environ. 876, 163208. https://doi.org/10.1016/j.scitotenv.2023.163208

Tan JQ, Yi H, Zhang ZJ, et al, 2022. Montmorillonite facilitated Pb (II) biomineralization by Chlorella sorokiniana FK in soil. J Hazard Mater. 423, 127007.https://doi.org/10.1016/j.jhazmat.2021.127007

Uroz S, Kelly LC, Turpault MP, et al, 2015. The mineralosphere concept: Mineralogical control of the distribution and function of mineral-associatec bacterial

communities. Trends Microbiol. 23, 751-762. https://doi.org/10.1016/j.tim.2015.10.004

Vance ED, Brookes PC, Jenkinson DS, 1987. An extraction method for measuring soil microbial biomass C. Soil Biol Biochem. 19, 703-707. https://doi.org/10.1016/0038-0717(87)90052-6

Walkly A, 1934. An examination of the Degtjareff method for determining soil organic matter and a proposed modification to the chromic acid titration method. Soil Sci 37:29–38

Wang J, Zhang P, Bao JT, et al, 2020. Comparison of cyanobacterial communities in temperate deserts: A cue for artificial inoculation of biological soil crusts. Sci Total Environ. 745, 140970. https://doi.org/10.1016/j.scitotenv.2020.140970

Wang X, Meng D, Li J, et al, 2023. Composition and dynamics of bacterial communities during flotation in a coal preparation plant. J Clean Prod. 385, 135691. https://doi.org/https://doi.org/10.1016/j.jclepro.2022.135691

Wang Y, Chen L, Li Z, et al, 2024. The role of iron-rich organic fertilizer in promoting the growth of Chinese cabbage and inhibiting the transformation of cadmium. Sci Total Environ. 908, 168430. https://doi.org/https://doi.org/10.1016/j.scitotenv.2023.168430

Weber B, Belnap J, Budel B, et al, 2022. What is a biocrust? A refined, contemporary definition for a broadening research community. Biol Rev. 97, 1768-1785. https://doi.org/10.1111/brv.12862

Wu HW, Cui HL, Fu CX, et al, 2024. Unveiling the crucial role of soil microorganisms in carbon cycling: A review. Sci Total Environ. 909, 168627. https://doi.org/10.1016/j.scitotenv.2023.168627

Wu L, Farias ME, Torres RM, et al, 2022. Salinity affects microbial composition and function in artificially induced biocrusts: Implications for cyanobacterial inoculation in saline soils. Soil Biol Biochem. 170, 108691. https://doi.org/10.1016/j.soilbio.2022.108691

Wu S, Konhauser KO, Chen B, Huang L, 2023. “Reactive Mineral Sink” drives soil organic matter dynamics and stabilization. npj Mater Sustain. 1, 3. https://doi.org/10.1038/s44296-023-00003-7

Xie Y, Wen X, Tu Y, et al, 2024.Mechanisms of artificial biological soil crusts development for anti-desertification engineering on the Qinghai-Tibetan Plateau. Environ Technol Innov. 33, 103542. https://doi.org/10.1016/j.eti.2024.103542

Xie Z, Liu Y, Hu C, et al, 2007. Relationships between the biomass of algal crusts in fields and their compressive strength. Soil Biol Biochem. 39, 567-572. https://doi.org/https://doi.org/10.1016/j.soilbio.2006.09.004

Xu L, Kou Y, Xiong W, et al, 2023. Soil depths and developmental stages of biological soil crusts are more important than shrub cover in structuring prokaryotic communities. Catena. 232, 107436. https://doi.org/10.1016/j.catena.2023.107436

Xu W, Zhao Y, Lian Y, et al, 2024. Co-development of biocrust and herbaceous plant communities in sandy areas after cyanobacterial inoculation. Plant Soil. 1-14. https://doi.org/10.1007/s11104-024-06794-5

Xue Z, Qu T, Li X, et al, 2024. Different contributing processes in bacterial vs. fungal necromass affect soil carbon fractions during plant residue transformation. Plant Soil. 494, 301-319. https://doi.org/10.1007/s11104-023-06277-z

Yang F, Huang J, Zhou C, et al, 2023a. Desert abiotic carbon sequestration weakening by precipitation. Environ Sci Technol. 57, 7174-7184. https://doi.org/10.1021/acs.est.2c09470

Yang S, Liu D, Zheng W, et al, 2023b. Microbial reduction and alteration of Fe (III)-containing smectites in the presence of biochar-derived dissolved organic matter. Appl Geochem. 152, 105661. https://doi.org/10.1016/j.apgeochem.2023.105661

Yang X, Zhou J, Huo T, et al, 2021. Metabolic insights into the enhanced nitrogen removal of anammox by montmorillonite at reduced temperature. Chem Eng J. 410,128290. https://doi.org/https://doi.org/10.1016/j.cej.2020.128290

Zhao Y, Lian Y-C, Zhao Y-Q, et al, 2024. Biocrust succession significantly influences soil virus composition and alpha diversity in a sandy desert. Appl Soil Ecol. 195, 105255. https://doi.org/10.1016/j.apsoil.2023.105255

Zhao Y, Wang N, Zhang ZS, et al, 2021a. Accelerating the development of artificial biocrusts using covers for restoration of degraded land in dryland ecosystems. L Degrad Dev. 32, 285-295. https://doi.org/10.1002/ldr.3714

Zhao Y, Xu WW, Wang N, 2021b. Effects of covering sand with different soil substrates on the formation and development of artificial biocrusts in a natural desert environment. Soil Tillage Res. 213, 105081. https://doi.org/10.1016/j.still.2021.105081

Zhao Y, Zhao YQ, Xu WW, et al, 2023. Acquiring high-quality and sufficient propagules/fragments for cyanobacteria crust inoculation and restoration of degraded soils in a sandy desert. L Degrad Dev. 34, 1593-1597. https://doi.org/10.1002/ldr.4532

Zhou XB, Zhao YG, Belnap JN, et al, 2020. Practices of biological soil crust rehabilitation in China: experiences and challenges. Restor Ecol. 28, S45-S55. https://doi.org/10.1111/rec.13148

Zhu X, Jackson RD, DeLucia EH, et al, 2020. The soil microbial carbon pump: From conceptual insights to empirical assessments. Glob Chang Biol. 26, 6032-6039. https://doi.org/10.1111/gcb.15319

Chapter V. Differences in soil organic carbon accumulation process between two typical clays based biocrusts

5.1 Introduction

Desertification is rapidly intensifying, with desert areas now covering more than one-fifth of the global land area (F. Yang et al., 2023). Soil organic carbon (SOC) plays a vital role in building resilient soil structures and ensuring optimal biogeochemical functions, making it essential for the restoration of desert regions (Chalchissa and Kuris, 2024; Chen et al., 2023; Li et al., 2023; Wu et al., 2023). Microorganisms are the primary drivers of SOC formation in biocrusts (Liang et al., 2017). Biocrusts are complex associations of organic microorganisms and inorganic soil minerals, providing crucial ecological functions such as fertilization, sand fixation, and supporting vegetation recovery (García-Carmona et al., 2020; Román et al., 2020; Zhang et al., 2022). Notably, biocrusts cover approximately 30% of the global dryland surface and are a dominant form of ground cover (Weber et al., 2022). Photosynthetic autotrophs within biocrusts capture atmospheric CO2 through photosynthesis, which is then used to form SOC. One study found that cryptogamic covers, including biocrusts, sequester 590 Tg/a of carbon in grasslands and deserts (Maier et al., 2018). Therefore, biocrusts are a significant contributor to SOC accumulation in desert areas.

SOC accumulation is influenced by both the formation and accumulation processes of SOC. The role of minerals in enhancing SOC stability through mechanisms like adsorption, encapsulation, and aggregation is well-documented (Wu et al., 2023; Xiao et al., 2023). The ability of minerals, especially clay minerals, to stabilize SOC is critical for its accumulation in various ecosystems, including oak forests, paddy soils, broadleaf forests, and shrubland grasslands (Jeewani et al., 2021; Liang et al., 2023; B. Wang et al., 2021; C. Wei et al., 2021). For SOC formation, microbial growth is a key driver (Liang et al., 2017). Previous research has highlighted that minerals and rocks provide physical support for microorganisms and plants, while also playing a role in nutrient cycling, soil fertility, and water quality. From an evolutionary standpoint, microbial colonization of minerals is a well-established strategy. Additionally, smaller clay minerals facilitate microbial colonization (Uroz et al., 2015; Wu et al., 2023; X. Yang et al., 2021). A study by Zhou et al. (2023) demonstrated that clay minerals enhance biocrust development by prolonging the water infiltration time on the soil surface.

Clay minerals are primarily categorized into 1:1 type and 2:1 type (Boumaiza et al., 2020). Kaolin and montmorillonite (MMT) are representative examples of 1:1 and 2:1 type clays, respectively (Zhang et al., 2022). Compared to 1:1 type clay, 2:1 type clay has a larger specific surface area (SSA) and higher cation exchange capacity (CEC), which are generally associated with a stronger adsorption potential (Six et al., 2002). While some studies have explored the relationship between these two types of clay and SOC (Han et al., 2016) most have focused on the stabilizing effects of clay on SOC,

often overlooking the role of clay in microbial growth or SOC formation (Jing et al., 2022; Liu et al., 2023). Furthermore, there are still some contradictions in current research regarding the effect of two different types of clay on the stability of SOC (Han et al., 2016). As Wattel‐Koekkoek et al. (2003) suggested, compared to kaolin, MMT significantly reduces the turnover rate of SOC and improves its stability. However, Xu et al. (2024) found that kaolin significantly reduced the mineralization rate of glucose and enhanced the accumulation of SOC. Therefore, more research is needed to better understand how different clay types influence the formation, stability, and accumulation of SOC.

The role of clay minerals in facilitating SOC formation and stabilization has been well-documented in various ecosystems, yet their significance in biocrust systems remains largely overlooked. Additionally, the effects of 1:1 and 2:1 type clays on SOC stabilization continue to be a topic of debate. Based on this, we propose the hypothesis that clay minerals may enhance SOC accumulation in artificial biocrusts by promoting both its formation and stability.

To investigate this, we examined the influence of kaolin (a 1:1 type clay) and montmorillonite (MMT, a 2:1 type clay) on SOC dynamics by co-inoculating them with *Microcoleus vaginatus* and cultivating the biocrusts for 84 days. Microbial growth was assessed through microbial biomass carbon (MBC), chlorophyll-a (Chl-*a*), and alpha diversity. SOC stability was evaluated using biological stability (mineralization quotient, qM), chemical stability (hot-water extractable organic carbon, HWEOC), and molecular structural stability. Additionally, solid-state nuclear magnetic resonance (^{13}C NMR) spectroscopy was employed to analyze structural variations in SOC bound to the two clay minerals. SOC content was monitored to determine the impact of different clay types on accumulation. By elucidating the mechanisms underlying SOC formation and stabilization in artificial biocrusts, this study provides valuable insights into effective restoration strategies for nutrient-deficient ecosystems, such as desert environments.

5.2 Materials and methods

5.2.1 Preparation of kaolin, MMT, sandy soil, and algal solution

Kaolin was purchased from Henan Yixiang Co., China, and washed three times with deionized water. MMT was obtained from Chifeng Ningcheng Bentonite Co., China, and subjected to ion exchange and washing by being placed separately in 1 M NaCl and deionized water at a 1:10 ratio (W/V) (Ma et al., 2004). The molecular formulas of the two types of clay were then determined by X-ray diffractometer (XRD) (Empyrean, Netherlands), which identified them as $Na_{0.3}Al_2[(Si, Al)_4O_{10}] (OH)_2 \cdot 2H_2O$ (JCPDS no:43-0688) and $Al_4(OH)_8(Si_4O_{10})$ (JCPDS no:99-0067) (Figure S4.1). Sandy soil was obtained from the Kubuqi Desert and its physical and chemical properties are presented in Table S5.1.

M. vaginatus (strain PCC 9802) was originally isolated from natural biocrusts in the Kubuqi Desert. Pure *M. vaginatus* was cultivated in BG-11 medium at 10 °C as stock cultures. Algal biomass for inoculation was prepared from stock cultures, whose cells were homogenized with sterilized glass homogenizers to ensure an even suspension. The algae were then cultured in BG-11 medium for 20 days under controlled conditions, with a temperature of 25 ± 1 °C and a daily light/dark cycle of 14/10 h (Zhixiang Wang et al., 2025). Illumination during the light period was provided by cool-white fluorescent light at 40 $\mu E \cdot m^{-2} \cdot s^{-1}$), as described by Wu et al. (2022)**.** The final large blocks of algae were crushed by a liquidizer (BG-JS2, Midea, China) and diluted with deionized water to obtain a homogeneous 3.2 μg/mL algal solution (dry algal weight)**.**

5.2.2 Experimental design

This study used constructed microcosms in ϕ150 × 15 mm circular culture dishes. Each culture dish was evenly spread with 200 g of sandy soil. Six experimental groups, the Kaolin group, the MMT group, the Algae group, the control group of the Kaolin group (C-kaolin group), the control group of the MMT group (C-MMT group), and the control group of the Algae group (C-Algae group) were established. Six replicates of each treatment group were prepared. The Kaolin group and the MMT group were provided with 3.72 g of kaolin and MMT, respectively, along with 30 mL of algal solution. (The amounts of the two types of clay to be added were determined based on the preliminary experiment results shown in Figure S2). The Algae group was only provided with 30 mL of algal solution. The C-kaolin group and the C-MMT group were supplemented with 3.72 g of kaolin and MMT, respectively, without any algal solution. In the C-Algae group, neither clay nor algal solution was added. All microcosms were initially supplied with 10 mL of BG-11 nutrient solution. During the subsequent 84-day cultivation period, no additional nutrients were added; only deionized water was used to maintain a relative soil moisture of 60%, equivalent to a soil water content of 10.92% (Wu et al., 2024). The microcosms were kept in a temperature-controlled incubator set at 25 ± 2 °C, with a daily cycle of 14 h of light and 10 h of darkness. Illumination during the light period was provided by cool- white fluorescent light at 40 $\mu E/(m^2 \cdot s)$. Regular sampling was performed to measure indicators, with surface biocrusts and underlying soil collected simultaneously during each sampling event.

5.2.3 Analytical methods

The external specific surface area (ESSA) of kaolin, MMT, and sandy soil was determined using the Brunauer-Emmett-Teller (BET) method with N_2 adsorption at 77 K. Prior to adsorption, the samples were degassed in a vacuum at 120 °C for 12 h (Zheng et al., 2024). The total specific surface area (TSSA) of MMT was measured by the methylene blue (MB) method (Santamarina et al., 2002). Specifically, 30 g of MMT was added to 500 mL of deionized water and stirred at 600 rpm for 5 min using a mechanical stirrer. Subsequently, a 10 g/L MB solution was added dropwise. After each addition of 20 mL of MB solution, stirring was continued at 400 rpm for 1 min. A drop

of the solution was then taken with a glass rod approximately 8 mm in diameter and placed on filter paper. The state of the droplet was observed. When a pale blue halo approximately 1 mm wide formed around the droplet on the filter paper and remained stable for 5 min without disappearing, the addition of MB solution was stopped. At this point, the TSSA of MMT can be calculated using Equation 1. The internal specific surface area (ISSA) of MMT was calculated by subtracting the ESSA from the TSSA.

$$S_{TSSA}=\frac{1}{319.87}C_{MB}VN_AA_{MB}\frac{1}{m_s} \quad \text{(Eq. 1)}$$

where C_{MB} represents the concentration of methylene blue (MB), equal to 10 g/L; V is the volume of the adsorbed MB solution, N_A is Avogadro's constant, equal to 6.02 × 10^{23} mol^{-1}; A_{MB} is the area covered by a single MB molecule, equal to 130 $Å^2$; m_s is the mass of the dry soil sample used in the test, set at 30 g; 319.87 is the molar mass of the MB molecule.

CEC was measured using the barium chloride extraction method (Ciesielski et al., 1997). A laser particle size analyzer (Malvern, Mastersizer 2000, Britain) was used to determine the particle size of the three substances. The microscopic morphologies of the six groups were examined by scanning electron microscope (SEM) (Phenom 6.0, Thermo Fisher Scientific, USA).

The content of SOC, available N (AN), total P (TP), and available P (AP) were determined using the $K_2Cr_2O_7$ oxidation (Walkly, 1934), the alkali dissolution diffusion method (Wang et al., 2024), the alkali fusion-Mo-Sb Anti spectrophotometric method, and the $NaHCO_3$-Mo-Sb anti spectrophotometric method, respectively (Tan et al., 2023). an elemental analyzer was used for total C (TC) and total N (TN) (Isoprime Ltd. Germany). The pH was determined with a pHmeter (S20 SevenEasy, Mettler Toledo, USA) at a ratio of 1:5 (W/V).

MBC was determined using the chloroform-fumigation-extraction method (Vance et al., 1987; Yu et al., 2023). Briefly, two identical samples were placed in separate dark sealed containers, one fumigated with $CHCl_3$ and the other not, for 24 h. Both samples were then extracted with 0.5 M K_2SO_4 at a ratio of 1:4 (W/V). The experimental conversion factor (E) was determined to be 0.45 for calculation of the result. Dissolved organic C (DOC) was measured from the control group without fumigation (Wang et al., 2022).

Chl-*a* was extracted with ethanol and measured according to Mugnai et al. (2018). Photosynthetic fluorescence parameters of the six systems were measured by a plant efficiency analyzer (PEA, Hansatech Instruments Ltd., UK). Specifically, the test samples were placed in the dark for more than 20 min and then exposed to a saturating pulse of 3000 μE m^{-2} s^{-1} to determine the maximum quantum yield F_v/F_m (Lan et al., 2017; L. Wu et al., 2022) and the performance index PI_{ABS} (Van Heerden et al., 2004). PI_{ABS} is a comprehensive performance parameter that reflects the overall efficiency of the main functional steps in the photosystem II (PSII) reaction center, including light energy absorption, excitation energy trapping, and conversion of excitation energy to electron transport (Van Heerden et al., 2004).

The NaOH absorption method was used to determine the mineralization process of SOC. Specifically, the samples were placed in containers with a 0.1 M NaOH solution, sealed, and kept away from light. After 25 days, the NaOH solution absorbing CO_2, was titrated with the 0.1 M H_2SO_4 solution. Basal respiration (Cbas), cumulative respiration (Ccum), metabolic quotient (qCO_2), and mineralization quotient (qM) were then calculated according to Lei et al. (2017).

Hot-water extractable organic carbon (HWEOC) was determined using the water bath method (Hou et al., 2019). Specifically, the sample was mixed with deionized water at a 1:10 ratio (W/V). After being shaken for 30 min, the mixtures were placed in a water bath at 70 ℃ for 18 h. The mixture was then thoroughly mixed on a vortex shaker for 3 s, and the supernatant was obtained by filtering. Finally, the SOC of the supernatant was determined. HWEOC was expressed as the percentage of SOC content before and after treatment.

The molecular structural stability of SOC ($SOC_{molecular}$) was characterized by ^{13}C NMR spectroscopy. After pre-treatment with 2% HF, the spectra of the samples were recorded on a Bruker AVANCE III 400 MHz instrument (Bruker, Germany). The spectral range of 10 to 220 ppm was the focus of the research. According to Hou et al. (2019), the chemical shift regions of -10-45, 45-110, 110-160, and 160-220 ppm correspond to alkyl C, O-alky C, aryl C, and carboxyl C, respectively. The areas under the curves for each chemical shift were defined as A_{-10-45}, A_{45-110}, $A_{110-160}$, and $A_{160-220}$, respectively. Alkyl C and aryl C are the recalcitrant carbon, while O-alky C is the labile carbon. The proportion of carboxyl ($P_{carboxyl}$) represents binding ability with SOC (Curti et al., 2021; Gu et al., 1994). The proportion of alkyl C (P_{alkyl}), O-alky ($P_{O\text{-}alky}$), aryl (P_{aryl}), $P_{carboxyl}$, and $SOC_{molecular}$ were calculated as: Equation 2 to 6, respectively:

$$P_{alkyl} = A_{-10-45}/(A_{-10-45}+A_{45-110}+A_{110-160}+A_{160-220}) \quad \text{(Eq. 2)}$$

$$P_{O\text{-}alky} = A_{45-110}/(A_{-10-45}+A_{45-110}+A_{110-160}+A_{160-220}) \quad \text{(Eq. 3)}$$

$$P_{aryl} = A_{110-160}/(A_{-10-45}+A_{45-110}+A_{110-160}+A_{160-220}) \quad \text{(Eq. 4)}$$

$$P_{carboxyl} = A_{160-220}/(A_{-10-45}+A_{45-110}+A_{110-160}+A_{160-220}) \quad \text{(Eq. 5)}$$

$$SOC_{molecular} = (P_{alkyl}+P_{aryl})/P_{O\text{-}alky} \quad \text{(Eq. 6)}$$

Samples were subjected to DNA extraction using the MagaBio DNA Soil Kit (Bioer Technology, China). Polymerase chain reaction (PCR) amplification targeted the bacterial 16S rDNA V3V4-1 region, utilizing the firwar and revers primers 338F (5′-ACTCCTACGGGAGGCAGCAG-3′) and 806R (5′-GGACTACHVGGGTWTCTAAT-3′) described by Lu et al. (2024) and Quast et al. (2013). The establishment of a database, testing of amplified sequences, and clustering of processed sequence data were conducted as described by Wang et al. (2023). The final operational taxonomic units (OTUs) were aligned with the Silva database (https://www.arb-silva.de/browser/). The ecological functions of functional bacterial groups were annotated using the functional annotation of prokaryotic taxa (FAPROTAX) database (S. Zhang et al., 2023).

5.2.4 Statistical analyses

Statical analyses included significance analysis (one-way ANOVA; Duncan's multiple ranges ($p<0.05$) in SPSS 20.0 (IBM, USA), correlation analysis relationships between ESSA, CEC, HWEOC, and qM (spearman rank correlation analysis) and between DOC, Shannon index, and MBC (Pearson correlation) (Z. Li et al., 2021; Puth et al., 2015).

5.3. Results

5.3.1 Influence of clay on SOC formation

5.3.1.1 Promotion effect on microbial growth

The most evident difference between the six trials, was the final color associated to the microbial development, mainly over the surfacers after 84 days (Figure 5.1). E.g. after 7 days, a noticeable green coloring was observed in the Kaolin and MMT groups, while after 14 days, the Kaolin group showed higher green saturation color comparing with MMT by day 14. Such changes are because MBC is a reliable indicator for determining microbial biomass (Finstad et al., 2023), and in both groups MBC biomass were significantly higher than in the other ones. From day 14 onwards, the MBC in the remained higher in Kaolin group than in MMT group, and after 84 days, the MBC from the Kaolin and MMT groups were 5.67 times and 4.36 times those of the Algae group (Figure 5.2). Thus, the addition of both types of clay significantly accelerates microbial growth ($p < 0.05$), and kaolin being the mineral that most stimulates its development.

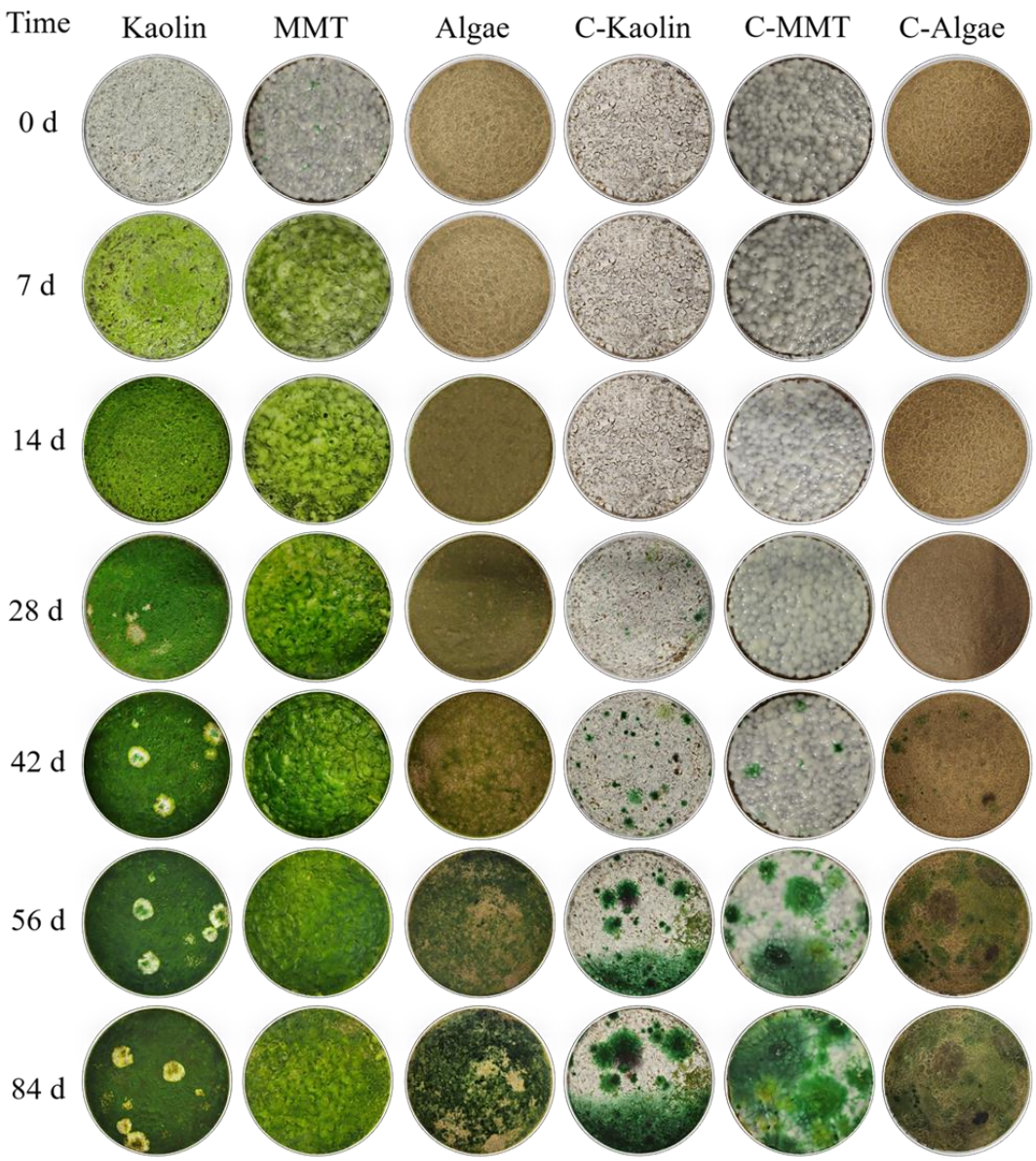

Figure 5.1. Dynamic changes during the development of microorganisms in the six treatments tested, at different times. C- represents blank control group

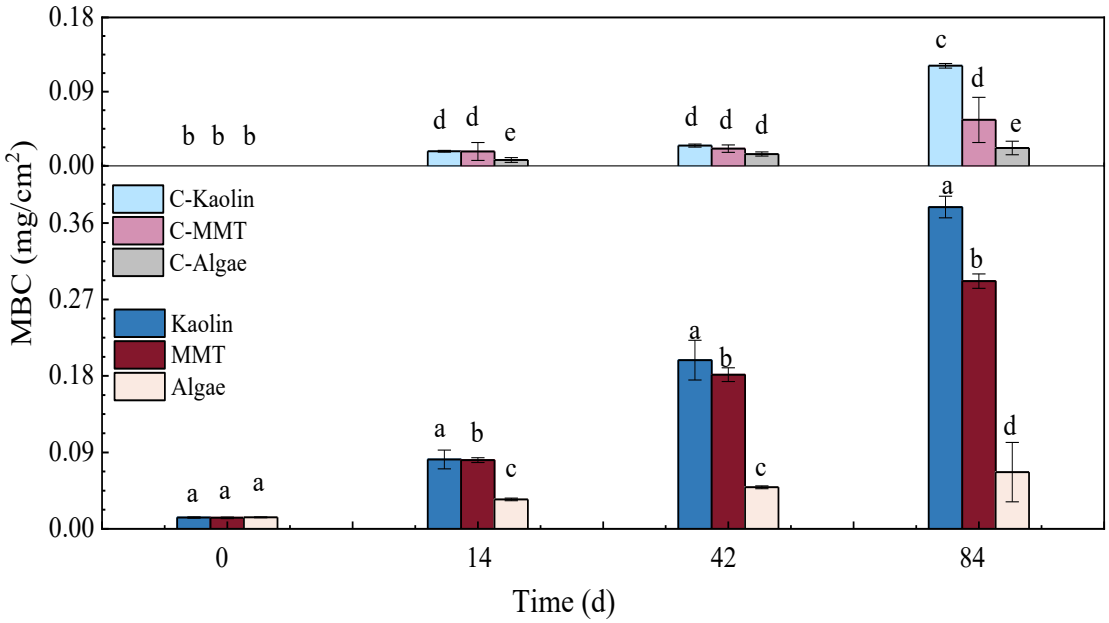

Figure 5.2. Microbial biomass carbon (MBC) after 0, 14, 42 and 84 days (d). a, b, c: significant diferences between trials per time ($p < 0.05$). C- represents blank control group

The increase in Chl-*a* during the assays reflects the presence of photosynthetic microorganisms (Figure 5.3a) (Mugnai et al., 2024). As the MBC (Figure 5.2), the presence of both types of clay increases the development of phototrophs ($p < 0.05$) in such a way that, the Chl-*a* contents in the Kaolin and MMT groups and after 84 days increases up to 2.44 and 1.59 times, respectively, compared with the group of Algae. This parameter alone does not reflect photosynthetic activity, therefore the associated photosynthetic efficiency must be analyzed (see below)

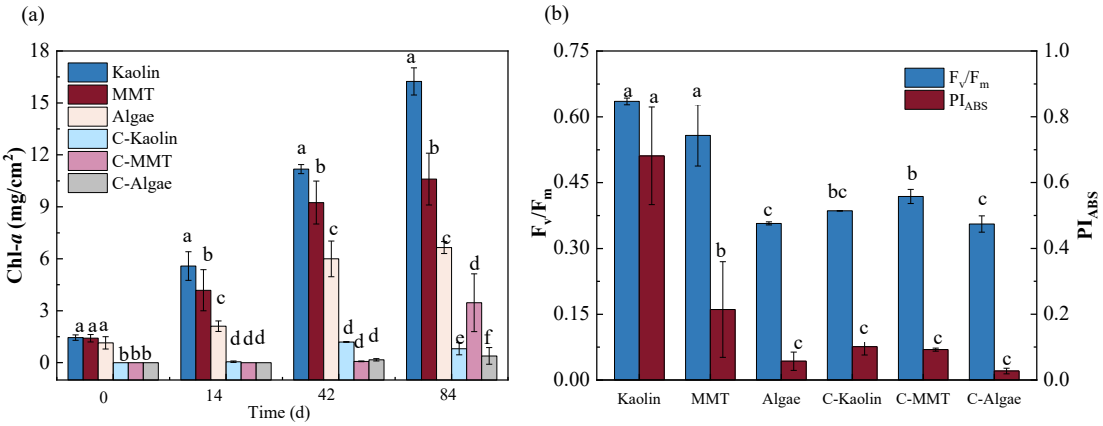

Figure 5.3 (a) Changes in chlorophyll-a (Ch-*a*) after 0, 14, 42 and 84 days (d); and (b) fluorescence parameters in each trial and on day 84. F_v/F_m: maximum quantum yield, PI_{ABS}: overall efficiency of reaction center in photosystem II (PSII). a, b, c and d: significant variations for $p<0.05$. C-: blank control group

The maximum quantum yield (F_v/F_m) and the overall efficiency of the reaction center in photosystem II (PII_{ABS}) obtained in the MMT and Kaolin groups were significantly higher than in the others (Figure 5.3b), e.g. F_v/F_m was 1.78 higher in Kaolin and 1.56 times in MMT groups than in Algae group). Although there are no statistically significant differences in F_v/F_m between the Kaolin and MMT groups, the PI_{ABS} of the Kaolin is 3.18 times than in MMT group. The former demonstrated that adding both clay minerals significantly enhanced the photosynthetic activity in biocrusts, and that kaolin showed a greater positive effect than MMT.

5.3.1.2 Influence on microbial community structure

The SEM images revealed the microscopic structures of the six experimental groups on day 0 (Figure S5.3) and day 84 (Figs. 5.4a to f). After growing during 84 days, the biocrust in the MMT group displayed an interesting “house-of-cards” assembly (P. Li et al., 2022); that is, a fragile but complex order arrange among microorganisms of the biocrusts (Figure 5.5c). In contrast, the Algae and Kaolin groups showed a higher abundance of filamentous algae, that may correspond to the originally inoculated, or their homologous counterparts (Figs. 5.5a, b, d-f).

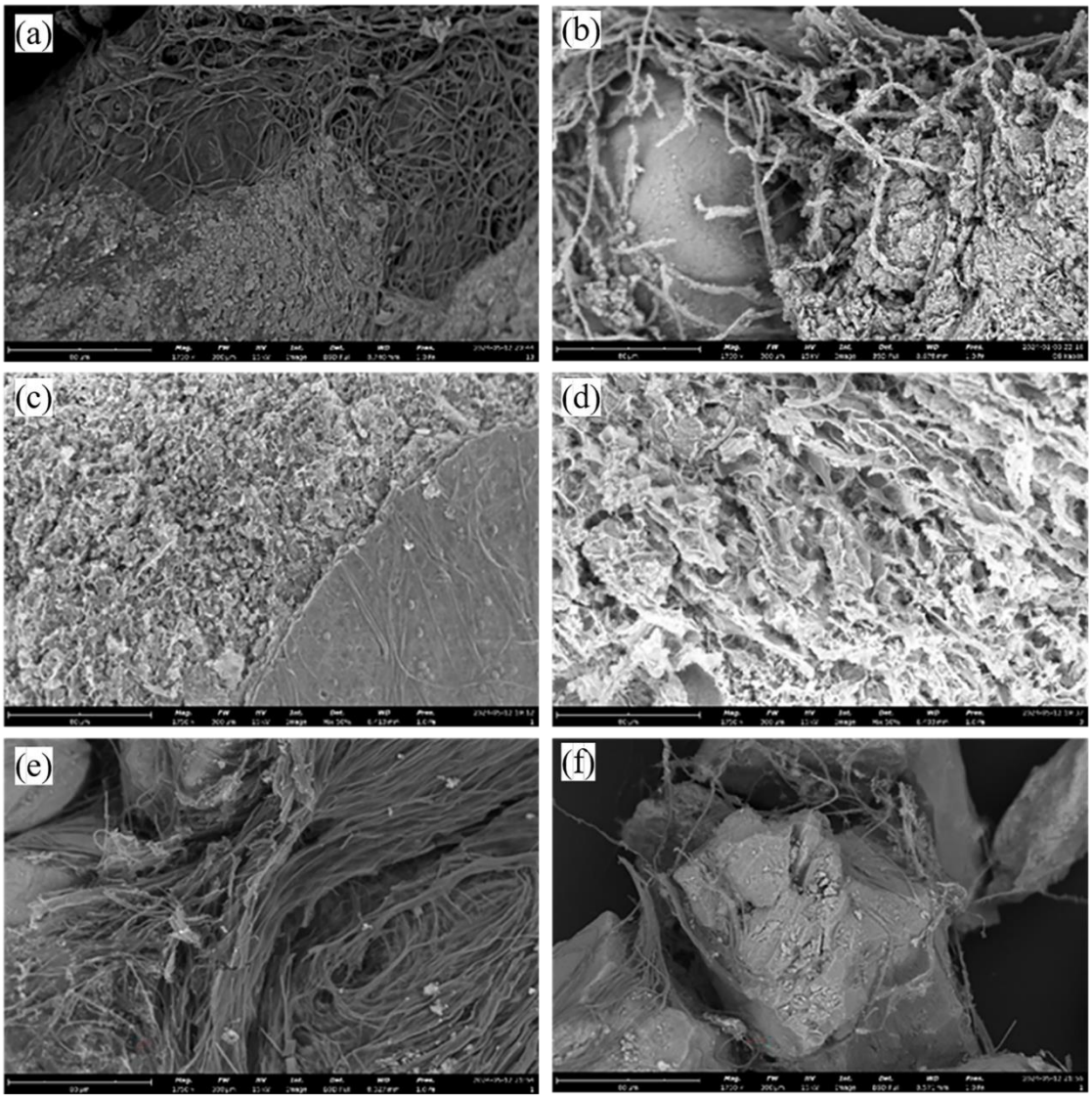

Figure 5.4. Images obtained from the scanning electron microscope, of biocrust samples after 84 days, from groups: (a) Kaolin, (b) C-kaolin, (c) MMT, (d) C-MMT, (e) Algae, and (f) C-Algae. C- represents blank control group

After 16S rDNA analyses, 24,526 sequences were obtained from 24 samples. These analyses cover 99% (Table 5.1); thus, it is possible to describe the bacterial community structure in each sample. All indices for evaluate Alpha diversity (e.g. Shannon, Simpson, ACE, and Chao1) (Zhang et al., 2022), displayed consistently the same diversity order ($p < 0.05$): Kaolin>MMT>Algae groups; meanwhile, the Shannon indexes for groups with the minerals, Kaolin and MMT, showed 1.82 and 1.42 times of the Algae group (Figure 5.5a, Table 5.1).

Table 5.1. Alpha diversity indexes of bacteria. Different letters assigned to values denote statistically significant differences ($p < 0.05$)

Group	Observed features	Shannon	Simpson	ACE	chao1	cover
Algae	968± 315bc	3.18± 0.24bc	0.67± 0.05bc	974.13± 317.40bc	969.92± 316.26bc	1.00
MMT	1146± 253abc	4.52± 1.07ab	0.75± 0.13b	1151.54± 254.78abc	1147.59± 254.41abc	1.00
Kaolin	1758± 969a	5.80± 2.07a	0.90± 0.07a	1767.55± 973.29a	1762.05± 973.17a	1.00
C-MMT	548± 66c	2.18± 0.165c	0.61± 0.04c	549.24± 65.976c	547.72± 65.72c	1.00
C-kaolin	1471± 136ab	3.56± 0.36bc	0.63± 0.10bc	1484.08± 140.57ab	1476.39± 139.11ab	1.00
C-Algae	640± 205c	2.65± 0.18c	0.60± 0.04c	645.01± 207.65c	641.61± 206.11c	1.00

Note: C- represents blank control group

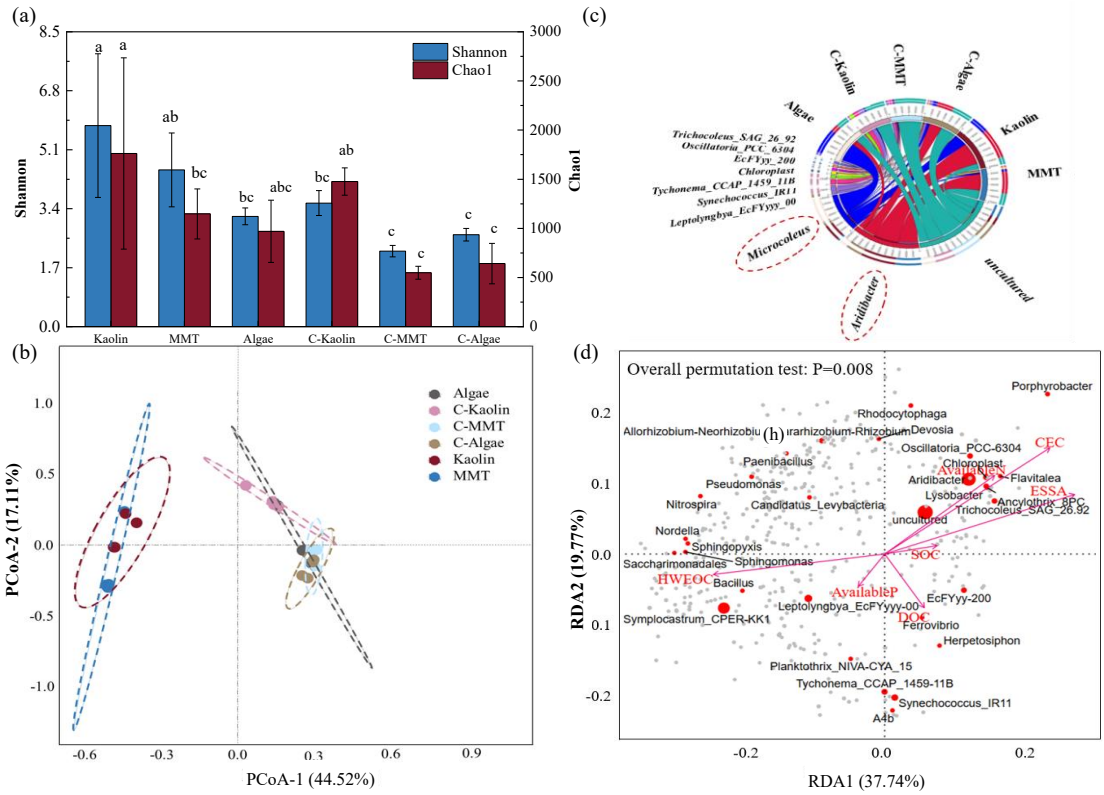

Figure 5.5 (a) The Shannon and Chao 1 indexes of bacteria in the six experimental groups on day 84. Different lowercase letters refer to significant variations ($p < 0.05$); (b) Principal coordinate analysis (PCoA) of bacterial communities at the OTU level; (c) Circos map of microbial community structure in the six groups at the genus level. (Only the top 10 dominant genera are shown); (d) Redundancy analysis (RDA) of environmental factors and bacterial communities. The length and direction of the arrows represent the degree of impact of environmental factors on the structure of the bacterial communities, as well as the positive or negative correlations between them. C- represents blank control group

The result suggested that the addition of both types of clay increased the diversity and richness of bacterial communities, and the promoting effect of kaolin was greater.

A total of 652 bacterial genera were identified across 24 samples. The distance between two clay–algae addition groups and the other four groups (Figure 5.5b) suggested that the addition of clay significantly altered the microbial community structure. Moreover, the principal coordinate analysis (PCoA) revealed that the bacterial microbial community structures of the MMT and Kaolin groups are highly similar. Figure 5.5c exposed that the addition of clay had an apparent impact on the abundance proportion of *Microcoleus* and *Aridibacter*. As *Microcoleus vaginatus* (the initially inoculated algae) belongs to *Microcoleus*, variations in the abundance of *Microcoleus sp.* may indicate changes in its differential reproduction rate in each experimental group in which it was inoculated. The abundance ratio of *Microcystis* in the three groups was: Algae> Kaolin>MMT groups. *Aridibacter*, a type of bacteria commonly associated with clay, increased in response to the addition of clay (Huber et al., 2014). The abundance ratio of *Aridibacter* was the inverse of *Microcoleus*, MMT >Kaolin> Algae groups. This suggests that MMT had a stronger influence on regulating microbial communities compared to kaolin. Using the FAPROTAX database, a total of 55 microbial pathways were annotated, with 7 representative pathways summarized in Table S5.2. The results show that the phototrophic pathway abundance in the MMT and Kaolin groups was significantly higher than in the Algae group, and phototrophic cyanobacteria played a major role in the pathway. Redundancy analysis (RDA) was used to explore the influence of seven environmental factors on the composition of the bacterial communities (Figure 5.5d). The results show that ESSA, CEC, and HWEOC were the primary factors affecting the bacterial community structure, among which ESSA and CEC had positive effects.

These results suggested that the addition of clay, especially MMT, significantly influenced the microbial community structure. ESSA and CEC were identified as the primary positive factors shaping this structure.

5.3.2 Influence of clay on SOC stability

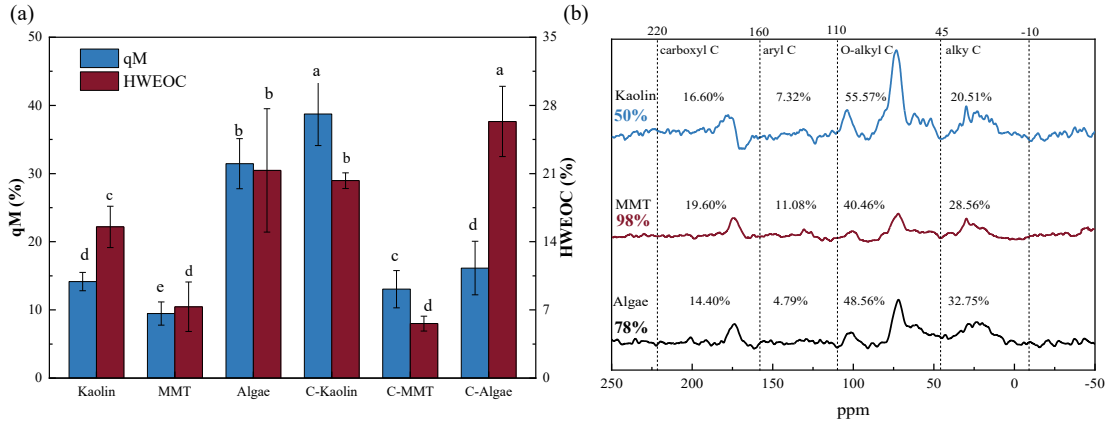

Figure 5.6 (a) Mineralization quotient (qM) and hot-water extractable organic carbon (HWEOC) on day 84. Different lowercase letters refer to significant variations ($p < 0.05$); (b) ^{13}C NEXAFS spectra of the Kaolin, MMT, and Algae groups. The chemical shift region -10-45,45-110,110-160, and 160-220 ppm represents alkyl C, O-alkyl C, aryl C, and carboxyl C, respectively. C- represents blank control group

Table 5.2 Spearman rank correlation analysis of ESSA, CEC, HWEOC, qM

Variable	Variable	Sample size (n)	Spearman's ρ	p-value
ESSA	HWEOC	18	-0.89	*** (< 0.001)
CEC	HWEOC	18	-0.82	*** (< 0.001)
ESSA	qM	18	-0.59	* (< 0.05)
CEC	qM	18	-0.58	* (< 0.05)

Note. ESSA: external specific surface area (ESSA); CEC: cation exchange capacity; HWEOC: hot-water extractable organic carbon; qM: mineralization quotient; Spearman's ρ: Spearman's rank correlation coefficient. C- represents blank control group

Mineralization is the main process for decomposing SOC (Breidenbach et al., 2022). Cbas, Ccum, qCO_2, and qM serve as important parameters for evaluating the mineralization of SOC, with qM being parameter that most directly characterizes the mineralization rate of SOC. Additionally, qM serves as an indicator of the biological stability of SOC, with smaller values indicating higher biological stability (Francaviglia et al., 2017). The ranking of qM was Aglae group > Kaolin group > MMT group, with the qMs of the MMT and Kaolin groups being 0.30 and 0.45 times that of the Algae group (Figure 5.6a). This indicates that the addition of both kaolin and MMT enhanced the biological stability of SOC, and MMT exhibited a stronger effect.

The parameters qM and HWEOC correspond to the biological and chemical stability of SOC, respectively. Lower values indicate higher stability (Hou et al., 2019). Both qM and HWEOC of the MMT group and Kaolin group are significantly lower than for the other groups ($p < 0.05$); while the HWEOC of the MMT group was 0.73 and 0.34 times higher than Kaolin and Algae groups, respectively (Figure 5.6a).

Table 5.2 shows that CEC and ESSA impact deeply on qM and HWEOC, particularly HWEOC. Notably, after 84 days of cultivation, XRD characterization of MMT and kaolin showed no significant change in interlayer spacing, indicating that SOC was not adsorbed into the interlayers in the two clays (Figure S5.1), consistent with previous findings (Baham and Sposito, 1994). Therefore, in this study, the SSA used for correlation analysis of MMT was based on the ESSA rather than the TSSA.

Figure 5.6b shows the Kaolin group demonstrated better adsorption capacity for labile carbon (O-alkyl C) and recalcitrant carbon (aryl C), that compared to the Algae group. In contrast, the MMT group, exhibited stronger retention effects for recalcitrant carbon (alkyl C and aryl C) but weaker adsorption of labile carbon. $SOC_{molecular}$ of the MMT group was 1.31 and 1.56 times higher than that in the Algae and Kaolin groups, respectively. Therefore, the addition of these minerals improved the biological and chemical stability of SOC, with MMT contributing more significantly to SOC stability than kaolin.

5.3.3 Influence of clay type on SOC accumulation

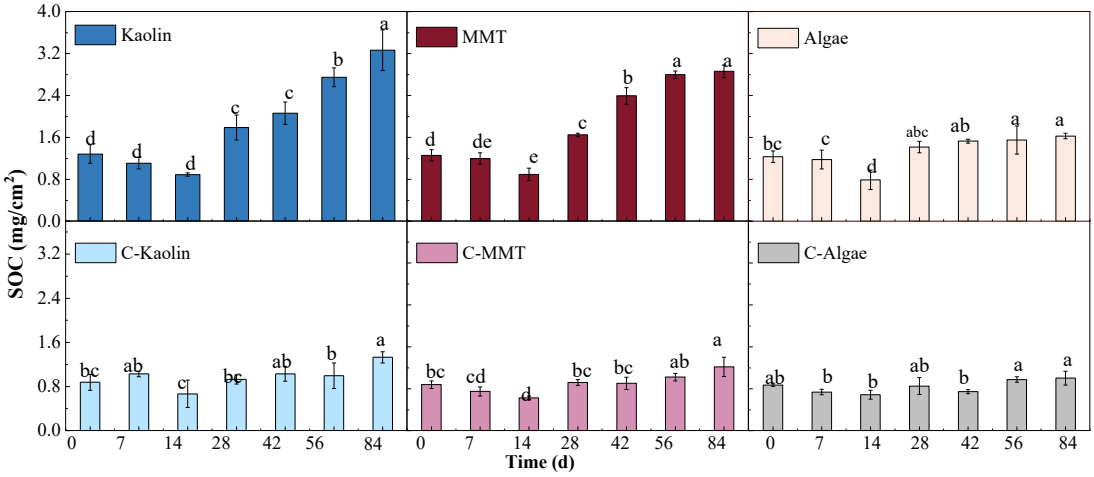

Figure 5.7 Changes of soil organic carbon (SOC) content over time for the six groups. Different lowercase letters refer to significant changes in SOC content over time for each group ($p < 0.05$). d: day. C- represents blank control group

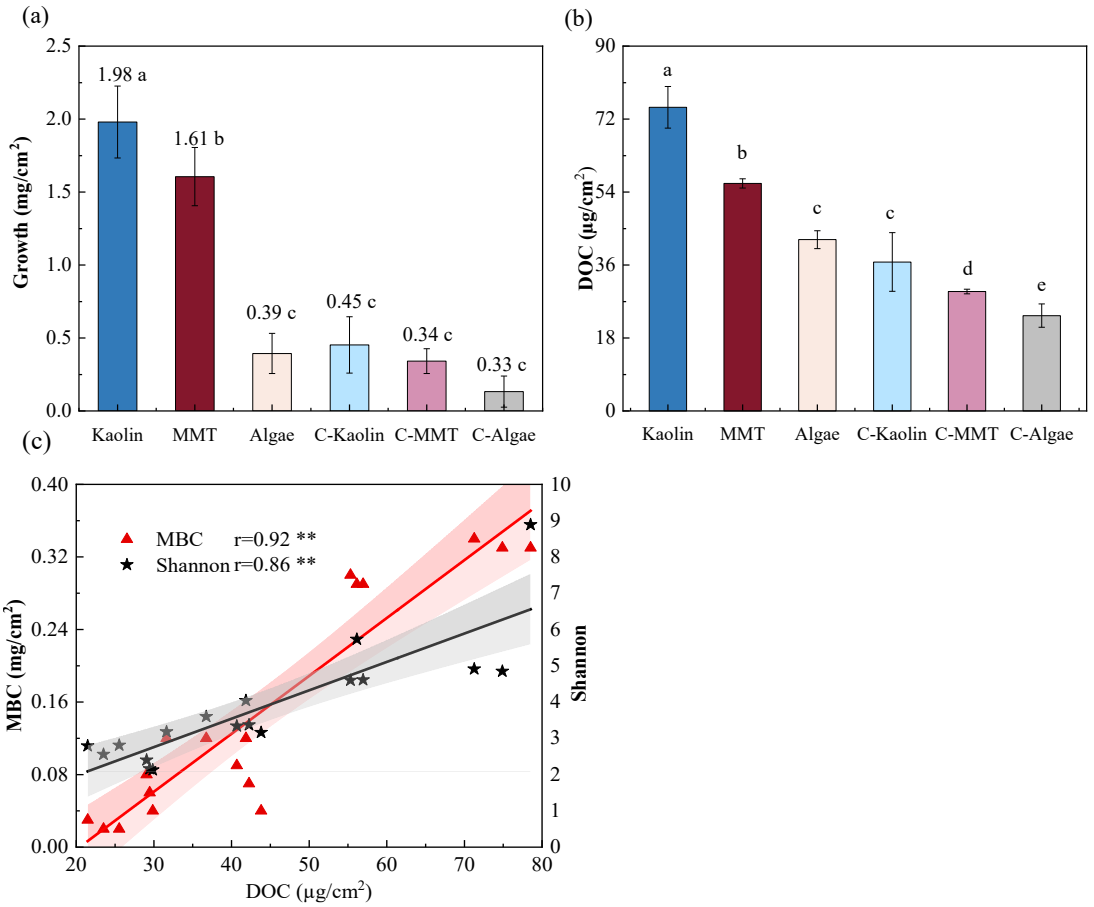

Figure 5.8 (a) soil organic carbon (SOC) growth of the six groups on day 84; (b) Dissolved organic carbon (DOC) of the six groups on day 84. Different lowercase letters refer to significant variations ($p < 0.05$); (c) Correlation analysis of microbial biomass carbon (MBC) and Shannon index with DOC. C- represents blank control group

As shown in Figure 5.7, the SOC content in all six groups followed a pattern of initial decline, followed by a subsequent increase. The decrease observed during days 0–14 was attributed to the slower formation and higher consumption of SOC by microbes. Between days 14 and 84, microbial proliferation led to a rapid increase in SOC content. Throughout this process, the facilitative impact of the two types of clay on SOC accumulation was visually evident, and the positive effect of kaolin was stronger. After 84 days, the growths of SOC in the Kaolin and MMT groups were 5.03 and 4.08 times that of the Algae group (Figure 5.8a), respectively.

DOC originates from the labile part of SOC, which is the most readily utilized by microorganisms (Li et al., 2023; F. Liu et al., 2023). The DOC of the Kaolin group was significantly higher than the other groups *($p < 0.05$)*, 1.78 and 1.33 times that of the Algae and MMT groups, respectively (Figure 5.8b). DOC showed a strong positive correlation between MBC, Shannon, and DOC (Figure 5.8c), indicating that the higher DOC content was the dominant reason for microbial growth.

5.4 Discussion

5.4.1 Synergistic effect of clays and cyanobacteria on accumulation of SOC

Undoubtedly, the formation and stability of SOC are the two major factors determining the accumulation of SOC. Microorganisms are the primary source of SOC, and microbial growth is a critical driver for SOC formation (Liang and Balser, 2011; H. W. Wu et al., 2024). Fine particles with highly reactive surfaces provide more available areas for microbial colonization, thus promoting microbial growth (Uroz et al., 2015). Zhao et al. (2021) showed a positive correlation between the biocrust cover and fine particle content (< 0.1 mm). In our study, 90% of the particles in MMT and kaolin were < 0.1 mm, explaining the significant changes of color, MBC (Figure 5.2), and Chl-*a* (Figure 5.3a) in the Kaolin group and MMT group. The spatial heterogeneity presented by numerous pores in clay minerals increases microbial diversity (Hartmann and Six, 2023). Compared to the Algae group, both the MMT and Kaolin groups exhibited higher alpha diversity, also visually verified. This explains why the addition of both types of clay promoted microbial growth in this study.

It is widely recognized that the protective effect of clay on SOC arises primarily from adsorption, in which SOC is adsorbed onto the clay surface or interlayer, forming a physical barrier between SOC and decomposers (Arthur et al., 2023; Islam et al., 2022; Kan et al., 2022; T. Wu et al., 2022). Consequently, the stronger the adsorption capacity of clay for SOC, the more favorable it is for the stability of SOC. The results of this study indicate that the addition of both clays in the clay-microalgae co-inoculation groups enhances the biological and chemical stability of SOC. Although the SOC molecular stability in the Kaolin group was lower than in the Algae group, the greater number of microorganisms and the more stable biological and chemical SOC stability

in the Kaolin group still resulted in a much higher SOC growth compared to the Algae group.

The influence of both clays on SOC formation and stability contributed to SOC growth in the Kaolin and MMT groups being 5.03 and 4.08 times higher than in the Algae group, respectively (Figure 5.8a). The SOC increases in the Kaolin and MMT groups were significantly higher than SOC growth in other groups. This demonstrated the synergistic effect of clays and cyanobacteria on SOC accumulation, with the two typical clays acting as synergists in this process.

5.4.2 Stronger effect of MMT on the stability of SOC

Our study demonstrated that in clay-microalgae inoculated systems, the addition of both clays improved the biological and chemical stability of SOC, with MMT showing a stronger positive effect (Figure 5.6). Table 5.2 shows the significant negative correlation between ESSA, CEC, and HWEOC (Spearman's ρ_{CEC} -0.82**; Spearman's ρ_{ESSA} -0.89**). The greater ESSA and higher CEC (Table S5.1) of MMT confer a higher adsorption potential, resulting in that of kaolin-HWEOC being 2.12 times that of MMT-HWEOC. Although the qM in the MMT group was also significantly higher than in the Kaolin group ($p < 0.05$), it showed a lower correlation with CEC and ESSA. This was due to differences in microbial growth among the six groups. For example, the lower microbial biomass in the C-algae group resulted in lower Ccum and qM, whereas the higher microbial biomass in the C-Kaolin group led to greater Ccum and qM (Table S5.3).

^{13}C NMR results (Figure 5.6b) indicated that MMT had a stronger adsorption capacity for recalcitrant carbon (alkyl C and aryl C), whereas kaolin showed stronger adsorption for labile carbon (O-alkyl C), including microbe polysaccharides (Mo et al., 2022). It also explained the result in Xu et al. (2024), that kaolin had a stronger inhibitory effect on SOC mineralization than MMT when polysaccharides were used as the carbon source. The results also were similar to those of previous studies, but in those cases they were assumed to be due to specific adsorption with unknown causes (Feng et al., 2005; Kallenbach et al., 2016; Wattel-Koekkoek et al., 2001). However, this study suggests that the larger ESSA and higher CEC enable MMT to have a good adsorption capacity for all types of organic carbon structures. This was supported by the order of $P_{carbonyl}$: MMT group > kaolin group > algae group, which indicates adsorption capacity with SOC (Curti et al., 2021; Gu et al., 1994). However, due to pore size limitations, the adsorption capacity of MMT for O-alkyl C, which is composed of large molecular structures (Mo et al., 2022), was restricted. The total adsorption average pore width (BET) of kaolin is 2.25 times that of MMT (Table S5.1), increasing the likelihood of O-alkyl C adsorption on kaolin. This was consistent with the findings of Wang et al. (2024), which also explains why MMT prefers lower molecular weight organic carbon (Han et al., 2021). This also emphasizes that the larger ESSA and higher CEC were the fundamental reasons for the increased $SOC_{molecular}$ value in MMT.

5.4.3 Stronger effect of kaolin on SOC formation

The experimental results indicated that the addition of both clays promoted SOC formation; however, the effect was more pronounced in the Kaolin group. Theoretically, MMT, with its unique layered structure, provides more pores than kaolin (Table. S4.1, Figs. 5.4c and 4.4d). In biocr4.ust systems, most microbes live in surface soils (Liao et al., 2024; Muñoz‐Martín et al., 2019), and the availability of surface water is critical for biocrust development (Kidron et al., 2022). The superior hydration capacity of MMT enables it to retain surface moisture for longer periods, theoretically favoring microbial growth. However, the MBC, Chl-*a*, and α-diversity in the Kaolin group were significantly higher than in the MMT group. Moreover, the alpha diversity in the C-MMT group was lower than in the C-Algae group, suggesting that factors in the MMT group might be limiting microbial growth. As shown in Figure 5.8a, DOC in the MMT group was significantly lower than in the Kaolin group ($p < 0.05$). This was likely due to MMT enhancing SOC stability, thereby reducing SOC decomposition. Given the limited SOC, this resulted in a lower DOC content, which was closely related to microbial growth (Li et al., 2023), thereby inhibiting microbial growth and SOC formation. Additionally, MMT exerted a stronger regulatory effect on microbial community structure compared to kaolin. These findings further support the idea that the high SOC stability induced by MMT inhibited microbial growth. Therefore, while both clays promoted SOC formation, kaolin had a stronger positive effect.

5.4.4 Recommendation for methods of applying the two types of clay in artificial biocrusts

The results of this study suggested that kaolin was more conducive to SOC formation, while MMT was more favorable for SOC stability. Although SOC growth in the Kaolin group was higher than in the MMT group after 84 days of biocrust development, it was noteworthy that the more complex spatial heterogeneity and greater water retention capacity of MMT may enhance microbial growth (Y. Li et al., 2024; Song et al., 2023). However, nutrient limitations hindered the effectiveness of MMT. Therefore, we propose the following recommendation for artificial biocrusts to improve nutrient supply in nutrient-limited ecosystems such as desert areas: During the initial phase, add 1:1 type clay to promote SOC formation. Then, in the later phase, add 2:1 type clay to enhance SOC stability. This approach may maximize the beneficial effects of both types of clay, thereby promoting the ultimate accumulation of SOC.

However, it is important to note that as an artificial simulation conducted in a laboratory, this study only demonstrated the theoretical feasibility of the approach. Substantial work remains to be done in the future. For instance, desert regions often severe conditions such as extreme precipitation, large diurnal temperature fluctuations, and high levels of ultraviolet radiation (Gong et al., 2024; Li et al., 2024; Wu et al., 2022). Further research is needed to explore the effects of clay on the resilience of artificial biocrusts under these harsh environmental conditions, as well as to optimize the clay addition strategy. Additionally, the long-term impacts of clay-based artificial

biocrusts on vegetation restoration and ecological rehabilitation in desert regions should be explored over extended timeframes, such as 10, 30, or even more years.

5.5 Conclusions

To investigate the role of clay minerals in SOC accumulation within artificial biocrust systems, two representative clays:kaolin (1:1 type) and montmorillonite (MMT, 2:1 type) -were introduced. Experimental results confirmed that both clays functioned as SOC synergists in artificial cyanobacterial biocrusts. After 84 days of cultivation, SOC content in the Kaolin and MMT groups increased by 5.03 and 4.08 times, respectively, compared to the Algae group. The higher dissolved organic carbon (DOC) content in the Kaolin group facilitated SOC formation, while the larger external specific surface area (ESSA) and higher cation exchange capacity (CEC) of MMT enhanced SOC stability. These findings underscore the critical role of clay minerals in SOC accumulation during biocrust development. Based on their distinct contributions, we propose a staged application strategy for artificial biocrust cultivation in nutrient-deficient environments such as deserts: 1:1 type clay should be applied in the early stages to promote SOC formation, followed by 2:1 type clay in later stages to improve SOC stability. This study provides both a theoretical foundation and a practical approach for restoring nutrient-limited ecosystems. However, further research is needed to validate these findings in real-world conditions. Future studies should include field inoculation experiments with clay-based artificial biocrusts and assess their long-term effects on ecological restoration in desert regions.

The main content in this chapter was published:

- ✓ **Zhang C**, Chen X, Zhou K, et al. Synergistic effects of clays and cyanobacteria on the accumulation dynamics of soil organic carbon in artificial biocrusts[J]. Journal of Environmental Management, 2025, 374: 124110. (Top; JCR Q1; IF 8.4)

5.6 References

Arthur, E., Tuller, M., Norgaard, T., Moldrup, P., Chen, C., Rehman, H.U., Weber, P.L., Knadel, M., de Jonge, L.W., 2023. Contribution of organic carbon to the total specific surface area of soils with varying clay mineralogy. Geoderma. 430, 116314. https://doi.org/10.1016/j.geoderma.2022.116314

Baham, J., Sposito, G., 1994. Adsorption of dissolved organic carbon extracted from sewage sludge on montmorillonite and kaolinite in the presence of metal ions. J. Environ. Qual. 23, 147–153. https://doi.org/10.2134/jeq1994.00472425002300010023x

Baker, N.R., 2008. Chlorophyll fluorescence: A probe of photosynthesis in vivo. Annu. Rev. Plant Biol. 59, 89–113. https://doi.org/10.1146/annurev.arplant.59.032607.092759

Boumaiza, H., Dutournie, P., Le Meins, J.-M., Limousy, L., Brendle, J., Martin, C., Michau, N., Dzene, L., 2020. Iron-rich clay mineral synthesis using design of experiments approach. Appl. Clay Sci. 199, 105876. https://doi.org/10.1016/j.clay.2020.105876

Breidenbach, A., Schleuss, P.M., Liu, S.B., Schneider, D., Dippold, M.A., de la Haye, T., Miehe, G., Heitkamp, F., Seeber, E., Mason-Jones, K., Xu, X.L., Huanming, Y., Xu, J.C., Dorji, T., Gube, M., Norf, H., Meier, J., Guggenberger, G., Kuzyakov, Y., Spielvogel, S., 2022. Microbial functional changes mark irreversible course of Tibetan grassland degradation. Nat. Commun. 13, 2681. https://doi.org/10.1038/s41467-022-30047-7

Chalchissa, F.B., Kuris, B.K., 2024. Modelling soil organic carbon dynamics under extreme climate and land use and land cover changes in Western Oromia Regional state, Ethiopia. J. Environ. Manage. 350, 119598. https://doi.org/10.1016/j.jenvman.2023.119598

Chen, X.L., Taylor, A.R., Reich, P.B., Hisano, M., Chen, H.Y.H., Chang, S.X., 2023. Tree diversity increases decadal forest soil carbon and nitrogen accrual. Nature. 618, 94–101. https://doi.org/10.1038/s41586-023-05941-9

Ciesielski, H., Sterckeman, T., Santerne, M., Willery, J.P., 1997. A comparison between three methods for the determination of cation exchange capacity and exchangeable cations in soils. Agronomie. 17, 9–16. https://hal.science/hal-00885821v1

Curti, L., Moore, O.W., Babakhani, P., Xiao, K.-Q., Woulds, C., Bray, A.W., Fisher, B.J., Kazemian, M., Kaulich, B., Peacock, C.L., 2021. Carboxyl-richness controls organic carbon preservation during coprecipitation with iron (oxyhydr)oxides in the natural environment. Commun. Earth Environ. 2, 229. https://doi.org/10.1038/s43247-021-00301-9

Feng, X., Simpson, A.J., Simpson, M.J., 2005. Chemical and mineralogical controls on humic acid sorption to clay mineral surfaces. Org. Geochem. 36, 1553–1566. https://doi.org/https://doi.org/10.1016/j.orggeochem.2005.06.008

Finstad, K.M., Nuccio, E.E., Grant, K.E., Broek, T.A.B., Pett-Ridge, J., McFarlane, K.J., 2023. Radiocarbon analysis of soil microbial biomass via direct chloroform extraction. Radiocarbon. 66, 854–862. https://doi.org/10.1017/RDC.2023.80

Francaviglia, R., Renzi, G., Ledda, L., Benedetti, A., 2017. Organic carbon pools and soil biological fertility are affected by land use intensity in Mediterranean ecosystems of Sardinia, Italy. Sci. Total Environ. 599, 789–796. https://doi.org/10.1016/j.scitotenv.2017.05.021

García-Carmona, M., Arcenegui, V., García-Orenes, F., Mataix-Solera, J., 2020. The role of mosses in soil stability, fertility and microbiology six years after a post-fire salvage logging management. J. Environ. Manage. 262, 110287. https://doi.org/10.1016/j.jenvman.2020.110287

Gong, Y., Yu, H., Hu, H., Huang, J., Ren, Y., Zhou, J., Peng, M., Chen, S., Alam, K., Zhao, W., Cheng, S., Zhu, Y., 2024. The Water Vapor Origin of a Rainstorm Event in the Taklamakan Desert. J. Geophys. Res. Atmos. 129, e2024JD041382https://doi.org/10.1029/2024jd041382

Gu, B., Schmitt, J., Chen, Z., Liang, L., McCarthy, J.F., 1994. Adsorption and desorption of natural organic matter on iron oxide: mechanisms and models. Environ. Sci. Technol. 28, 38–46. https://doi.org/10.2134/jeq1994.00472425002300010023x

Han, L., Sun, K., Jin, J., Xing, B., 2016. Some concepts of soil organic carbon characteristics and mineral interaction from a review of literature. Soil Biol. Biochem. 94, 107–121. https://doi.org/10.1016/j.soilbio.2015.11.023

Han, L., Yang, Y., Sun, K., Zhang, B., Chen, Y., Fang, L., Xing, B., 2021. Different mechanisms driving the preferential adsorption of dissolved organic matter by goethite and montmorillonite. Chem. Geol. 585, 120560. https://doi.org/https://doi.org/10.1016/j.chemgeo.2021.120560

Hartmann, M., Six, J., 2023. Soil structure and microbiome functions in agroecosystems. Nat. Rev. EARTH Environ. 4, 4–18. https://doi.org/10.1038/s43017-022-00366-w

Hou, Y.H., Chen, Y., Chen, X., He, K.Y., Zhu, B., 2019. Changes in soil organic matter stability with depth in two alpine ecosystems on the Tibetan Plateau. Geoderma. 351, 153–162. https://doi.org/10.1016/j.geoderma.2019.05.034

Huber, K.J., Wüst, P.K., Rohde, M., Overmann, J., Foesel, B.U., 2014. *Aridibacter famidurans* gen. nov., sp nov and *Aridibacter kavangonensis* sp nov., two novel members of subdivision 4 of the *Acidobacteria* isolated from semiarid savannah soil. Int. J. Syst. Evol. Microbiol. 64, 1866–1875. https://doi.org/10.1099/ijs.0.060236-0

Islam, M.R., Singh, B., Dijkstra, F.A., 2022. Stabilisation of soil organic matter: Interactions between clay and microbes. Biogeochemistry. 160, 145–158. https://doi.org/10.1007/s10533-022-00956-2

Jeewani, P.H., Van Zwieten, L., Zhu, Z., Ge, T., Guggenberger, G., Luo, Y., Xu, J., 2021. Abiotic and biotic regulation on carbon mineralization and stabilization in

paddy soils along iron oxide gradients. Soil Biol. Biochem. 160, 108312. https://doi.org/10.1016/j.soilbio.2021.108312

Jing, F., Sun, Y., Liu, Y., Wan, Z., Chen, J., Tsang, D.C.W., 2022. Interactions between biochar and clay minerals in changing biochar carbon stability. Sci. Total Environ. 809, 151124. https://doi.org/10.1016/j.scitotenv.2021.151124

Kalisz, A., Kornaś, A., Skoczowski, A., Oliwa, J., Jurkow, R., Gil, J., Sękara, A., Sałata, A., Caruso, G., 2023. Leaf chlorophyll fluorescence and reflectance of oakleaf lettuce exposed to metal and metal (oid) oxide nanoparticles. BMC Plant Biol. 23, 329. https://doi.org/10.1186/s12870-023-04305-9

Kallenbach, C.M., Frey, S.D., Grandy, A.S., 2016. Direct evidence for microbial-derived soil organic matter formation and its ecophysiological controls. Nat. Commun. 7, 13630. https://doi.org/10.1038/ncomms13630

Kan, Z., Liu, Wen-Xuan, Liu, Wen-Sheng, Lal, R., Dang, Y.P., Zhao, X., Zhang, H., 2022. Mechanisms of soil organic carbon stability and its response to no-till: A global synthesis and perspective. Glob. Chang. Biol. 28, 693–710. https://doi.org/10.1111/gcb.15968

Keqiang, Z., Zijia, Z., Cui, Z., Ling, X., Delong, M., Li, W., Shaoxian, S., Sancheze, R.M.T., Farias, M.E., 2023. Rapid artificial biocrust development by cyanobacterial inoculation and clay amendment. L. Degrad. Dev. 34, 3728–3743. https://doi.org/10.1002/ldr.4716

Kidron, G.J., Lichner, L., Fischer, T., Starinsky, A., Or, D., 2022. Mechanisms for biocrust-modulated runoff generation – A review. Earth-Science Rev. 231, 104100. https://doi.org/10.1016/j.earscirev.2022.104100

Lan, S.B., Ouyang, H.L., Wu, L., Zhang, D.L., Hu, C.X., 2017. Biological soil crust community types differ in photosynthetic pigment composition, fluorescence and carbon fixation in Shapotou region of China. Appl. SOIL Ecol. 111, 9–16. https://doi.org/10.1016/j.apsoil.2016.11.009

Lan, S.B., Wu, L., Zhang, D.L., Hu, C.X., Liu, Y.D., 2011. Ethanol outperforms multiple solvents in the extraction of chlorophyll-*a* from biological soil crusts. SOIL Biol. Biochem. 43, 857–861. https://doi.org/10.1016/j.soilbio.2010.12.007

Lei, C., Pi, M., Kuang, P., Guo, Y., Zhang, F., 2017. Organic dye removal from aqueous solutions by hierarchical calcined Ni-Fe layered double hydroxide: Isotherm, kinetic and mechanism studies. J. Colloid Interface Sci. 496, 158–166. https://doi.org/https://doi.org/10.1016/j.jcis.2017.02.025

Li, P., Hu, M., Liu, M., Zhang, H., Liu, G., Xing, Y., Xia, X., Guo, J., 2022. Thixotropic and hydration effects of Mg/Al-layered double hydroxide and sodium montmorillonite composite dispersion on oil well cement paste. Cem. Concr. Compos. 134, 104785. https://doi.org/https://doi.org/10.1016/j.cemconcomp.2022.104785

Li, S., Yang, S., Wei, X., Jiao, S., Luo, W., Chen, W., Wei, G., 2023. Reduced trace gas oxidizers as a response to organic carbon availability linked to oligotrophs in

desert fertile islands. ISME J. 17, 1257–1266. https://doi.org/10.1038/s41396-023-01437-6

Li, Y., Wei, Z., Wang, H., Wu, P., Zhang, S., You, Z., Liu, T., Huang, L., Song, Y., 2024. Impact of hydrate spatial heterogeneity on gas permeability in hydrate-bearing sediments. Energy. 293, 130717. https://doi.org/10.1016/j.energy.2024.130717

Li, Z., Gao, X., Lu, D., 2021. Correlation analysis and statistical assessment of early hydration characteristics and compressive strength for multi-composite cement paste. Constr. Build. Mater. 310, 125260. https://doi.org/https://doi.org/10.1016/j.conbuildmat.2021.125260

Li, Z., Lu, H., Zhang, K., Wu, Y., 2024. Mechanism of developing early strength of Portland cement-desert sand system under radiation in desert conditions. Case Stud. Constr. Mater. 21, e03693. https://doi.org/https://doi.org/10.1016/j.cscm.2024.e03693

Liang, C., Balser, T.C., 2011. Microbial production of recalcitrant organic matter in global soils: implications for productivity and climate policy. Nat. Rev. Microbiol. 9, 75. https://doi.org/10.1038/nrmicro2386-c1

Liang, C., Schimel, J.P., Jastrow, J.D., 2017. The importance of anabolism in microbial control over soil carbon storage. Nat. Microbiol. 2, 17105. https://doi.org/10.1038/nmicrobiol.2017.105

Liang, G., Stark, J., Waring, B.G., 2023. Mineral reactivity determines root effects on soil organic carbon. Nat. Commun. 14, 4962. https://doi.org/10.1038/s41467-023-40768-y

Liao, K., Chen, C., Ye, W., Zhu, J., Li, Y., She, S., Wang, P., Tao, Y., Lv, A., Wang, X., Chen, L., 2024. The adaptability, distribution, ecological function and restoration application of biological soil crusts on metal tailings: A critical review. Sci. Total Environ. 927, 172169. https://doi.org/10.1016/j.scitotenv.2024.172169

Liu, D., Li, M., Yu, R., Li, H., Shen, Y., Tian, Q., Bu, H., Huang, C., Tan, W., 2023. Interlayer organic matter within hydroxy-interlayered clay minerals enhances soil organic carbon stability under long-term organic fertilization. Appl. Clay Sci. 239, 106963. https://doi.org/10.1016/j.clay.2023.106963

Liu, F., Zhao, Q., Ding, J., Li, L., Wang, K., Zhou, H., Jiang, M., Wei, J., 2023. Sources, characteristics, and in situ degradation of dissolved organic matters: A case study of a drinking water reservoir located in a cold-temperate forest. Environ. Res. 217, 114857. https://doi.org/https://doi.org/10.1016/j.envres.2022.114857

Lu, Z., Wang, H., Wang, Z., Liu, J., Li, Y., Xia, L., Song, S., 2024. Critical steps in the restoration of coal mine soils: Microbial-accelerated soil reconstruction. J. Environ. Manage. 368, 122200. https://doi.org/https://doi.org/10.1016/j.jenvman.2024.122200

Ma, Y.-L., Xu, Z.-R., Guo, T., You, P., 2004. Adsorption of methylene blue on Cu (II)-exchanged montmorillonite. J. Colloid Interface Sci. 280, 283–288. https://doi.org/10.1016/j.jcis.2004.08.044

Maier, S., Tamm, A., Wu, D., Caesar, J., Grube, M., Weber, B., 2018. Photoautotrophic organisms control microbial abundance, diversity, and physiology in different types of biological soil crusts. ISME J. 12, 1032–1046. https://doi.org/10.1038/s41396-018-0062-8

Mo, X., Wang, M., Wang, Y., Chen, X., Zhang, A., Zeng, H., Zheng, Y., Kong, D., Wang, J., 2022. Molecular-level characteristics of soil organic carbon in rhizosheaths from a semiarid grassland of North China. Soil Biol. Biochem. 170, 108682. https://doi.org/https://doi.org/10.1016/j.soilbio.2022.108682

Mugnai, G., Chamizo, S., Certini, G., Li, H., Rossi, F., Adessi, A., 2024. The contribution of the phototrophic fraction in the fertility of different successional stages of induced biological soil crusts. Biol. Fertil. Soils 1–16. https://doi.org/10.1007/s00374-024-01840-x

Mugnai, G., Rossi, F., Felde, V., Colesie, C., Büdel, B., Peth, S., Kaplan, A., De Philippis, R., 2018. The potential of the cyanobacterium *Leptolyngbya ohadii* as inoculum for stabilizing bare sandy substrates. SOIL Biol. Biochem. 127, 318–328. https://doi.org/10.1016/j.soilbio.2018.08.007

Muñoz-Martín, M.Á., Becerra-Absalón, I., Perona, E., Fernández-Valbuena, L., Garcia-Pichel, F., Mateo, P., 2019. Cyanobacterial biocrust diversity in Mediterranean ecosystems along a latitudinal and climatic gradient. New Phytol. 221, 123–141. https://doi.org/10.1111/nph.15355

Puth, M.-T., Neuhäuser, M., Ruxton, G.D., 2015. Effective use of Spearman's and Kendall's correlation coefficients for association between two measured traits. Anim. Behav. 102, 77–84. https://doi.org/https://doi.org/10.1016/j.anbehav.2015.01.010

Quast, C., Pruesse, E., Yilmaz, P., Gerken, J., Schweer, T., Yarza, P., Peplies, J., Glöckner, F.O., 2013. The SILVA ribosomal RNA gene database project: improved data processing and web-based tools. Nucleic Acids Res. 41, 590–596 https://doi.org/10.1093/nar/gks1219

Román, J.R., Chilton, A.M., Cantón, Y., Muñoz-Rojas, M., 2020. Assessing the viability of cyanobacteria pellets for application in arid land restoration. J. Environ. Manage. 270, 110795. https://doi.org/10.1016/j.jenvman.2020.110795

Santamarina, J.C., Klein, K.A., Wang, Y.H., Prencke, E., 2002. Specific surface: determination and relevance. Can. Geotech. J. 39, 233–241. https://doi.org/10.1139/t01-077

Six, J., Conant, R.T., Paul, E.A., Paustian, K., 2002. Stabilization mechanisms of soil organic matter: implications for C-saturation of soils. Plant Soil. 241, 155–176. https://doi.org/10.1023/A:1016125726789

Song, X., Chen, C., Zhou, H., Shang, J., Ren, T., 2023. Effect of high-temperature treatment on water vapour sorption of montmorillonite. Geoderma. 436, 116563. https://doi.org/10.1016/j.geoderma.2023.116563

Tan, J., Wang, X., Zhang, M., Meng, D., Hu, Y., Li, Y., Song, S., Wu, L., Sánchez, R.M.T., Farías, M.E., Xia, L., 2023. Chlorella sorokiniana FK-montmorillonite

interaction enhanced remediation of heavy metals in tailings. Sci. Total Environ. 876, 163208. https://doi.org/https://doi.org/10.1016/j.scitotenv.2023.163208

Uroz, S., Kelly, L.C., Turpault, M.P., Lepleux, C., Frey-Klett, P., 2015. The Mineralosphere Concept: Mineralogical Control of the Distribution and Function of Mineral-associatec Bacterial Communities. TRENDS Microbiol. 23, 751–762. https://doi.org/10.1016/j.tim.2015.10.004

Van Heerden, P.D.R., Strasser, R.J., Krüger, G.H.J., 2004. Reduction of dark chilling stress in N_2-fixing soybean by nitrate as indicated by chlorophyll a fluorescence kinetics. Physiol. Plant. 121, 239–249. https://doi.org/10.1111/j.0031-9317.2004.0312.x

Vance, E.D., Brookes, P.C., Jenkinson, D.S., 1987. An extraction method for measuring soil microbial biomass C. Soil Biol. Biochem. 19, 703–707. https://doi.org/10.1016/0038-0717(87)90052-6

Walkly, A., 1934. An examination of the Degtjareff method for determining soil organic matter and a proposed modification to the chromic acid titration method. Soil Sci. 37, 29–38. https://doi.org/10.1097/00010694-193401000-00003

Wang, B., Liang, C., Yao, H., Yang, E., An, S., 2021. The accumulation of microbial necromass carbon from litter to mineral soil and its contribution to soil organic carbon sequestration. Catena. 207, 105622. https://doi.org/10.1016/j.catena.2021.105622

Wang, S., Redmile-Gordon, M., Shahbaz, M., Ge, T., Zhang, M., Wu, Y., Liu, J., Huang, Q., Cai, P., 2022. Microbial formation and stabilisation of soil organic carbon is regulated by carbon substrate identity and mineral composition. Geoderma. 414, 115762. https://doi.org/10.1016/j.geoderma.2022.115762

Wang, X., Meng, D., Li, J., Lu, Z., Zhang, Z., Zhang, C., Song, S., Peng, Y., Xia, L., 2023. Composition and dynamics of bacterial communities during flotation in a coal preparation plant. J. Clean. Prod. 385, 135691. https://doi.org/https://doi.org/10.1016/j.jclepro.2022.135691

Wang, X., Xu, Y., Ou, Q., Chen, W., van der Meer, W., Liu, G., 2024. Adsorption characteristics and mechanisms of water-soluble polymers (PVP and PEG) on kaolin and montmorillonite minerals. J. Hazard. Mater. 466, 133592. https://doi.org/https://doi.org/10.1016/j.jhazmat.2024.133592

Wang, Y., Chen, L., Li, Z., Duan, S., Zhang, X., Fang, J., Xiao, Y., 2024. The role of iron-rich organic fertilizer in promoting the growth of Chinese cabbage and inhibiting the transformation of cadmium. Sci. Total Environ. 908, 168430. https://doi.org/https://doi.org/10.1016/j.scitotenv.2023.168430

Wang, Z., Pan, J., Lu, Z., Xia, L., Song, S., Hu, Y., Li, Y., 2025. Microcoleus vaginatus: A novel amendment for constructing artificial soil from tailings. Environ. Technol. Innov. 37, 103939. https://doi.org/https://doi.org/10.1016/j.eti.2024.103939

Wattel-Koekkoek, E.J.W., van Genuchten, P.P.L., Buurman, P., van Lagen, B., 2001. Amount and composition of clay-associated soil organic matter in a range of

kaolinitic and smectitic soils. Geoderma 99, 27–49. https://doi.org/https://doi.org/10.1016/S0016-7061(00)00062-8

Wattel-Koekkoek, E.J.W., Buurman, P., Van Der Plicht, J., Wattel, E., Van Breemen, N., 2003. Mean residence time of soil organic matter associated with kaolinite and smectite. Eur. J. Soil Sci. 54, 269–278. https://doi.org/10.1046/j.1365-2389.2003.00512.x

Weber, B., Belnap, J., Budel, B., Antoninka, A.J., Barger, N.N., Chaudhary, V.B., Darrouzet-Nardi, A., Eldridge, D.J., Faist, A.M., Ferrenberg, S., Havrilla, C.A., Huber-Sannwald, E., Issa, O.M., Maestre, F.T., Reed, S.C., Rodriguez-Caballero, E., Tucker, C., Young, K.E., Zhang, Y.M., Zhao, Y.G., Zhou, X.B., Bowker, M.A., 2022. What is a biocrust? A refined, contemporary definition for a broadening research community. Biol. Rev. 97, 1768–1785. https://doi.org/10.1111/brv.12862

Wei, C., Wang, Q., Ren, M., Pei, Z., Lu, J., Wang, H., Wang, W., 2021. Soil aggregation accounts for the mineral soil organic carbon and nitrogen accrual in broadleaved forests as compared to that of coniferous forests in Northeast China: Cross-sites and multiple species comparisons. L. Degrad. Dev. 32, 296–309. https://doi.org/10.1002/ldr.3725

Wu, H.W., Cui, H.L., Fu, C.X., Li, R., Qi, F.Y., Liu, Z.L., Yang, G., Xiao, K.Q., Qiao, M., 2024. Unveiling the crucial role of soil microorganisms in carbon cycling: A review. Sci. Total Environ. 909, 168627. https://doi.org/10.1016/j.scitotenv.2023.168627

Wu, L., Farias, M.E., Torres, R.M., Xia, L., Song, S.X., Saber, A.A., Lan, S.B., 2022. Salinity affects microbial composition and function in artificially induced biocrusts: Implications for cyanobacterial inoculation in saline soils. SOIL Biol. Biochem. 170, 108691. https://doi.org/10.1016/j.soilbio.2022.108691

Wu, L., Zhang, C., Vadiveloo, A., Montes, M.L., Xia, L., Song, S., Fernandez, M.A., Lan, S., 2024. Efficient nutrient recycling from wastewater to deserts: A comparative study on biocrust cyanobacteria performance. Chem. Eng. J. 491, 151927. https://doi.org/https://doi.org/10.1016/j.cej.2024.151927

Wu, S., Konhauser, K.O., Chen, B., Huang, L., 2023. “Reactive Mineral Sink” drives soil organic matter dynamics and stabilization. npj Mater. Sustain. 1, 1–12. https://doi.org/10.1038/s44296-023-00003-7

Wu, S.F., An, G.L., Wang, L.W., Zhang, C., 2022. Smart temperature difference management in summer desert enabled by ammonia-based resorption cycle. Energy Convers. Manag. 254, 115274. https://doi.org/10.1016/j.enconman.2022.115274

Wu, T., Ost, A.D., Audinot, J.-N., Wiesmeier, M., Wirtz, T., Buegger, F., Häusler, W., Höschen, C., Mueller, C.W., 2022. Association of fresh low-molecular-weight organic compounds with clay-sized mineral fraction in soils of different organic carbon loading. Geoderma. 409, 115657. https://doi.org/10.1016/j.geoderma.2021.115657

Xiao, K.Q., Zhao, Y., Liang, C., Zhao, M., Moore, O.W., Otero-Fariña, A., Zhu, Y.G., Johnson, K., Peacock, C.L., 2023. Introducing the soil mineral carbon pump. Nat. Rev. Earth Environ. 4, 135–136. https://doi.org/10.1038/s43017-023-00396-y

Xu, J., Liu, J., Fu, Q., Zhang, M., Guo, B., Li, H., Chen, X., Qiu, G., 2024. Soil carbon turnover and balance in the priming effects of basalt, montmorillonite, and kaolinite in a Luvisol soil. J. Soils Sediments. 24, 732–743. https://doi.org/10.1007/s11368-023-03676-8

Yang, F., Huang, J., Zhou, C., Yang, X., Mamtimin, A., Zheng, X., Huo, W., Ji, F., Han, D., Meng, L., Gao, J., Song, M., Wang, Y., Zhu, C., 2023. Desert Abiotic Carbon Sequestration Weakening by Precipitation. Environ. Sci. Technol. 57, 7174–7184. https://doi.org/10.1021/acs.est.2c09470

Yang, X., Zhou, J., Huo, T., Lv, Y., Pan, J., Chen, L., Tang, X., Zhao, Y., Liu, H., Gao, Q., Liu, S., 2021. Metabolic insights into the enhanced nitrogen removal of anammox by montmorillonite at reduced temperature. Chem. Eng. J. 410, 128290. https://doi.org/https://doi.org/10.1016/j.cej.2020.128290

Yu, F., Zhang, W., Hou, X., Li, Y., Tong, J., 2023. How nutrient loads influence microbial-derived carbon accumulation in wetlands: A new insight from microbial metabolic investment strategies. Environ. Res. 217, 114981. https://doi.org/https://doi.org/10.1016/j.envres.2022.114981

Yuyuan, Z., Zhiwei, G., Haocheng, S., Liang, W., Shuang, Z., Xipeng, L., Qicheng, C., Haisheng, C., 2024. The role of oxygen vacancy in CaO-$Ca_{12}Al_{14}O_{33}$ materials derived from hydrocalumite for enhanced CO_2 capture cyclic performance. Chem. Eng. J. 481, 147955.

Zhang, M., Zhang, T., Zhou, L., Lou, W., Zeng, W., Liu, T., Yin, H., Liu, H., Liu, X., Mathivanan, K., 2022. Soil microbial community assembly model in response to heavy metal pollution. Environ. Res. 213, 113576. https://doi.org/10.1016/j.envres.2022.113576

Zhang, S., Pei, L., Zhao, Y., Shan, J., Zheng, X., Xu, G., Sun, Y., Wang, F., 2023. Effects of microplastics and nitrogen deposition on soil multifunctionality, particularly C and N cycling. J. Hazard. Mater. 451, 131152. https://doi.org/https://doi.org/10.1016/j.jhazmat.2023.131152

Zhang, X., Yao, M.-C., Chen, L., Sheng, G.-P., 2022. Lewis Acid-Base Interaction Triggering Electron Delocalization to Enhance the Photodegradation of Extracellular Antibiotic Resistance Genes Adsorbed on Clay Minerals. Environ. Sci. Technol. 56, 17684–17693. https://doi.org/10.1021/acs.est.2c05785

Zhao, Y., Xu, W.W., Wang, N., 2021. Effects of covering sand with different soil substrates on the formation and development of artificial biocrusts in a natural desert environment. SOIL TILLAGE Res. 213, 105081. https://doi.org/10.1016/j.still.2021.105081

Chapter VI. Conclusions

6.1 Main conclusions

The Earth is an interconnected, holistic ecosystem. Nutrient-poor soils cover a considerable portion of the planet's surface and play an indispensable role in global water, carbon, and nutrient cycles. The capacity of these soils to retain water and sequester carbon significantly influences regional and even global climate patterns, thereby affecting the climatic conditions on which all life depends. Thus, the present study focuses on enhancing water retention and carbon sequestration in nutrient-poor soils. Using three typical types e.g., saline-alkali soil, phosphogypsum-covered soil, and desert soil, we introduced salt-tolerant polymers, natural biocrusts, and clay-based artificial biocrusts. By clarifying the interactions between inorganic components (e.g., clay, phosphogypsum, salinity, cation exchange capacity, pH) and organic components (e.g., polymeric materials, microorganisms, SOC), we aimed to drive a synergistic enhancement effect, thereby achieving restoration outcomes superior to those obtained using single materials or methods. The specific conclusions are as follows:

(1) Chapter II: Aridity and rapid evaporation of soil moisture are major drivers of soil salinization. Therefore, enhancing soil water retention has been recognized as an effective strategy to mitigate soil salinization. In response to this prominent issue of saline-alkali soils, we correspondingly developed the ST-SAP and obtained the following conclusions. With the three strong hydrophilic groups (R-SO_3H, R-COOH, R-$CONH_2$), ST-SAP has excellent swelling ability, which reaches up to 69.04 g/g under high salt condition; ST-SAP can effectively realize multiple reswelling under high salt condition; The complexation reaction between Ca^{2+} and three hydrophilic groups of ST-SAP contributes to its remarkable stability under high salt condition; With 2 wt% ST-SAP, the moisture of saline-alkali soil could be prolonged to 28 days. These findings highlight the strong potential of ST-SAP for practical applications in saline-alkali land management and agricultural water conservation

(2) Chapter III:

(3) Chapter IV: SOC plays a crucial role in enhancing soil structure and maintaining key biogeochemical functions. Simultaneously, SOC is one of the critical indicators of soil fertility and is often used to assess soil quality. Therefore, SOC is essential for the rehabilitation of desertified soil. To investigate the impact of clay minerals on the dynamics of SOC accumulation in artificial biocrust systems, we determined that the optimal addition of montmorillonite was 1.4 g dm^{-2}, leading to a 3.45-fold increase in SOC content after 84 days of cultivation. Three key findings emerged from the montmorillonite-based artificial biocrust system. First, montmorillonite significantly accelerated microbial growth; second, it specifically regulated microbial communities, promoting the proliferation of photosynthetically active microorganisms; third, the growth of microbial biomass driven by

montmorillonite was the primary factor driving SOC accumulation. Based on these results, we propose that montmorillonite acts as an accelerator for the biocrust carbon pump during the formation of artificial biocrusts. While this study provides valuable insights, it is limited to laboratory conditions. Future research in natural settings is needed to examine the effects of montmorillonite-based artificial biocrusts on processes such as water infiltration, surface runoff, evaporation, and soil erosion in desertified areas, thereby enhancing our understanding of ecosystem functions and biodiversity under desert environmental conditions.

(4) Chapter V: To investigate the role of clay minerals in SOC accumulation within artificial biocrust systems, two representative clays—kaolin (1:1 type) and montmorillonite (MMT, 2:1 type)—were introduced. Experimental results confirmed that both clays functioned as SOC synergists in artificial cyanobacterial biocrusts. After 84 days of cultivation, SOC content in the Kaolin and MMT groups increased by 5.03 and 4.08 times, respectively, compared to the Algae group. The higher dissolved organic carbon (DOC) content in the Kaolin group facilitated SOC formation, while the larger external specific surface area (ESSA) and higher cation exchange capacity (CEC) of MMT enhanced SOC stability. These findings underscore the critical role of clay minerals in SOC accumulation during biocrust development. Based on their distinct contributions, we propose a staged application strategy for artificial biocrust cultivation in nutrient-deficient environments such as deserts: 1:1 type clay should be applied in the early stages to promote SOC formation, followed by 2:1 type clay in later stages to improve SOC stability. This study provides both a theoretical foundation and a practical approach for restoring nutrient-limited ecosystems. However, further research is needed to validate these findings in real-world conditions. Future studies should include field inoculation experiments with clay-based artificial biocrusts and assess their long-term effects on ecological restoration in desert regions.

6.2 Innovations

For the three types of nutrient-poor soils, the innovations of this thesis are as follows:

Chapter II presents the novel synthesis of a salt-tolerant superabsorbent polymer (ST-SAP) for saline-alkali soils, which exhibits superior water absorption and retention. The research enabled clear identification of the complexation patterns between Ca^{2+} ions and three hydrophilic groups (R-$CONH_2$, R-SO_3H, R-COO^-), and yielded detailed three-dimensional computed tomography (3D-CT) images of the Ca salt distribution within the polymer.

Chapter III presents the first investigation into the interaction between phosphogypsum and the overlying biocrusts. It is revealed that phosphogypsum facilitates the growth of the biocrusts. Interactions between phosphogypsum and biocrusts promote microbial cycling of C, N, P, and S, ultimately leading to significant improvements in the physical and chemical properties of the phosphogypsum stockpile

surface. Based on these findings, we propose that the application of biocrusts may represent a promising approach for *In situ* green management of phosphogypsum.

Chapter IV presents a pioneering investigation into the role of clay, exemplified by montmorillonite, in the microbial carbon pump of biocrusts. Three key findings were revealed: 1) MMT accelerates microbial growth; 2) MMT optimizes the microbial community structure by favoring microbes with high photosynthetic activity and oligotrophic adaptability; and 3) The MMT-enhanced microbial growth serves as the primary driver for soil organic carbon (SOC) accumulation. Based on these critical results, we propose that role of MMT as a "accelerator" of the biocrust carbon pump during the construction of artificial biocrusts.

Chapter V investigates, for the first time, the differential effects of two typical clay types on the formation and stabilization of soil organic carbon (SOC) in nutrient-poor soils. The results revealed that 1:1-type clay (exemplified by kaolin) is more conducive to SOC formation, whereas 2:1-type clay (exemplified by montmorillonite, MMT) favors SOC stabilization. Consequently, a targeted clay application strategy is proposed: for the establishment of biocrusts on nutrient-poor soils, 1:1-type clay should be applied in the initial phase, followed by the addition of 2:1-type clay in the later stages.

Academic achievements during the Ph.D. program

■ Articles published in international journals during Ph. D. studying

1) **Zhang C**, García-Meza JV, Zhou KQ, et al. Superabsorbent polymer used for saline-alkali soil water retention[J]. Journal of the Taiwan Institute of Chemical Engineers, 2023, 145: 104830. (JCR Q1; IF 6.3)

2) **Zhang C**, Zhou KQ, Wang Z, et al. Montmorillonite as an "accelerator" for the microbial carbon pump during artificial biocrust construction[J]. Plant and Soil, 2025: 1-17. (JCR Q1; IF 4.1)

3) **Zhang C**, Chen X, Zhou K, et al. Synergistic effects of clays and cyanobacteria on the accumulation dynamics of soil organic carbon in artificial biocrusts[J]. Journal of Environmental Management, 2025, 374: 124110. (Top; JCR Q1; IF 8.4)

4) Zhou KQ, Zhang ZJ, **Zhang C**, et al. Rapid artificial biocrust development by cyanobacterial inoculation and clay amendment[J]. Land Degradation & Development, 2023, 34(12): 3728-3743. (JCR Q1; IF 3.7)

5) Wang XZ, Meng DL, Li JB, Lu ZJ, Zhang ZJ, **Zhang C**, et al. Composition and dynamics of bacterial communities during flotation in a coal preparation plant[J]. Journal of Cleaner Production, 2023, 385: 135691. (Top; JCR Q1; IF:10)

6) Li JB, Meng DL, Wang XZ, Lu ZJ, **Zhang C**, et al. First insight into indigenous microorganisms in coal slurry involved in polyacrylamide biodegradation[J]. Fuel, 2023, 332: 126006. (Top; JCR Q1; IF:7.5)

■ Articles in preparation

1) **Zhang C**, et al. Occurrence of biocrusts and their positive effects on microbial nutrient cycling on phosphogypsum. (Under review)

Supplementary information

Supplementary information for chapter II

To investigate the water retention properties of ST-SAP in saline-alkali soil of high salinity, the saline-alkali soil of Lop Nur was selected. The saline-alkali soil samples were composed of 0-30 cm topsoil at different sampling points, whose properties are shown in Table S2.1.

Table S2.1. The properties of saline-alkali soil from Lop Nur, Xinjiang Province, China.

Properties	Result
CEC	6.452 $cmol^+/kg$
Total dissolved salt	18.13%
pH	8.29
Soluble cation contents （Na^+, K^+, Ca^{2+}, Mg^{2+}）	4.13 wt% Na^+； 0.50 wt% K^+ 0.75 wt% Ca^{2+}； 0.45 wt% Mg^{2+}

To study the adsorption of Ca^{2+} by ST-SAP, the materials (0.1000 g) were put in different concentrations of $CaCl_2$ solution until swelling equilibrium. The experimental data were fitted with the Langmuir and Freundlich models, whose equations are described as follows:

Langmuir model:

$$Q_e = k_l Q_m C_e / (1 + k C_e) \quad \text{(Eq. 1)}$$

Freundlich model:

$$Q_e = k_f C_e^{(1/n)} \quad \text{(Eq. 2)}$$

In which C_e (g/L) and Q_e(g/g): equilibrium concentrations of the solution; Q_e (g/g) and Q_m (g/g): balanced and maximum adsorption ratio of ST-SAP, respectively; k_l (L/g) and k_f (g/g): Langmuir and Freundlich constants, respectively, and *1/n*: adsorption intensity index.

The fitting model parameters were listed in Table S2.2. Freundlich model was more suitable to describe the adsorption process, whose R^2 reached 0.998. The 1/n reflects the effect of concentration on the adsorption capacity, which was 0.191 less than 0.5, indicating that Ca^{2+} was easily adsorbed in the ST-SAP structure. Referring to the Langmuir model, the maximum adsorption capacity of Ca^{2+} towards ST-SAP was 0.259 g/g.

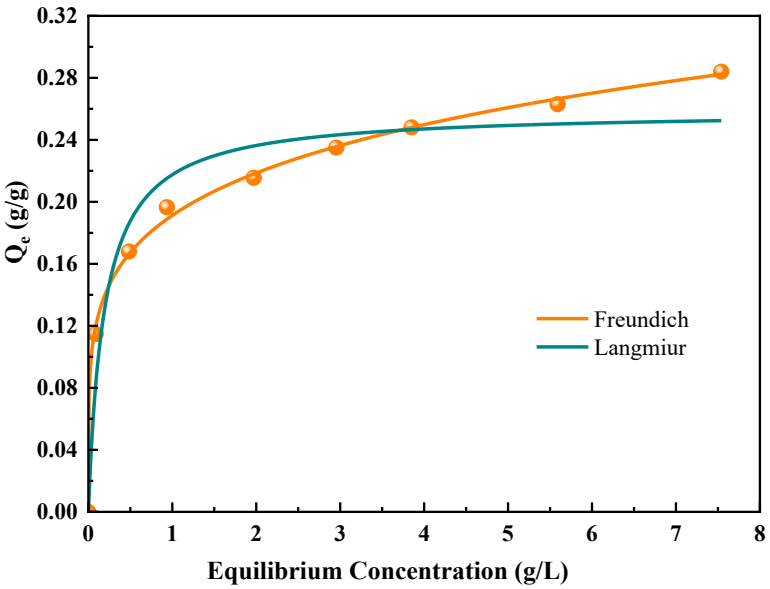

Figure S 2.2. Adsorption isotherm for Ca^{2+} absorption

Table S 2.2 Adsorption isotherm parameters for the adsorption of Ca^{2+} by the salt-tolerant superabsorbent polymer (ST-SAP)

Langmuir			**Freundlich**		
Q_m (g/g)	k_l (L/g)	R_1^2	1/n	k_f (L/g)	R_2^2
0.259	5.282	0.937	0.193	0.191	0.998

Supplementary information for chapter III

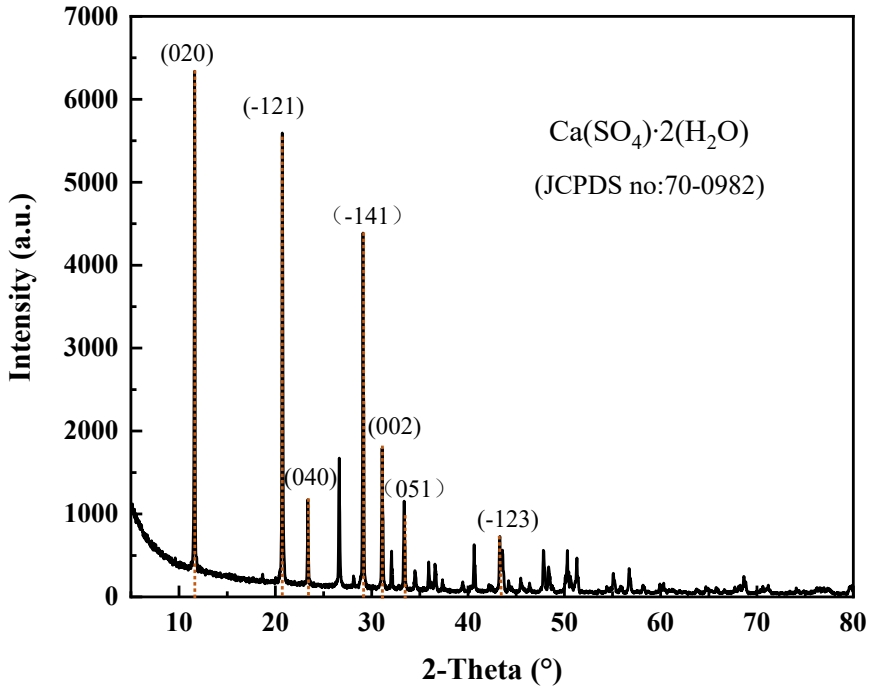

Figure S3.1 XRD pattern of phosphogypsum

Table S3.1 Physical and chemical properties of phosphogypsum (PG)

Properties	PG stack	CJ/T 340-2016	Properties	PG stack	CJ/T 340-2016
SOC（mg/g）	4.23	11.60-46.40	pH (1:2.5)	3.39	5.0-8.3
TC (mg/g)	10.00	/	Soluble F^-（mg/kg）	156.42	/
TN (mg/g)	0.50	/	WR 0.25 （%）	0.46	/
AN (mg/kg)	9.60	40-200	MWD (mm)	0.09	/
AP (mg/kg)	69.09	5-60	Exchangeable Ca^{2+} (cmol/kg)	2673.91	
TP (mg/g)	46.06	/	As (mg/kg)	0.061	< 30
CEC (cmol+/kg)	0.03	≥ 10	Cd (mg/kg)	0.096	< 0.4
Particle size (μm)	D90 73.77	/	Cr (mg/kg)	0.38	< 100
	D50 32.27		Cu (mg/kg)	0.41	< 40
	D10 5.02		Ni (mg/kg)	0.26	< 40

Note: CJ/T 340-2016 is the Urban Construction Industry Standard of the People's Republic of China for Planting Soil for Greening

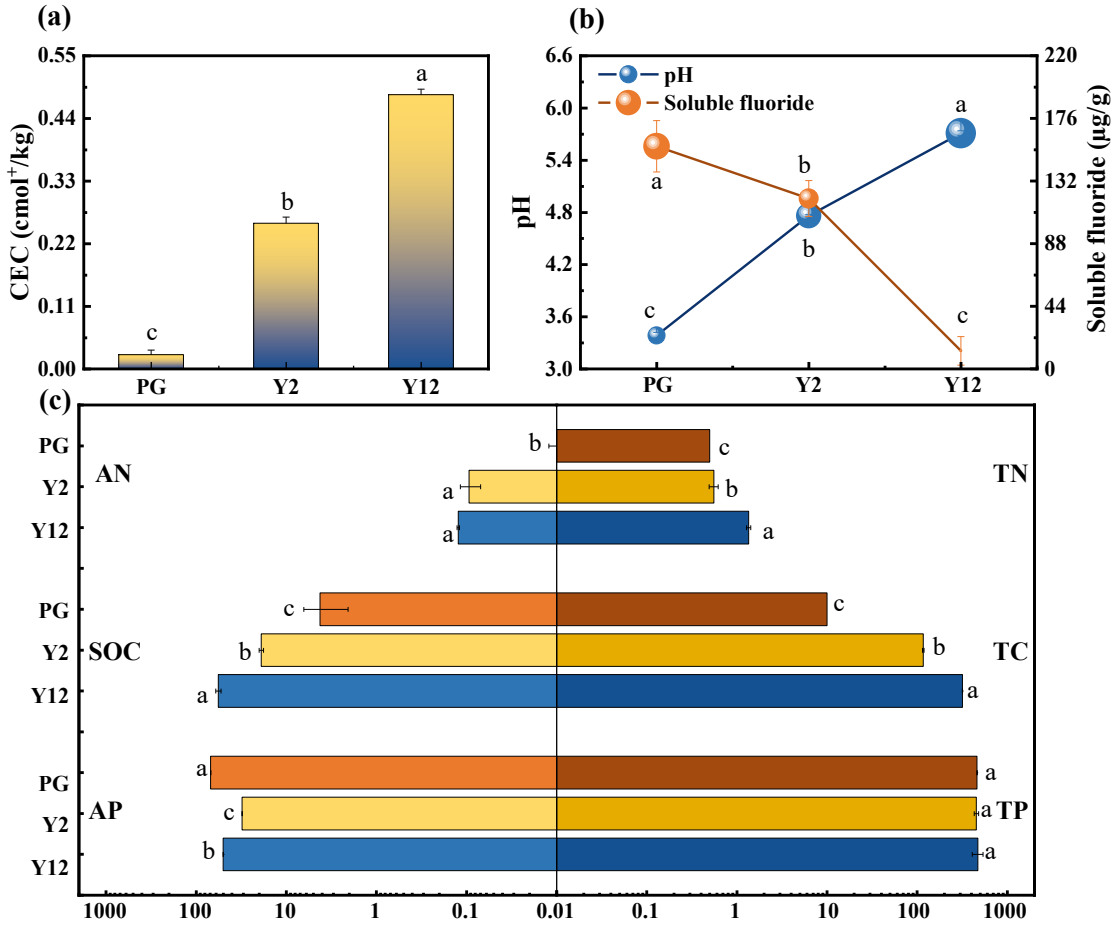

Figure S3.2 Properties of the biocrust layers. (a) Cation exchange capacity (CEC); (b) pH and soluble F content; (c) available N (AN), soil organic C (SOC), available P (AP), total C (TC), total N (TN), and total P (TP). a, b, c: significant differences ($p < 0.05$). Error bar: standard deviation

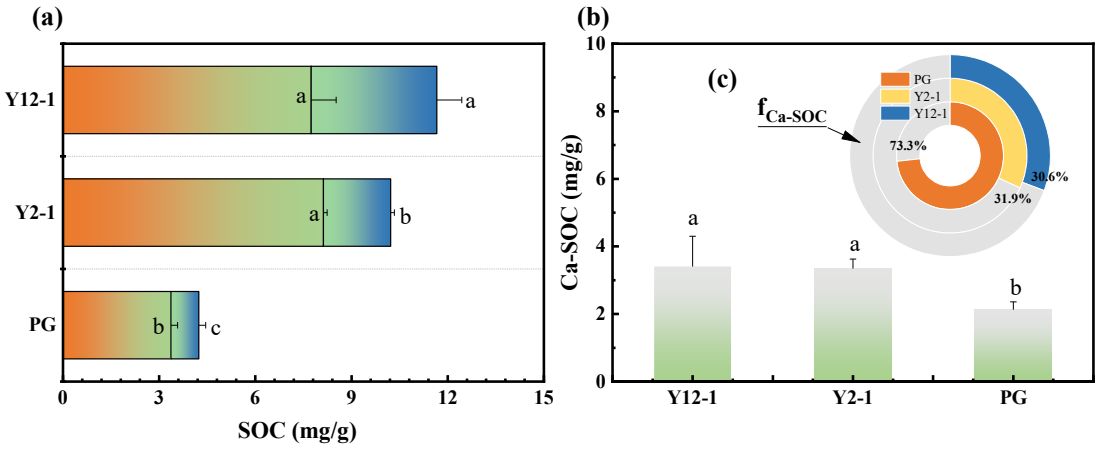

Figure S3.3 Properties of the phosphogypsum layers. (a) Mineral-associated organic matter (MaOM) and particulate organic c (POC); (b) Ca-bound to organic C of soil (Ca-SOC); (c) The proportion of Ca-SOC to total SOC ($f_{Ca\text{-}SOC}$). a, b and c: to statistically significant differences ($p < 0.05$). Error bars: standard deviations

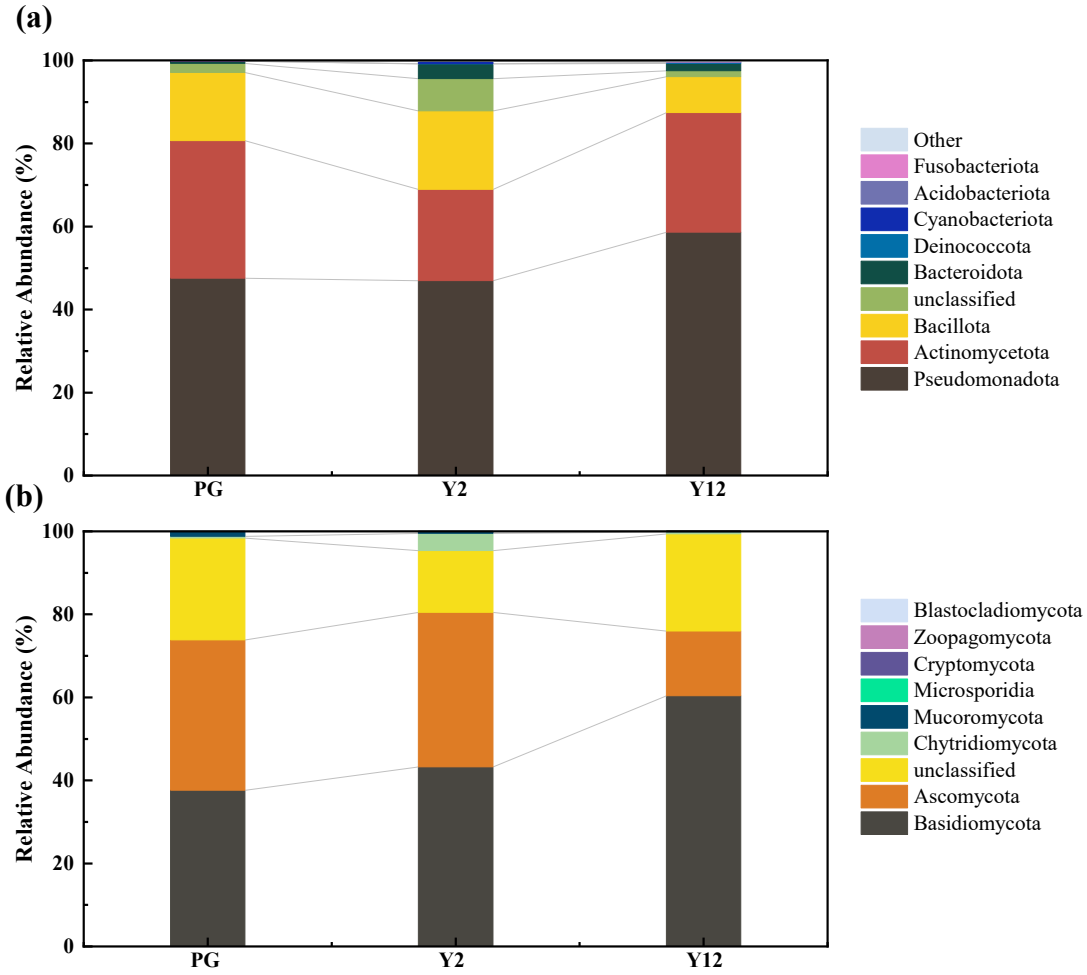

Figure S3.4 Abundance map at the phylum level of bacteria (a), fungi (b)

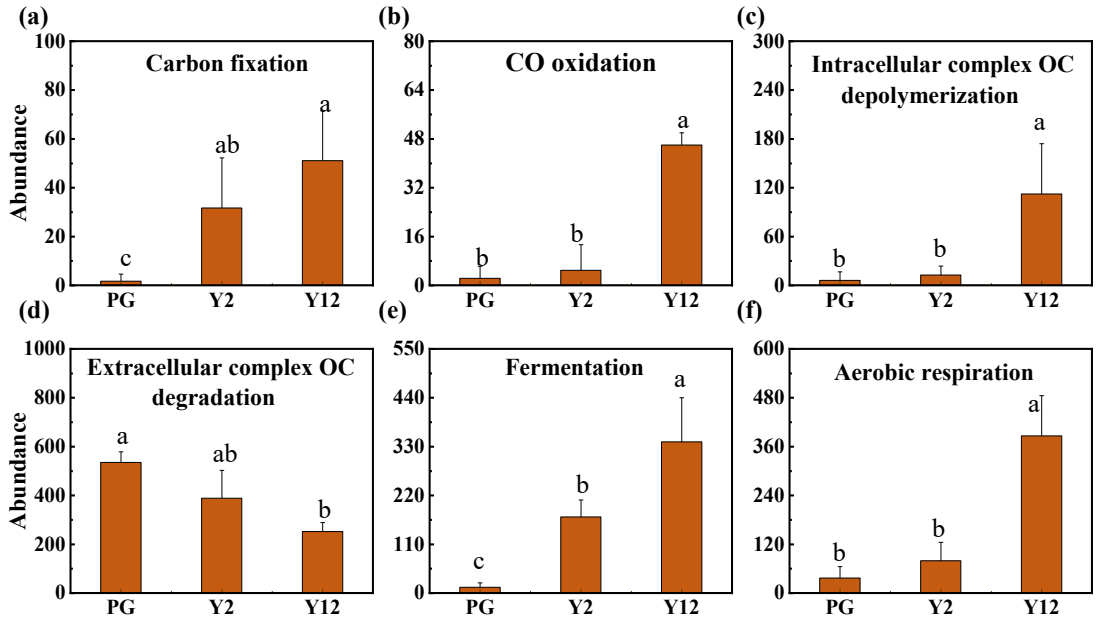

Figure S3.5 Relative abundance of gene clusters related to the carbon cycle. Different letters assigned to values denote statistically significant differences ($p < 0.05$). Error bars denote standard deviations

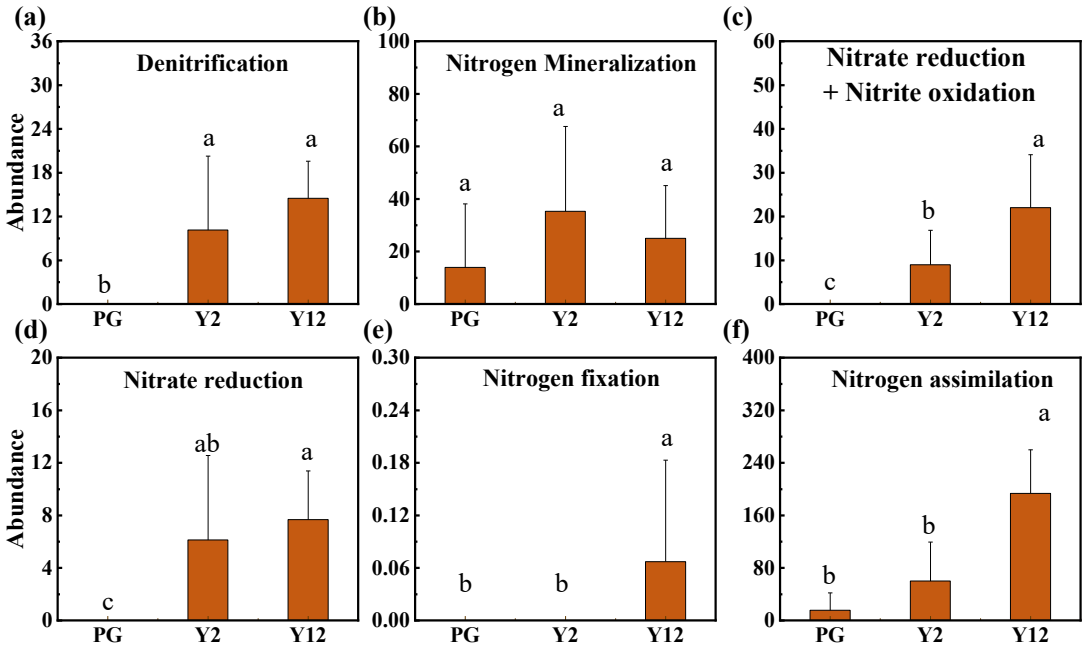

Figure S3.6 Relative abundance of gene clusters related to the N cycle. Different letters assigned to values denote statistically significant differences ($p < 0.05$). Error bar: standard deviation

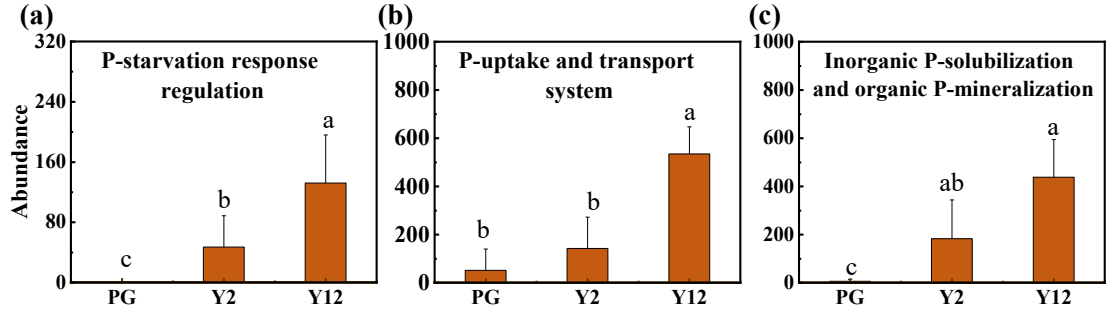

Figure S3.7. Relative abundance of gene clusters related to the P cycle. a, b and c; significant difference ($p < 0.05$). Error bars: standard deviations

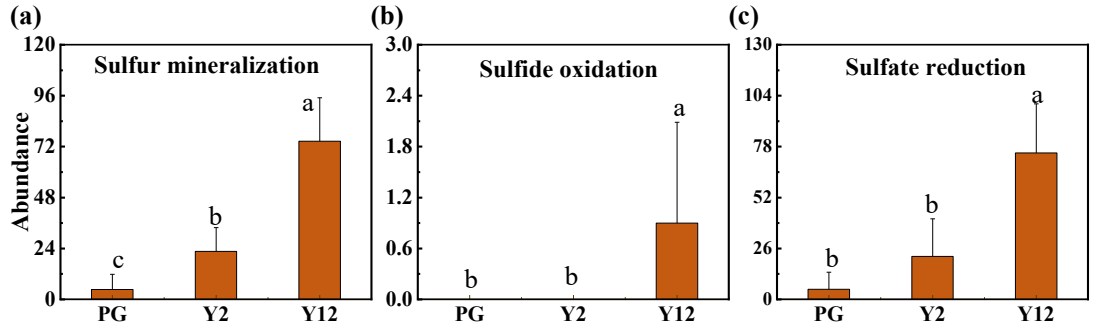

Figure S3.8. Relative abundance of gene clusters related to the S cycle. A, B AND C: significant differences ($p < 0.05$). Error bar; standard deviations

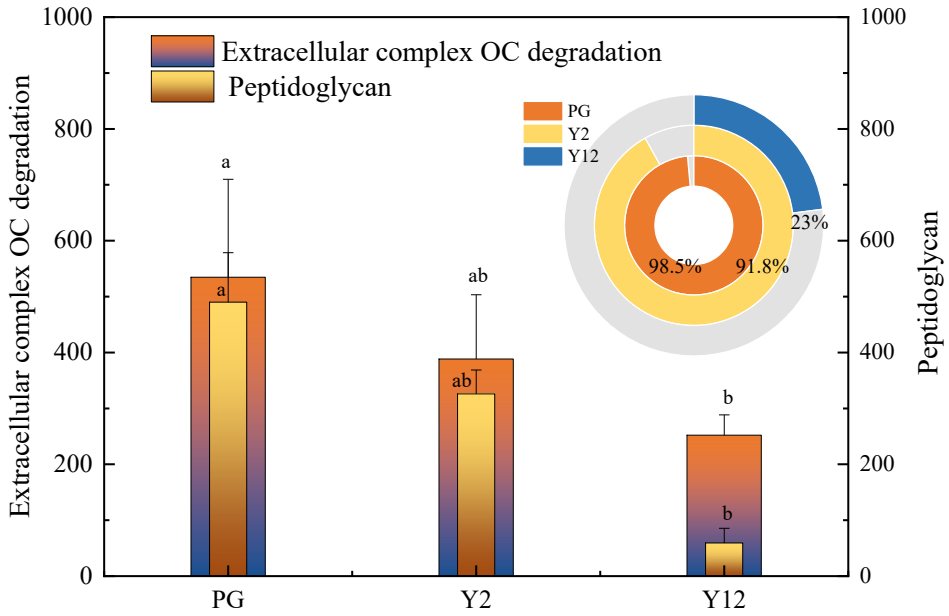

Figure S3.9. Abundance of genes involved in extracellular complex organic carbon (OC) degradation and peptidoglycan. The ring diagram in the upper-right corner shows the proportion of peptidoglycan degradation genes relative to the total extracellular complex OC degradation gene abundance. Different letters assigned to values denote statistically significant differences ($p < 0.05$). Error bars denote standard deviations

Supplementary information for chapter IV

Table S4.1 Physical and chemical properties of the sandy soil and montmorillonite

Properties		Sandy soil	montmorillonite
SOC（mg/g）		0.63±0.04	0.47±0.01
TC (mg/g)		4.0±0.14	3.12±0.26
TN (mg/g)		0.4±0.58	0.11±0.01
AN (μg/g)		11.25±0.15	3.78±0.07
AP (μg/g)		0.58±0.03	0.43±0.01
CEC (cmol+/kg)		0.13±0.01	122.23±0.05
pH (1:5)		8.4±0.01	10.17±0.04
Particle size (um)	D_{90}	289.63	5.93
	D_{50}	174.44	2.10
	D_{10}	120.23	0.74

Note: SOC: soil organic C, TC: total C, TN: total N, AN: available N, AP: available P

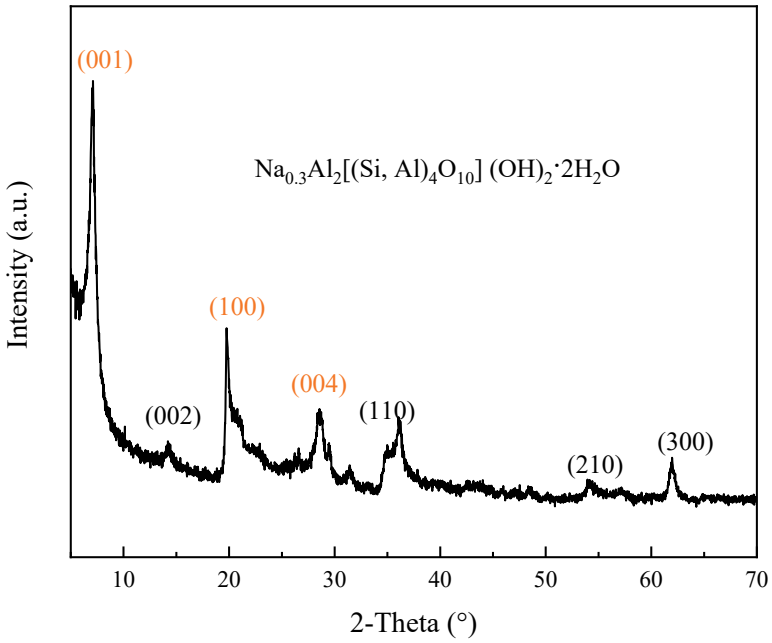

Figure S4.1. X-ray Diffraction (XRD) pattern of the Na-based montmorillonite. Its structure was identified as $Na_{0.3}Al_2[(Si, Al)_4O_{10}] (OH)_2 \cdot 2H_2O$ (JCPDS no:43-0688)

Table S4.2 Partial functions of microbial communities. Different letters assigned to values denote statistically significant differences ($p < 0.05$).

Function	0-M	0.7-M	1.4-M	2.1-M	CK-M	CK-Soil
Photoautotrophy-cyanobacteria	0.129± 0.020b	0.054± 0.030b	0.226± 0.009a	0.223± 0.011a	0.145± 0.021ab	0.096± 0.028b
Photoheterotrophy	$2.30\times10^{-3}\pm 4.30\times10^{-4}$a	$5.38\times10^{-3}\pm 1.66\times10^{-3}$a	$2.01\times10^{-3}\pm 1.62\times10^{-3}$a	$1.89\times10^{-3}\pm 3.86\times10^{-4}$a	$1.62\times10^{-3}\pm 3.60\times10^{-4}$a	$3.75\times10^{-3}\pm 1.63\times10^{-3}$a
Phototrophy	0.132± 0.020b	0.059± 0.028b	0.229± 0.008a	0.225± 0.011a	0.147± 0.021ab	0.100± 0.027b
Photosynthesis	0.010± 0.002b	0.007± 0.001b	0.024± 0.002a	0.024± 0.003a	0.012± 0.002b	0.009± 0.002b
Photosynthesis-antenna proteins	$2.33\times10^{-3}\pm 5.91\times10^{-4}$b	$9.21\times10^{-4}\pm 4.11\times10^{-4}$b	$7.74\times10^{-3}\pm 8.92\times10^{-4}$a	$7.43\times10^{-3}\pm 9.90\times10^{-4}$a	$2.80\times10^{-3}\pm 6.54\times10^{-4}$b	$1.70\times10^{-3}\pm 5.50\times10^{-4}$b

Supplementary information for chapter V

Table S5.1 The physical and chemical properties of montmorillonite (MMT), kaolin, and sandy soil

Properties		Kaolin	MMT	Sandy soil
SSA (m^2/g)	External	13.65	53.11	2.30
	Internal	/	782.56	/
	Total	13.65	835.67	2.30
CEC (mmol/100g)		3.57	122.34	0.66
The total adsorption average pore width (nm) (BET)		43.60	19.41	8.91
Particle size (um)	D90	6.61	5.93	289.63
	D50	2.88	2.10	174.44
	D10	0.95	0.74	120.23
SOC (mg/g)		0.52	0.47	0.63
TC (mg/g)		4.8	3.12	4.00
TN (mg/g)		0.3	0.11	0.4
AN (μg/g)		4.16	3.78	11.25
AP (μg/g)		0.65	0.43	0.58
pH (1:5 W/V)		7.1	10.17	8.41

Note: SSA: Specific surface area; CEC: cationic capacity; BET: Brunauer-Emmett-Teller; SOC: soil organic C; TC: total carbon; TN: total N; AN: available N; AP: available P

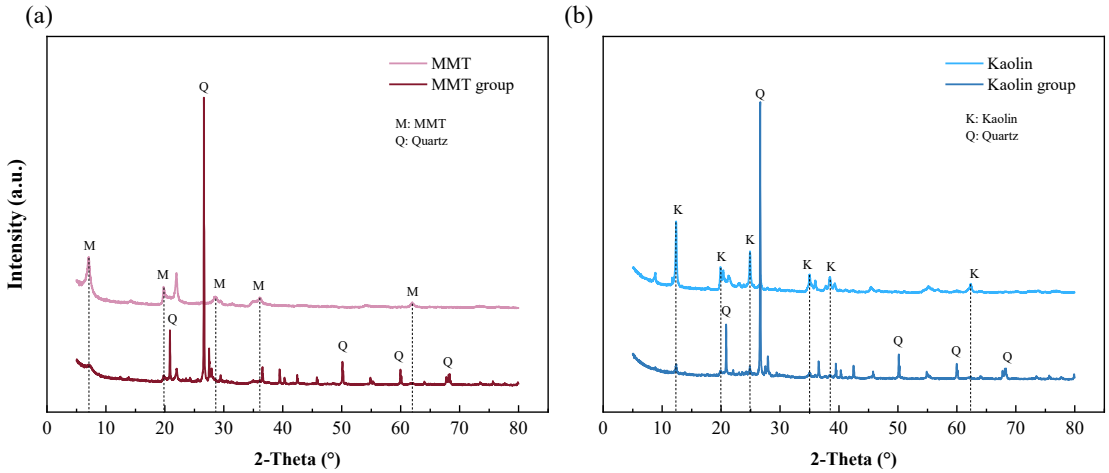

Figure S5.1 X-ray Diffraction spectra of montmorillonite (MMT) (a) and kaolin (b) before and after algae inoculation, separately. MMT: MMT before inoculation with algae; MMT group: MMT after 84 days of inoculation with algae, kaolin: kaolin before inoculation with algae; kaolin group: kaolin after 84 days of inoculation with algae

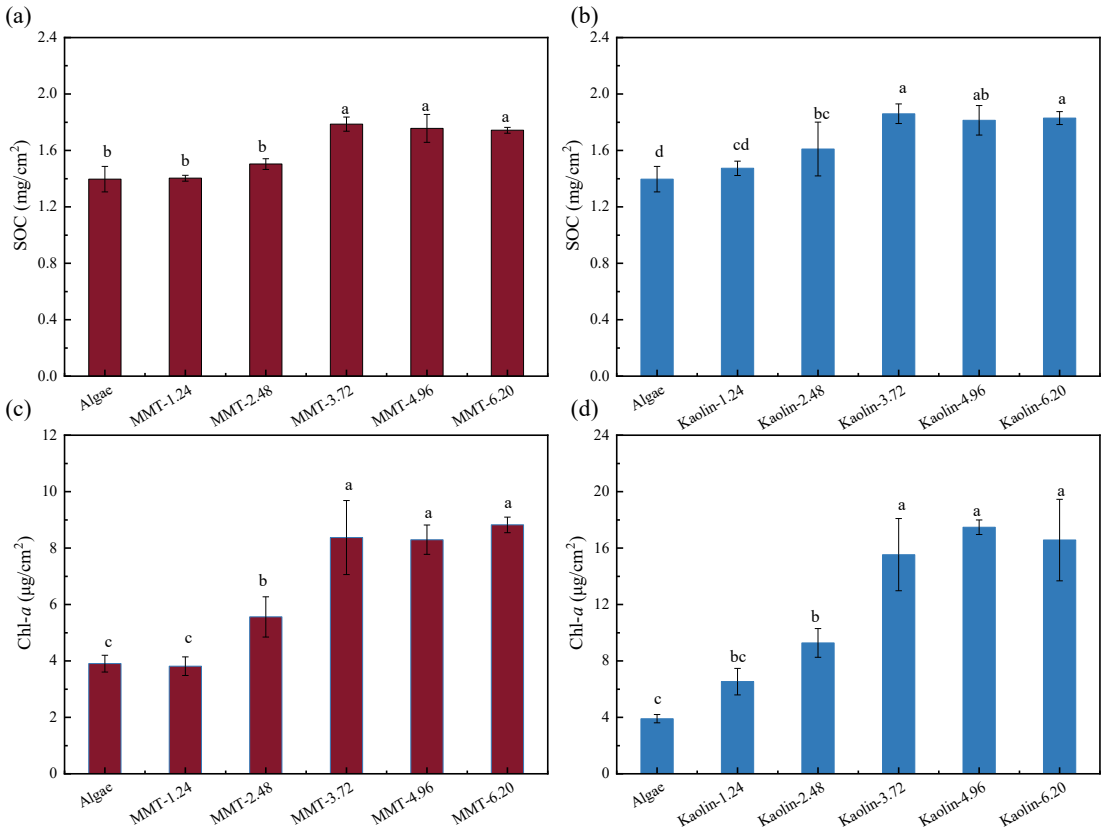

Figure S5.2 On day 30, SOC content (a) and Chl-*a* (c) in different MMT addition groups; SOC content (b) and Chl-*a* (d) in different kaolin addition groups. SOC: soil organic carbon; Chl-*a*: chlorophyll-a; MMT: montmorillonite. Algae, MMT-1.24, MMT-2.48, MMT-3.72, MMT-4.96, and MMT-6.20 represent MMT addition levels of 0 g, 1.24 g, 2.48 g, 3.72 g, 4.96 g, and 6.20 g, respectively, with an algae solution addition of 30 mL in all cases. Similarly, kaolin-1.24, kaolin-2.48, kaolin-3.72, kaolin-4.96, and kaolin-6.20 represent kaolin addition levels of 0, 1.24, 2.48, 3.72, 4.96, and 6.20 g, respectively, with an algae solution addition of 30 mL in all cases

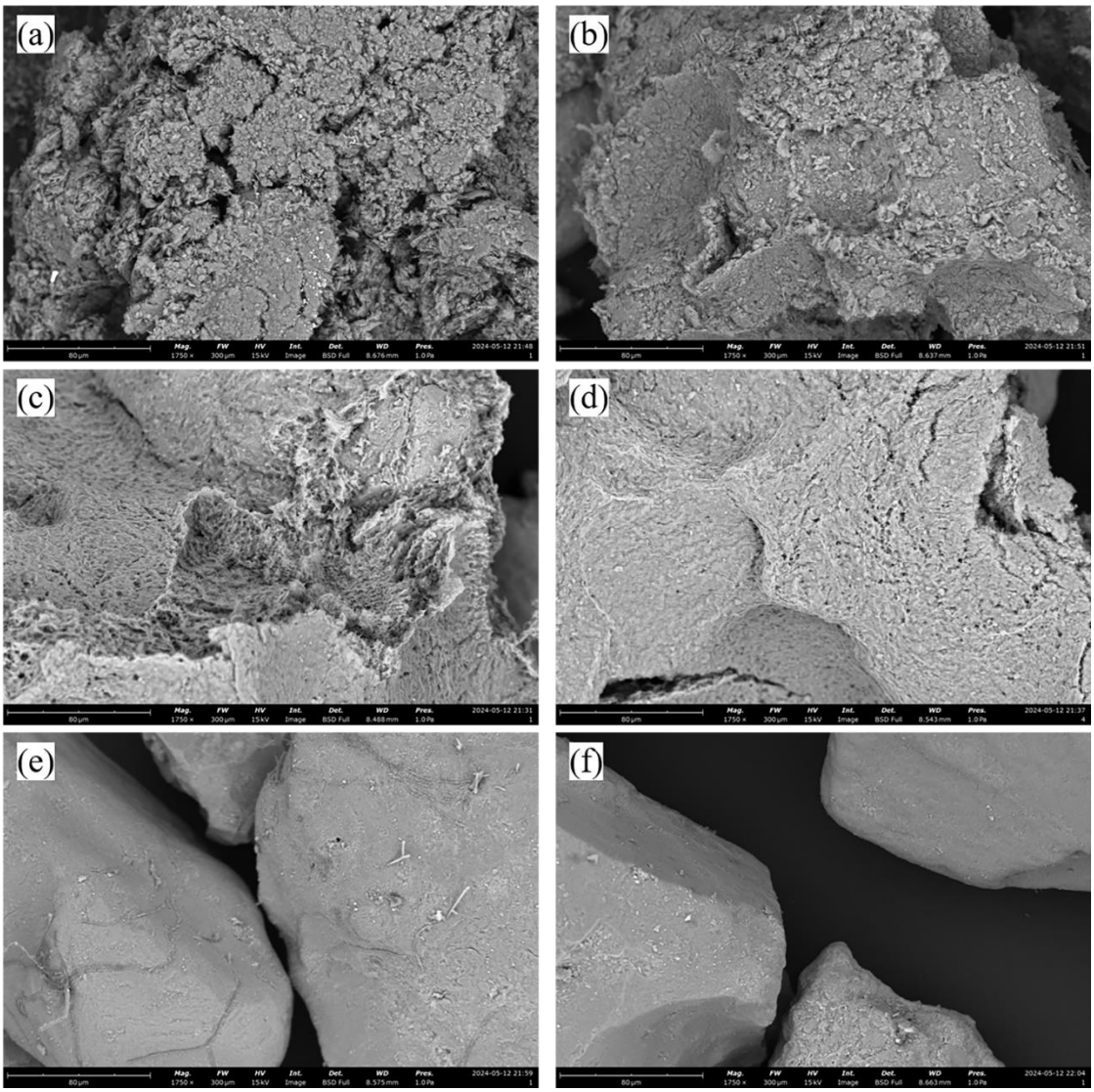

Figure S5.3 (a-f) Scanning electron microscope (SEM) images at day 0 of kaolin (a), C-kaolin (b), MMT (c), C-MMT (d), Algae (e), and C-Algae group (f)

Table S5.2. Predicted functional abundances using the FAPROTAX database

Function prediction	Kaolin	MMT	Algae	C-kaolin	C-MMT	C-algae
photosynthetic_ cyanobacteria	0.21± 0.05a	0.22± 0.01a	0.15± 0.04b	0.21± 0.01a	0.15± 0.02b	0.13± 0.05b
nonphotosynthetic _cyanobacteria	0.0007± 0.0006ab	0.0003± 0.0003c	0.0003± 0.0001c	0.0005± 0.0002c	0.0011± 0.0002a	0.0003± 0.0001c
photoautotrophy	0.21± 0.05a	0.22± 0.01a	0.15± 0.04b	0.21± 0.01a	0.15± 0.016b	0.13± 0.05b
photoheterotrophy	0.00016± 0.0001c	0.0014± 0.0001bc	0.0018± 0.001abc	0.00023± 0.00003c	0.0021± 0.0009ab	0.0032± 0.0017a
phototrophy	0.21± 0.05a	0.23± 0.01a	0.15± 0.04b	0.21± 0.01a	0.15± 0.02b	0.13± 0.05b
Chemohetero-trophy	0.0167± 0.02a	0.0223± 0.01a	0.0209± 0.006a	0.0176± 0.0016a	0.0065± 0.002a	0.0156± 0.0016a
aerobic_chemohet erotrophy	0.017± 0.005ab	0.011± 0.005bc	0.021± 0.006a	0.018± 0.002ab	0.006± 0.002c	0.014± 0.003ab

Note. FAPROTAX database: the functional annotation of prokaryotic taxa database

Table S5.3 Mineralization parameters of soil organic carbon (SOC)

Parameters	Algae	MMT	Kaolin	C-MMT	C-Kaolin	C-Algae
Cbas (mg CO_2–C cm^{-2} soil d^{-1})	0.047± 0.0061ab	0.040± 0.0041b	0.057± 0.020ab	0.044± 0.007ab	0.066± 0.032a	0.044± 0.010ab
Ccum (mg CO_2–C cm^{-2} soil)	0.511± 0.060a	0.271± 0.049d	0.363± 0.035c	0.155± 0.032e	0.438± 0.052b	0.162± 0.039e
qCO_2 (mg CO_2–C cm^{-2} h^{-1} $Cmic^{-1}$)	0.010± 0.007a	0.001± 0.0002c	0.001±0. 0001c	0.002± 0.003bc	0.004± 0.0005bc	0.006± 0.002b
qM (%)	31.447± 3.684b	9.476± 1.695d	14.165± 1.348c	13.040± 2.700cd	38.749± 4.626a	16.143± 3.923c

Note: Cbas: basal respiration, Ccum: cumulative respiration, qCO2: metabolic quotient, qM: mineralization quotient, CK: control check